NASA TT F-10,359

# LAWS OF TURBULENT FLOW IN SMOOTH PIPES

J. Nikuradse

Translated from "Gesetzmässigkeiten der turbulenten Stromung in glatten Rohren

VDI (Verein Deutscher Ingenieure)- Forschungsheft 356 Supplement to "Engineering Research" ("Forschung auf dem Gebiet des Ingenieurwesens"), Edition B, Volume 3, pp. 1 - 36, September/October 1932.



NATIONAL AERONAUTICS AND SPACE ADMINISTRATION
WASHINGTON OCTOBER 1966

Table of contents

# LAWS OF TURBULENT FLOW IN SMOOTH PIPES

J. Nikuradse

## ABSTRACT

The laws of turbulent flow in smooth pipes in the widest possible range of Reynolds numbers were determined by means of an experimental setup wherein turbulent water flows in circular pipes could be observed up to Re $3240 \cdot 10^3$. It was shown that the velocity distribution changes with the Re number. Measured distributions were in good agreement with those reported by Bazin and Stanton. The exponent n of Prandtl's exponential law had the fixed value of $n = 1/7$ in the Blasius range of drag up to Re $100 \cdot 10^3$. At very low Re the exponent was larger. Above Re $100 \cdot 10^3$ there is a lowering of the exponent. Turbulent exchange magnitudes were determined as a function of wall distance. Above Re $100 \cdot 10^3$ the distribution of this magnitude over the cross section is independent of the Re number. Measured velocity distributions and law of drag were compared with v Karman's distributions and were found to be in good agreement at high Re where the influence of viscosity is absent. If $\lambda = \frac{dp}{dx}\frac{2d}{au}$ is the pipe coefficient of drag, the Blasius drag formula $\lambda = \frac{0.316}{Re^{1/4}}$ is confirmed up to Re $= 100 \cdot 10^3$. For higher Re the drag coefficient becomes $\lambda = 0.0032 + \frac{0.221}{Re^{0.237}}$. Correlations between the average velocity $\bar{u}$ and maximum velocity U are determined and certain conclusions with reference to the v. Karman drag formula and the present one are drawn.

## Introduction

Until now the experimental knowledge of turbulent flow, which has been the /1* subject of numerous studies, was still not sufficient to produce a satisfactory theory of turbulence. The older studies, which were primarily aimed at the laws of flow resistance in pipes, could satisfy neither the theoretician nor the practician. The results of these experiments remained unclear as long as they were not related to the physically correct parameter, to the Reynolds number (Re). In many cases no consideration was given to the fact that the velocity

*Numbers given in the margin indicate the pagination in the original foreign text.

distribution in the pipe developed only after a long "starting zone". H. Blasius (ref. 1) succeded in arranging the experimental material on flow in smooth pipes from the point of view of similarity. He obtained an empirical formula that represents the law of drag fairly accurately in a range of Reynolds number to about $Re = \frac{\bar{u}.d}{v} = 100 \cdot 10^3$ ($\bar{u}$ = average velocity, d = pipe diameter, v = kinematic viscosity). For setting up his drag formula Blasius used the experiments of Saph and Schoder, (ref. 2) who worked with water and measured the pressure loss in 15 drawn brass pipes with diameter d = 2.77 mm to 53 mm in the range of Reynolds number from $Re = 1.4 \cdot 10^3$ to $104 \cdot 10^3$: Blasius found the formula $\lambda = 64/Re$ for laminar flow and $\lambda = 0.316\ Re$ for turbulent flow ($\lambda$ = drag coefficient). The experiments of Saph and Schoder show that the transition of laminar flow to turbulent flow takes place at about Re = 2000 and 3000. In addition to the experiments with water of Saph and Schoder, Blasius used the experiments of Nusselt (ref. 3) for drawing up his law of similitude. Nusselt studied the pressure losses for the flow of compressed air in a pipe with diameter d = 2.201 cm. When the drag coefficient is calculated from these experiments and plotted as a function of the Reynolds number, the same results are obtained as those that were obtained from the experiments of Saph and Schoder. Nusselt's values, which lie in the range of Reynolds number $6 \cdot 10^3$ to about $150 \cdot 10^3$ agree very well with the resistance formula of Blasius. Thereby the similarity for different fluids, water and air, is confirmed. Blasius also used the experiments of Lang, which were made in a copper pipe of d = 6 mm up to Reynolds number $Re = 326 \cdot 10^3$. The purpose of the experiments was to make a comparison between high velocities with small pipe diameter on the one hand and low velocities with large pipe diameter on the other hand. This comparison led to a very satisfactory confirmation of the law of similitude.

After the drawing up of the law of similitude, Ombeck (ref. 4) set himself the task of determining the dependence of the drag coefficient on the Reynolds number from experiments with air over a large range of Reynolds numbers, and thereby verifying the formula of Blasius. The experiments were carried out in circular pipes made of different materials and of different diameters (d = 2.004 cm to d = 10 cm), and extended to about $Re = 450 \cdot 10^3$. From these experiments Ombeck obtained a formula similar to that of Blasius, with insignificant deviations. These lie, as Ombeck himself states, in the uncertainty of the determination of the kinetic viscosity. Considering the circumstance, he found a good agreement with the Blasius formula up to $Re = 100 \cdot 10^3$.

For the purpose of verifying the law of similitude, Stanton and Pannell (ref. 5) performed numerous experiments in circular pipes with different diameters (d = 0.361 cm to d = 12.62 cm) with water and air at different temperatures. The experiments were in the range of Reynolds numbers $2.2 \cdot 10^3$ to $430 \cdot 10^3$. The results of these experiments confirmed the law of similitude /2 in the best way: up to Reynolds number $100 \cdot 10^3$ the testing points were in line with those of Blasius. Beyond that an increasing deviation upward from the line was observed with increasing Reynolds number. Lees (ref. 6) used the Stanton-Pannell results as the basis for drawing up his empirical formula for the law of resistance and found $\lambda = 0.0714 + \frac{0.6104}{Re^{0.35}}$

Jakob and Erk (ref. 7) carried out experiments with water on the pressure drop in relation to throughput in drawn brass pipes of diameter d = 7 cm and 10 cm in the range of Reynolds numbers between $86 \cdot 10^3$ and $462 \cdot 10^3$. Within the distribution of the testing points about 1% confirmed the measurements of Stanton and Pannell. Jakob and Erk derived a drag formula from their own experiments which agrees almost precisely with that of Lees.

Of more recent experiments, those of Hermann (ref. 8) on the law of resistance in a still greater range of Reynolds numbers must be mentioned: Hermann carried out the experiments with water in a copper pipe of diameter d = 5 cm and a brass pipe of diameter d = 6.8 cm in the range of Reynolds numbers between $20 \cdot 10^3$ and $1900 \cdot 10^3$ and starting zones between 88 and 600 pipe radii. He studied the dependence of the drag coefficient on the Reynolds number and for short starting zones and low Reynolds numbers he found a good agreement with the law of drag which Stanton and Pannell and Jakob and Erk and others previously had established. Hermann observed a starting effect (decrease of drag coefficient with the starting zone) with a starting distance of up to 600 pipe radii: in addition he obtained an increase in the starting zone with increasing Reynolds number. The experimental results show that approximately 200 r should be considered as the starting zone. Hermann derived from these experiments a formula which is analogous to that of Lees. At the end he presents a table for conversion of the drag coefficient for any starting zone between 88 and 600 radii. L. Schiller (ref. 9), under whose direction Hermann worked, reported in 1929 in Aachen at the Congress for Aerodynamics and Related Subjects about the results cited above, whereby it turned out that the drag coefficients above the highest Reynolds numbers reached by Stanton and Pannell and Jakob and Erk were substantially higher than those found at Göttingen. The higher resistance apparently showed that Hermann had a rotation in his test pipe which caused an increase in drag. This fact induced L. Prandtl (ref. 10) to suggest that a flow straightener be built into the pipe intake and the measurements be repeated. The results of the check measurements, as reported by L. Schiller in a postscript to his Aachen lecture, was that there was no more starting effect after 250 pipe radii and that with a sharp intake no more starting effect was to be observed after a zone of 100 r, which agrees with the Göttingen measurements. Here it must also be mentioned that the extensive Göttingen measurements, not published, show about starting distance that there is no starting effect from 100 r on with a rounded intake either.

Among the first good experiments on the velocity distribution of turbulent flows are those of Stanton (ref. 11). The measurements were made with air in pipes of 500 cm length and a diameter d = 4.93 cm and d = 7.4 cm and extended over the Reynolds numbers between $14 \cdot 10^3$ and $60 \cdot 10^3$. Data about the pressure gradient at which the velocity distribution was recorded are missing. A further similar measurement with water was made by the author (ref. 12) in a circular pipe of 2.8 cm diameter at a Reynolds number of about $180 \cdot 10^3$. Furthermore, measurements exist on the velocity distribution in channels and pipes of non-circular cross section, which are not related to this work.

From the works cited one will see that the experimental findings are not adequate to clarify the turbulence problem. For this reason we had set ourselves the task at Göttingen, to expand the existing investigations in two directions: on the one hand to extend the scope of the experiments to very high

Reynolds numbers and on the other hand in addition to ascertaining the law of drag also to clarify the velocity distributions, the knowledge of which is of great importance to the study of turbulent flow, in relation to the Reynolds number. We have carried out a large series of experiments on the velocity distribution and pressure drop in smooth pipes with the highest attainable measuring accuracy and in as large a range of Reynolds numbers as possible. Through suitable interpretations we have succeeded in showing:

1. which laws exist in the relationship between drag and velocity distribution.
2. by which formulas the drag law and the law for velocity distribution can be expressed.
3. which laws apply to the exchange magnitude and the Prandtl mixing path theory.

In these investigations full use was made of the theoretical results of Karman's consideration of similitude (ref. 13). The experiments confirmed these results very well above the limit at which the influence of viscosity on the turbulence phenomena disappears.

The experiments (ref. 14) were carried out during 1928/29 at the Kaiser Wilhelm Institut für Strömungsforschung under the direction of Prof. Dr. L. Prandtl. The theoretical treatment of the experimental results could not be completed until the summer of 1931. The experimental installation and apparatus were built in the shops of the Kaiser Wilhelm Institut für Strömungsforschung.

I should like to express in this place my heartfelt thanks to my highly respected chief Prof. Dr. L. Prandtl, who supported me at all times with his valuable counsel.

## I. Experimental Part /3

### 1. Apparatus

Three different experimental installations were used for the study of flow phenomena in circular pipes;

a) For low Reynolds numbers of about $3 \cdot 10^3$ to $60 \cdot 10^3$ a tank with overflow was used, which tank was fed from the water supply;
b) For higher Reynolds numbers to about $1400 \cdot 10^3$ the water was circulated by means of a rotary pump;
c) To reach still higher Reynolds numbers to about $2500 \cdot 10^3$ the water stored in the tank was driven out by means of compressed air;
d) With the last two installations the Reynolds number was further increased by raising the temperature of the water, whereby in the 3rd case a maximum value of Re = $3300 \cdot 10^3$ could be reached.

Re a): As a perfectly constant water column with small throughput quantity such as is required at lower Reynolds numbers was difficult to obtain with a

rotary pump alone, the following arrangement was made. The water flows through a feed pipe zl (Fig. 1) from the water system into the open water tank wk. With the outlet valve ah open the water rises in the ascending pipe str as high as the water in tank wk. As the feed pipe delivered a somewhat greater amount of water than flowed out through the test pipe vr, the excess water was delivered through the ascending pipe str to the collecting vessel ft from which it was carried off through outlet pipe fr, so that a constant water level was obtained. In order to get a uniform flow of water in the test pipe a straightener gl was built into the cylindrical part of the outlet from water tank wk. This was to prevent the great vorticity, which was caused in the water tank by the inflowing water, from being continued in the test pipe. Through the conical part of the outlet the water received an acceleration which had a further stabilizing effect. The water was then brought through a pipe zr of 25 cm diameter and 250 cm length to the head of the test pipe. Test pipes of the following sizes were used (Table 1).

Table 1

Dimensions of the Test Pipes

| d mm | $l_e$ mm | $l_I$ mm | $l_{II}$ mm | $l_a$ mm | x mm | $\frac{x}{d}$ | Designations |
|---|---|---|---|---|---|---|---|
| 10 | 550 | 500 | 500 | 450 | 2,000 | 200 | $vr_1$ |
| 20 | 1,330 | 500 | 500 | 170 | 2,500 | 125 | $vr_2$ |
| 30 | 1,960 | 500 | 500 | 40 | 3,000 | 100 | $vr_3$ |
| 50 | 3,300 | 1,000 | 1,000 | 70 | 6,000 | 120 | $vr_4$ |
| 100 | 4,000 | 1,500 | 1,000 | 550 | 7,050 | 70.5 | $vr_5$ |

d = internal diameter of pipe; $l_e$ = length of intake; $l_I$ = measuring section I; $l_{II}$ = measuring section II; $l_a$ = length of outlet; x = total length; $\frac{x}{d}$ = relative total length.

In order to obtain a uniform intake into the test pipe, feed pipe zr to the test pipe is conically narrowed in all tests, to the diameter of the test pipe. In this reducing piece al (Fig. 4) [ i.e. 5 ] there was a sharp-edged constriction during the tests with overflow, which should guarantee a turbulent flow even with the lowest Reynolds numbers studied. A relief valve eh was mounted at the highest point of the feed pipe immediately before the narrowing. The test pipe with the velocity measuring apparatus was mounted on two carriages, which permitted convenient displacement during conversion. The carriages ran on tracks on the edge wall of the supply canal. In the longitudinal direction of the carriage lay an optical track on which the riders stood, which carried the test pipe and made an adjustment in the horizontal direction possible. At the end of the test pipe was the velocity measuring apparatus, which will be described in detail below. Underneath, in the supply channel vk

stood the measuring tank mb (Fig. 4) [i.e. 5].

Re b): For the experiments with circulation (Fig. 2) the water was taken from the supply canal vk and conveyed to the water tank wk by the rotary pump which was driven by a motor am (power: 14 kW, speed variable between 1120 and 1900 rpm). From the water tank it returned through the test pipe vr to the supply canal. Coarse control was achieved through the starter an of the drive motor and the slide valve sb that was inserted between rotary pump kp and water tank wk. The fine adjustment took place through a throttle valve dv on the velocity measuring apparatus (Fig. 5). The rotary pump was capable of maintaining a pressure up to 2 atm on the water surface in water tank wk. The pressure was generated by the water compressing the air present in the tank above the water. Generally a water column of 500 cm was maintained (dimensions of tank wk; height 6500 mm; diameter 1500 mm). The testing arrangement just described permitted water flows up to about $Re = 1000 \cdot 10^3$ to be created at normal temperatures. The testing section was otherwise exactly as with the arrangement first described.

Re c): The compressed air installation consisted of a compressor capable of creating a pressure of about 10 atm in the pressure tank dk (Fig. 1). The pressure tank was connected through an Arca regulator a with water tank wk; the regulator, which will be described in detail below, provided for constant pressure in the discharge of water from the water tank. As the outflow time was limited (shortest period about 45 sec) the quick-acting valve sh located between the water tank and the test pipe provided for quick opening and closing of the experimental passage. The quick-acting valve was controlled by compressed air. About 0.1 sec was required for the opening and closing. To prevent a reduced pressure from occuring in the water pipe through the closing of the quick-acting valve, the relief valve sv, which was placed at the highest point of the feed pipe zr between the quick-acting valve and the test pipe, provided for equalization with the ambient air. As in these tests measurements were made in the free jet, the velocity measuring apparatus gm was open and an ascending pipe sr was placed on it. The free jet was caught by the jet destroyer st, which was mounted on a third carriage, and returned to the supply canal through deflection and quieting vessel br. The feed pipe zr in these experiments was only 1500 mm long, due to lack of space.

Re d): In order to reach still higher Reynolds numbers the kinematic viscosity $v = \frac{\mu}{\varrho}$ of the water was reduced by increasing the temperature. /4
The same method was also used in part for the measurements with circulation, because the tests by means of this installation required much less time and effort than with the last mentioned test arrangement. The water was heated with steam in a tank. The tank delivered about 1.1 liter/sec water at 40° C. By reducing the amount delivered the water temperature could be increased to ca 95° C, which due to the cooling in the testing apparatus corresponded to a temperature of about 40° C in the test pipe. The tank was next to the wall of the hydraulic laboratory and discharged through a hose zf into the supply canal vk. As a result of the increase in the temperature of the water the Reynolds numbers amounted to $Re = 1400 \cdot 10^3$ with the second installation and $Re = 3240 \cdot 10^3$ with the third installation. A general view of the installation for c) and d) is seen in Fig. 3.

2. Measuring Devices

a) Velocity measuring apparatus with throttle and swinging outlet

The velocity measuring apparatus (Fig. 4) consists of the housing m, the cover d, the spindles sp and su, the slide schl and the movable pito tube pt. The housing has windows f on either side for observation purposes. There is a wall w in the middle, which is to prevent the fluid from flowing back into the measuring chamber. The cover d is screwed rigidly to the housing so a ready seal is obtainable. A valve e is placed on the cover for venting.

Spindles sp and su are provided for moving the pito tube and at the same time they support slide schl. Spindle sp has a thread of 1 mm pitch and pushes the slide horizontally; it is turned from the outside and is sealed by a stuffing box. The revolutions of spindle sp are transferred to a counter zw. This is so arranged that the roll for the last digit position (unit position) is rigidly attached to the counter shaft, so that the counter advances the units instead of one number and consequently the second place of the numbers is in the unit position. Thereby 0.1 mm displacement can be read conveniently. With the movement of the slide back and forth the pitot tube is simultaneously moved in the same direction.

The vertical movements of the pitot tube holder ph are effected by spindle su, which has no thread, but a groove. Through the turning of the spindle the worm gears are turned. The worm wheel z has an internal thread with 1 mm pitch and screws the pitot tube holder ph up and down while it is secured against turning by the guide flanks fl. The counting was done by means of counter $zw_2$ in the same manner as with spindle sp.

The total pressure to be measured is carried outside through the pito tube holder ph on which pitot tubes pt of various diameters can be mounted, and through hose s. As the velocity distribution was measured 0.1 to 0.2 mm behind the outlet end of the test pipe, the static pressure must also be measured in this plane of cross section; for this reason a boring scht of about 0.8 mm diam was made in the flange of the test pipe. This boring was ca 2 mm from the edge of the jet. The pressure prevailing here was equal to the pressure at the edge of the jet.

In order to be able to regulate the throughput quantities accurately a throttle valve dv (Fig. 4) is mounted on the velocity measuring apparatus. The position of the throttle cone dk can be adjusted by means of the screw spindle srsp (Fig. 5) [i.e. 4] with measuring scale msk.

The swinging outlet sch serves to lead the liquid quickly to a measuring tank for quantity measurement and again to lead it off. A ball bearing kl permits it to be swung very rapidly.

The velocity measuring apparatus, the throttle device and the swinging outlet are mounted together and lie on a carriage wg (Fig. 4) [i.e. 5] which is likewise movable on the tracks previously mentioned, in the longitudinal direction of the supply tank.

b) Measuring Tank

A cylindrical measuring tank mb (Fig. 5) with a capacity of about 700 liters with 1000 mm diameter and 900 mm height was used for the quantity measurement; it could be moved under the swinging outlet sch. A drain with stopcock ab was placed in the bottom of the measuring tank. Before the drain cock there was installed a water-gauge glass ws with millimeter graduation for reading the water level in the tank. The measuring tank stood on four screw feet sf to make it adjustable horizontally. A perforated round wooden disk was floating on the water in the measuring tank, which was to damp the oscillations of the water surface, whereby the time for reading was shortened. A smaller similar measuring tank of 178 mm diameter and 700 mm height was used for the measurement of smaller quantities. For more exact ascertainment of the diameter of the measuring tank the height of rise of the water level was determined as a function of the amount of water (ca 10 kg), formerly established by weighing.

c) Micromanometer

The accuracy of reading the ordinary water manometer was not sufficient for the small pressure differences that occurred. An instrument had to be created whose reading accuracy met our demands but which also at the same time could be used for high pressures. This problem was solved as follows for pressures from 0.02 to about 500 mm water column. In a vertical glass tube with three stopcocks $h_1$, $h_2$, $h_3$ (Fig. 6) two glass tubes are fused in between every two cocks. Between the two free upper legs of these tubes a T piece with 120° angle between the legs was fused in so that one leg stood vertically upwards. This end of the T piece could be closed by a stopcock $h_5$. The stopcock $h_4$ in another leg of the T piece permitted the breaking of the connection between the two glass tubes. The free ends $a_3$ and $a_4$ of the glass tubes could be closed by pinchcocks. When this device is to be used as a water manometer, the two pressure lines are closed at $a_1$ and $a_2$ and the stopcocks $h_1$, $h_2$ and $h_4$ are opened. With mercury filling the pressure line is closed at $a_3$ and $a_4$ and opened at $h_3$. For checking the zero point during operation $h_3$ is opened with the water manometer and $h_4$ with the mercury manometer. The reading zone has a length of about 500 mm. An increase in the accuracy of measurement was achieved through a reading microscope mi. On a solid baseplate of brass a square precision tube is rigidly mounted, on which the two slides sl are movably arranged. Each slide carries a reading microscope with cross hairs. The moving is effected by rack and pinion. The worm drive sn (Fig. 7) which can be engaged and disengaged makes possible a precise fine adjustment. The lower slide carries the scale m with millimeter gradation, the upper one carries the vernier n with division in fiftieths. A swingable magnifying glass lu is placed in front of the vernier. The illumination is effected by the strip lamp la (Fig. 6) which /6 is movably placed behind a pane of frosted glass mg. By means of adjustable shields bl (Fig. 7) the zone of the meniscus under observation is darkened, so it is contrasted black against the illuminated frosted glass. The manometer can be adjusted by means of level and regulating screws to be precisely vertical.

d) Arca Regulator

The Arca regulator, a present from the firm Arca-Regler AG, Berlin W3, maintains the desired pressure in the water tank. The mode of operation is as follows. The water pipe is connected at wl. A branch $l_1$ leads through choke dr which regulates the throughput. The water acts on piston k and flows through pipe $l_2$ to the poppet valve $t_v$ which closes with high pressure in the water tank and opens again with low pressure. The tension spring sf permits adjustment to a specific pressure prior to the beginning of the experiment. The membrane bellows mb transmits the pressure by means of lever h to poppet valve tv. If the pressure in the water tank declines the poppet valve tv also opens. Thereby the discharge $l_2$ is released. The water in the water pipe is now no longer blocked, piston ko is forced upward by piston spring kf and with it the control piston sk. The latter now clears the water passage under the lifting piston hk. The water pressure now raises the lifting piston and thereby the regulator valve rv lifts, by which the connection between compressed air tank dk and water tank wk is again established. When the predetermined pressure is again reached in water tank wk, this acts through the membrane bellows and the poppet valve tv closes. Thereby the pressure on the piston ko increases and presses the latter downward. Then the water flow wl under lifting piston hk is again shut off and the outlet wa is opened. The lifting spring hf again presses the regulator valve rv shut. In that the membrane bellows mb is not connected with the air space in the tank, but below in the water space, the water pressure is kept constant at the outlet during the discharge independent of the superimposed water column height.

e) Quick closing valve (Ref. 15)

The quick closing valve (Fig. 9) is operated by compressed air of about e atm and can be opened or closed in about 0.1 to 0.2 sec. The process in opening and closing the quick acting valve is as follows:

Turning the control wheel sr first opens a small valve ha by means of a cam, which lets compressed air through pipe l in below lifting piston hk. The latter is raised and with it the cone k as far as the stop schr, which is adjustable. Now the seat surfaces of cone k are free, and the latter is rotated by the rotating piston drk. The compressed air enters the control piston sk through the inlet lc and fills the chambers ka (see section A-A). If the control wheel sr and likewise the control piston sk are turned electrically or manually, the slots at c and d open, the compressed air flows through slots c into chambers ku and presses the rotating piston drk and consequently also cone k of the valve. The air that is present in chambers ko escapes through slots d into the open. When cone k and the rotating piston drk have been turned 90° the small valve ha closes and lets out the air under the lifting piston hk at the same time. The latter and the cone are again forced down by an adjustable spring f. The closing is effected by the turning backward of control wheel sr through the same arrangements in reverse order.

To prevent cone k from oscillating an oil damping device is provided (section B-B). The damping piston dmk is rigidly connected to the rotating piston drk. The chambers kd are filled with oil through an inlet e connected with

Fig. 1. Experimental installation /5

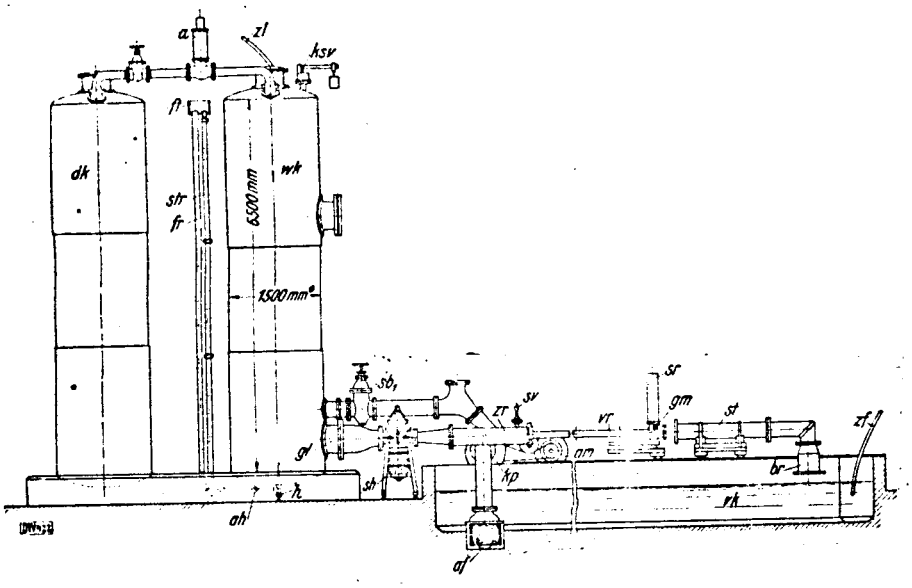


| | |
|---|---|
| zl | feed pipe |
| wk | water tank |
| dk | compressed air tank |
| $sb_1$ | slide valve between wk and kp |
| $sb_2$ | slide valve between wk and zr |
| str | ascending pipe |
| fr | outlet pipe |
| ft | collecting vessel |
| ah | outlet valve |
| h | blowout valve |
| gl | straightener |
| zr | feed pipe |
| ksv | safety valve for water tank |
| br | quieting vessel |
| sv | relief valve |
| vr | test pipe |
| gm | velocity measuring apparatus |
| sr | ascending pipe |
| a | Arca regulator |
| kp | rotary pump |
| am | drive motor |
| vk | supply canal |
| an | starter for electric motor |
| zf | feed hose |
| af | drain |
| qws | mercury water level meter |
| sh | quick closing valve |
| st | jet destroyer |

Fig. 2. View of experimental installation with water circulation. /5

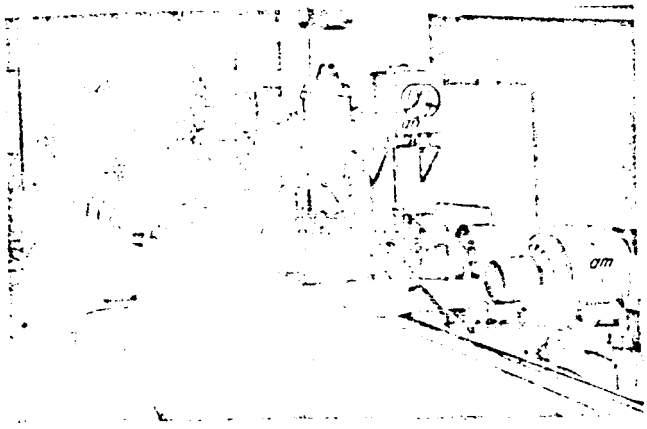

Fig. 3. View of installation for shock experiments.

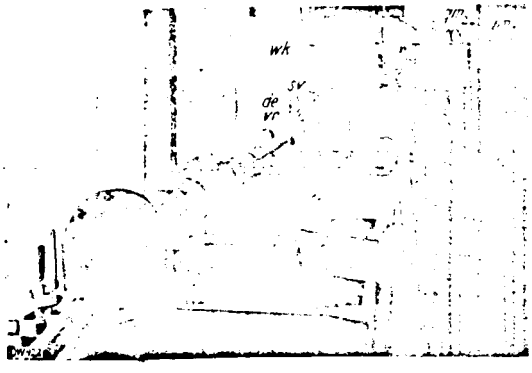

| | |
|---|---|
| de | pressure adjustment |
| qm, $qm_2$ | mercury manometers |
| wm | water manometer |

Fig. 4. The big velocity measurement apparatus with throttle and swinging outlet. /5

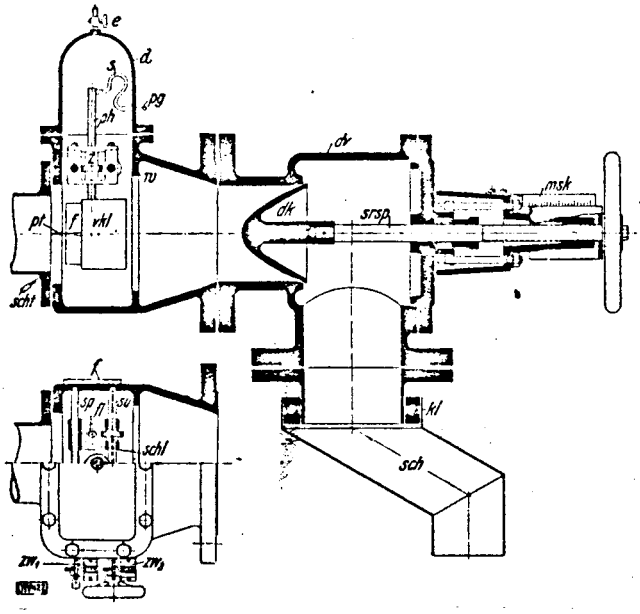


| | |
|---|---|
| m | housing |
| d | cover |
| sp, su | spindles |
| schl | slide |
| pt | pitot tube |
| ph | pitot tube holder |
| f | window |
| pg | pipe attachment for total pressure |
| z | worm wheel |
| fl | guide flanks |
| s | hose |
| srsp | screw spindle |
| dr | throttle cone |
| msk | measuring scale |
| kl | ball bearing |
| dv | throttle valve |
| w | wall |
| e | venting valve |
| vkl | fairing for pitot tube holder |
| sch | swinging outlet |
| $zw_1$, $zw_2$ | counters |
| scht | hose sleeve |

Fig. 5. A part of the experimental installation /5

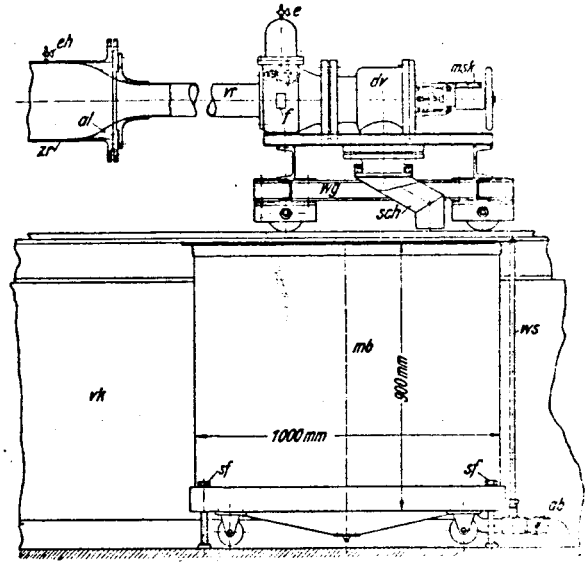


| | |
|---|---|
| zr | feed pipe |
| eh | relief valve |
| al | reducing piece |
| vr | test pipe |
| e | venting valve for the velocity measuring apparatus |
| f | window of the velocity measuring apparatus |
| vk | supply canal |
| dv | throttle valve |
| msk | measuring scale of the throttle valve |
| sch | rotating outlet |
| wg | carriage |
| mb | measuring tank |
| ws | water gauge glass |
| ab | drain cock |
| sf | screw feet |

Figs. 6 and 7. View and closeup of the micromanometer /6

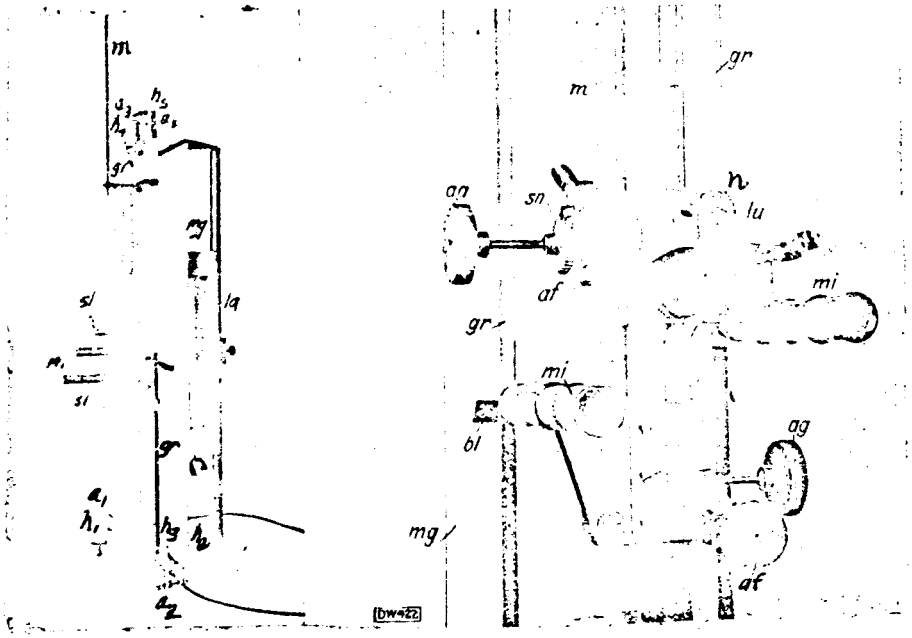


| | |
|---|---|
| $h_1$, $h_2$, $h_3$, $h_4$, $h_5$ | valves |
| $a_1$, $a_2$, $a_3$, $a_4$ | pressure line connections |
| mi | reading microscope |
| bl | shield |
| sl | slide |
| m | scale |
| sn | worm drive |
| n | vernier |
| lu | magnifying glass |
| ag | drive wheel for coarse adjustment |
| af | drive wheel for fine adjustment |
| gr | glass tube |
| mg | frosted glass pane |
| la | strip lamp |

Fig. 8. The Arca regulator

/7

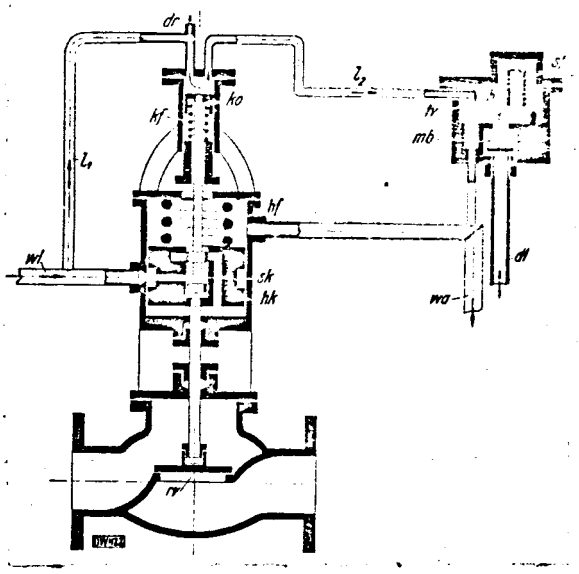


| | |
|---|---|
| wl | water pipe |
| $l_1$ | branch |
| $l_2$ | discharge |
| dr | throttle |
| ko | piston |
| kf | piston spring |
| hf | lifting spring |
| sk | control piston |
| hk | lifting piston |
| sf | tension spring |
| h | lever |
| tv | poppet valve |
| mb | membrane bellows |
| dl | pressure pipe |
| wa | water discharge |
| rv | regulator valve |

Fig. 9. The quick closing valve

/7

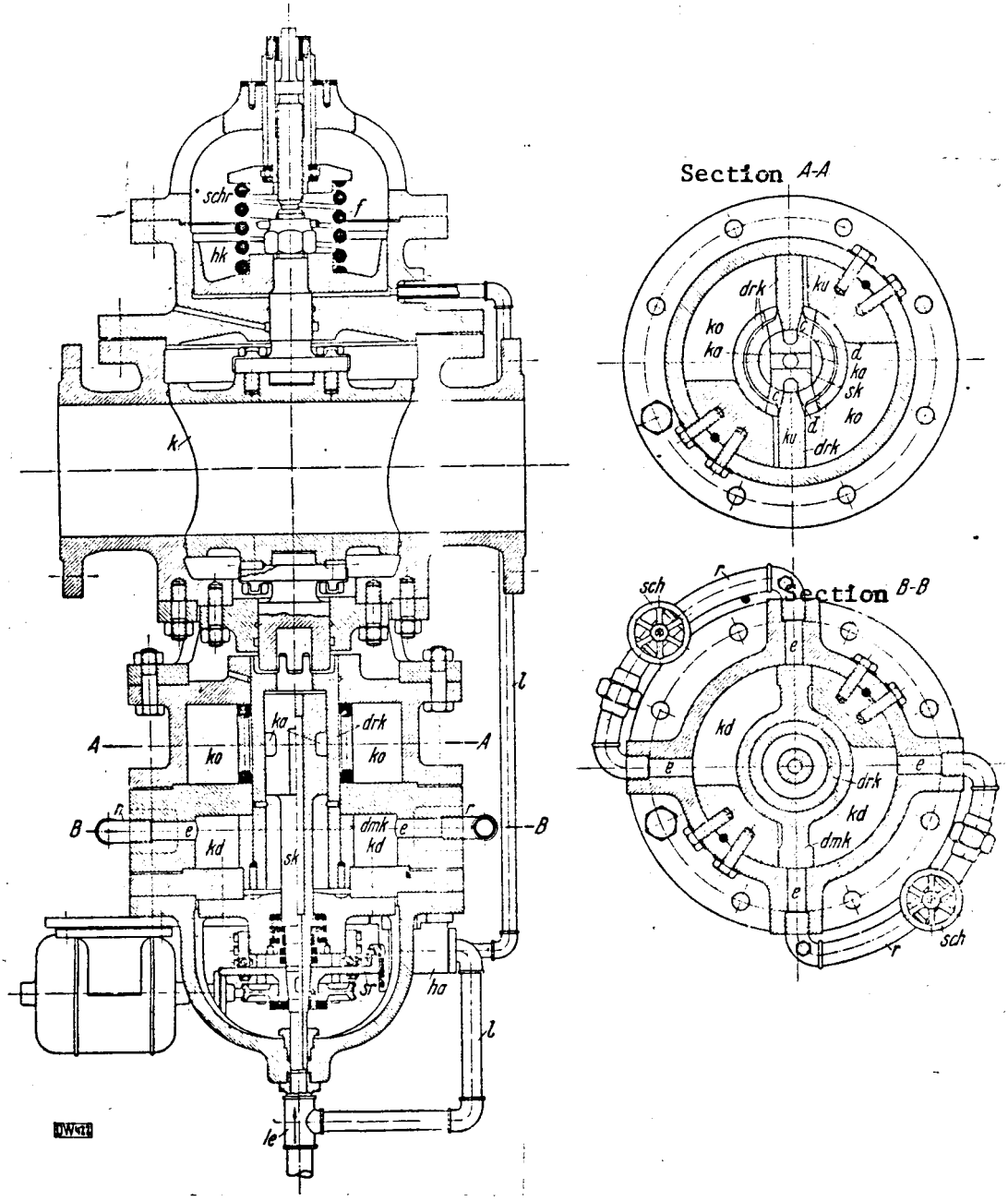


sr....control wheel
ha....valve
k.....cone
schr..stop
drk...rotating piston
sk....control piston
ka.....chamber of control piston
c, d....slots
ku, ko..compressed air chambers
l.....compressed air
hk.....lifting piston
f.....spring
dmk.....damper piston
kd.....oil chamber
le.....compressed air chamber
r.....pipe line
sch ....slide valve
e.....oil intake

the pipeline r and slide valves sch. By the rotation of the damping piston, oil is forced through the pipe toward the back and by adjustment of slide valve sch it is more or less throttled. In the moment when damper piston dmk closes the supply boring e, the oil, except for leaks, is completely shut off. A hard impact is prevented by this oil cushion.

/7

3. Experiments

a) Quantity Measurements

The quantity measurements up to Re = $300 \cdot 10^3$ were undertaken in the measuring tank. As no guarantee was given that the measuring tank was precisely cylindrical, it had to be calibrated. A weighed amount of water was put into the tank and the water level read in the water gauge glass. The calibration showed a uniform diameter everywhere. The cross section of the large measuring tank was F = 7850 $cm^2$, that of the smaller one F = 248 $cm^2$. In each measurement the lower level was read before the higher level after water was poured /8 in. The reading was done with perfectly still water and with a mirror to avoid parallax. This manner of reading made an accuracy of from 0.1 to 0.2 mm possible. By means of the swinging outlet the water could be brought to the measuring tank in 0.1 to 0.2 sec. The duration of the inflow into the measuring tank was determined with a stopwatch. The stopwatch was checked as to accuracy and had 1/10 sec gradations. The swinging outlet could then be swung back as quickly. The duration of the inflow was between 100 and 600 sec. If we assume that with a measuring duration of 100 sec measurements are accurate within 0.2 sec, and furthermore that the water level in the water gauge is read accurately within 0.2 mm, then in the most favorable case the error in quantity measurement amounted to 0.3%. With a measuring duration of 600 sec the error was reduced to 0.05%. The greatest error produces and error of 0.13% for the average velocity u. The amount was determined as the average of several observations (4 to 6) and occasionally from two observations.

b) Temperature Measurements

The temperature was generally measured with a thermometer at the outlet. In order to be sure that the water in the pipe had the same temperature as it had at the outlet, the water flowing out through the relief valve (Fig. 4) [i.e. 5] was measured. The thermometer had been calibrated and had 1/10 degree graduations. Thus about 1/20 to 1/30° could be estimated, whereby an error in the kinematic viscosity was limited to 0.05 to 0.08%. At the higher temperatures the error in the kinematic viscosity is still smaller. The measurements were undertaken at temperatures from 9° to 38° C. At ordinary water temperature the constancy of temperature is easy to achieve: at higher temperatures on the other hand there was some difficulty. As mentioned, the higher temperatures were obtained by water of 80 to 90° C flowing from a tank into the supply canal vk, (500 to 800 cc/sec). Through preliminary tests it was found what amount and temperature of this water was required in order to maintain a certain temperature of the test water continuously. Cooled water corresponding to the inflow was discharged through the drain af (Fig. 1) from the deepest part of supply canal vk.

c) Determination of Pipe Radius

If the pressure gradient $\frac{dp}{dx}$ is related to the dynamic pressure of the average velocity $\overline{q} = \varrho \frac{\bar{u}^2}{2}$ there will be obtained the dimensionless number $\lambda$ which is designated the drag coefficient.

$$\lambda = \frac{dp}{dx} \cdot \frac{2r}{q} = \frac{dp}{dx} \cdot \frac{4\pi^2}{\varrho Q^2} \cdot r^5,$$

where $\varrho$ is the density of the water
Q is the throughput per unit of time
r is the pipe radius

This formula gives the result that the drag coefficient $\lambda$ which was to be determined from our experiments is proportionate to the fifth power of the pipe radius. Therefore as accurate a determination of this as possible was required. The pipe radius was determined from the weight of the water which filled the test pipe completely, and the length of the pipe. The weight determination was done with an accuracy of ± 0.01%. The length could be measured accurately to 0.2 mm, which corresponds to an error of ±0.007%. If the calculation is made with the error of weight and pipe length in the most unfavorable case, the pipe radius r will be about 0.001% in error. This error is of no consequence for the determination of drag coefficient $\lambda$.

d) Measurements of Static Pressure

The measurement of the static pressure is made under the assumption that the static pressure is the same over the entire measuring cross section. Since the static pressure can be measured quite accurately through cleanly made wall borings, if the wall is parallel to the flow direction, the measurements of the pressure gradient were made in that way. In each measuring cross section four borings were made in the test pipe, which borings were connected by an annular equalizing chamber ak (Fig. 10). The connection with the manometer could be established by means of a nozzle tü and hose. The free leg of the manometer was connected in the same way with the next measuring cross section.

ak....equalizing chamber
tü....nozzle

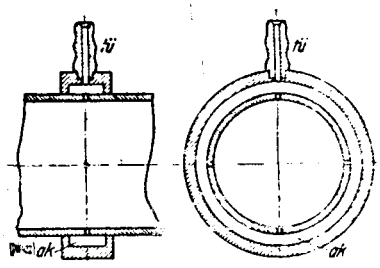


Fig. 10. Measuring cross section for the determination of the static pressure.

The pressure gradient was measured in this way over a measuring distance 1. Very often a suction or pressure effect occurred through imperfect borings (the elevation produced a suction effect and the indentations a pressure effect). In order to obtain a faultless reading of the pressure gradient the most favorable form of the boring was sought and the sharp-edged form was identified as being the one. In order to determine the effect of size, borings of 0.5 mm diameter were first made and these were gradually enlarged to 1.2 mm diameter. It was found that at least within the range that was studied, the size of the boring is without influence on the pressure indication.

In preparing the sharp-edged borings a precisely fitting brass pin was pushed into the pipe at the site of the boring. Thereby, the formation of large burrs and denting were prevented. By polishing with fine emery paper on a wooden pin all the burr was easily removed. To check a boring site was cut open and examined with a microscope under 50 x magnification. No burr could be found.

The borings were examined individually for quality prior to the attachment of the equalizing chamber. Every two borings were connected through a micromanometer. The testing was now made with the greatest throughput obtainable in order to magnify possible errors as much as possible. In case such occurred the pipe was polished again.

Furthermore, the pressure differences were measured over two measuring distances $l_1$ and $l_2$. The pressure gradient indications were only regarded as correct when with the same length of the two measuring distances identical pressure differences were determined. To compensate for an error in pressure difference the pipe was reversed in relation to the direction of flow. Then with the same Reynolds number the same pressure difference must be indicated.

To achieve greater accuracy in the pressure gradient necessary for the evaluation, even longer measuring distances were used, as shown in Table 1. /9 The length of the measuring distances was determined with an accuracy to 0.2 mm. The pressure differences were measured to 50 cm water column, respectively mercury column, with a micromanometer of the described type. Greater pressure differences were ascertained with an ordinary mercury U-manometer of 250 cm height.

e) Velocity Measurements

The measurements of velocity were carried out so that the dynamic pressure of the pitot tube was connected with reference to the static pressure of the pressure boring that lay in the measuring cross section and 2 mm from the edge of the flow, so that the manometer indicated the dynamic pressure directly. The velocity was calculated with the formula

$$u = 44{,}3\sqrt{h} \quad \text{cm/s} \qquad (1)$$

wherein h is the measured dynamic pressure height in cm water column and u is the velocity in cm/sec.

This formula is derived from Bernouilli's equation which is obtained from

Euler's equation of motion for frictionless fluids subject only to gravity through integration along a streamline. The Bernouilli equation then takes the following form:

$$\frac{p}{\varrho} + \frac{u^2}{2} + H = \text{const}, \qquad (2)$$

where H is the height of the point under consideration above a horizontal level chosen at random.

When the Bernouilli equation is multiplied by density we obtain the following pressure equation:

$$p + \varrho \frac{u^2}{2} + \varrho H = p_0. \qquad (3)$$

If outside forces (gravity) are disregarded (because H in our case has the same value at both test openings) the pressure equation is:

$$p + \varrho \frac{u^2}{2} = p_0. \qquad (4)$$

$p_0$ is the value of the highest pressure that appears at the mouth of the pitot tube. It corresponds to velocity zero and is called total pressure; p is the static pressure. If $p_0 - p = hy$ (with y = density and h = height of the manometer column) from equation (4) we obtain:

$$\varrho \frac{u^2}{2} = h\gamma \qquad (5)$$

or with

$$\varrho = \frac{\gamma}{g}$$

$$u = \sqrt{2gh} = 4{,}43\sqrt{h} \quad \text{cm/s}.$$

The velocity distribution was measured with a pitot tube 0.1 to 0.2 mm behind the discharge cross section of the test pipe. The reliability of the measurement at this distance behind the discharge cross section is shown by comparison with the velocity distributions that were measured 2 and 5 mm before the discharge cross section (Fig. 11). A further measurement of the velocities at different Reynolds numbers in the pipe axis at the discharge and at the same time 20 d before the discharge gave identical values. The measurements were therefore undertaken behind the discharge cross section in order to avoid pressure field disturbances, but above all also because in this way it is possible to measure the velocities right up to the wall of the pipe.

As knowledge of the static pressure in the measuring cross section was very important for measuring the velocity distribution, this comparative measurement was carried out with a probe that was installed instead of the pitot tube. In order to eliminate as far as possible the influence of the pitot tube holder on the static pressure a fairing vk1 (Fig. 5) [i.e. 4] with symmetrical profile was placed so that the probe lay in the axis of symmetry of the profile. The side borings of the probe lay in the measuring cross section. The probe was connected through a micromanometer with a boring in the wall which likewise lay in the measuring cross section. As no pressure difference could be detected by the manometer, it can be concluded that the static pressure outside the jet was of equal magnitude also. It is therefore justified to measure the static pressure in velocity measurements through borings in the flange. In

addition a value $\frac{x}{d}$ (in which x is the pipe length and d the pipe diameter) was sought by velocity measurements, at which $\frac{x}{d}$ value the velocity distribution is independent of pipe length. For this purpose the velocity distributions at Reynolds number Re = 900·10 and with $\frac{x}{d}$ = 100, 65 and 40 were recorded: this was done by cutting off the pipe at these lengths. At all these values the velocity distributions were independent of the pipe length. As in the main tests the starting distance was $\frac{x}{d}$ = 50 further investigations could be omitted. This result is reproduced in a dimensionless graph in Fig. 12.

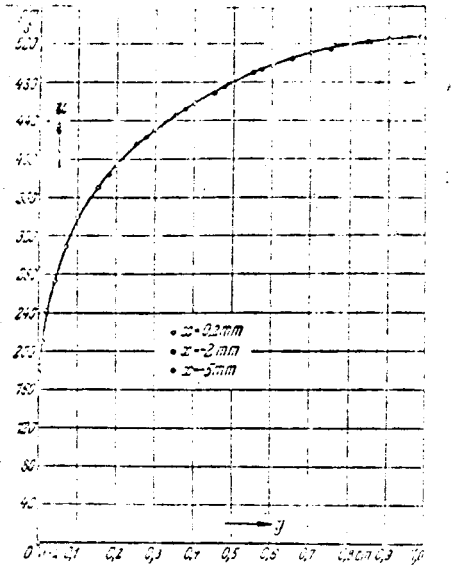


Fig. 11. Velocity distributions with x = 0 mm, x = -2 mm, and x = -5 mm.

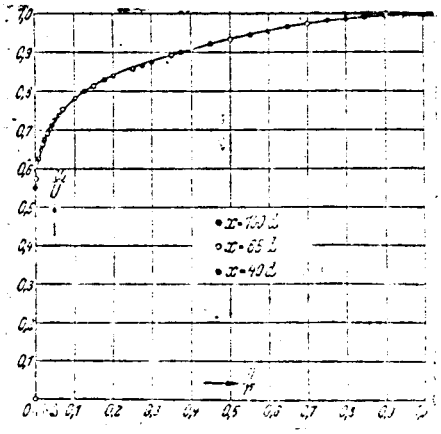


Fig. 12. Velocity distributions with x = 100 d, x = 65 d and x = 40 d.

For the measurements of the velocity distribution pitot tubes were used, of 0.21 mm and 0.30 mm internal diameter and 30 mm length, which for hydrodynamic reasons was conical. The position of the pitot tube at the edge of the test pipe is shown in Fig. 13. In this position the indication of the pitot tube does not correspond to the dynamic pressure prevailing there. This is explained by the fact that only a part of the pitot tube opening lies in the water jet and the rest is outside it, so that the water that flowed in flows out again to the side. But because exact knowledge of the dynamic pressure also in the vicinity of the wall is important, a method was used that makes the correction of the velocity measurement in this area possible. For this purpose the velocity distribution was measured with three pitot tubes of different internal diameter, namely 0.3, 0.582 and 1.045 mm at the same Reynolds number. These measurements served to determine by extrapolation the velocity distribution that would have been measured with the pitot tube of diameter zero. In Fig. 13 the distance from the wall is plotted as abscissa and the velocity as ordinate. If a straight line is laid through points of equal velocity (parallel

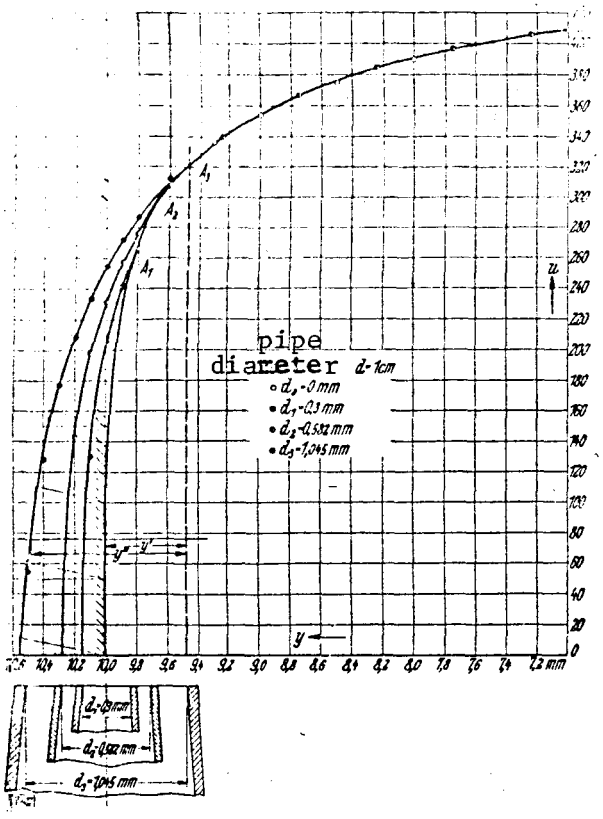


Fig. 13. Reduction of pitot tube opening to zero.

to the abscissa axis) and in the individual points the pertinent internal diameters of the pitot tubes are plotted as vertical distances, a curve can be laid through the terminal points of these distances, which through extrapolation produces a point of intersection with the straight line. This is a point of a new curve which would have been obtained with pitot tube of internal diameter zero. If the pitot tube opening lies entirely in the water jet, a correction is superfluous, as Fig. 13 shows.

For these positions the measured velocity curve coincides with the theoretical curve in point $A_i$ (i = 1, 2, 3). The distance of point $A_i$ from the wall is therefore equal to the internal radius $r_i$ (i = 1, 2, 3) of the opening in the pitot tube used for measuring. In order to determine the correction for any desired pitot tube opening a perpendicular to the abacissa axis (broken line in figure) is drawn through such a point $A_i$ and the distances Y' and Y" of this straight line are determined from two points on the theoretical and the measured curves that correspond to the same velocity.

In this way value couples are ascertained for various Reynolds numbers, which are reproduced in a dimensionless graph in Fig. 14. If we have measured a velocity distribution and want to convert this near the wall to the velocity distribution that would be obtained with the pitot tube opening zero, then this graph is used in the manner that the velocities that lie in the distance y" are displaced to the corresponding distance y'.

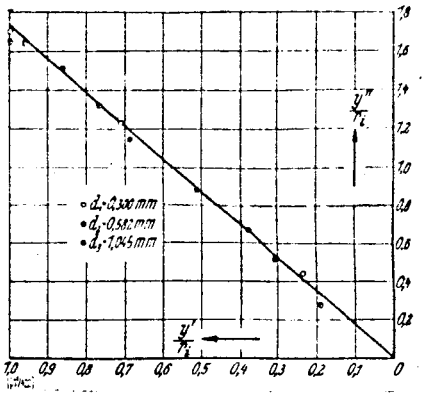

Fig. 14. $\frac{y'}{r_i}$ in relation to $\frac{y''}{r_i}$

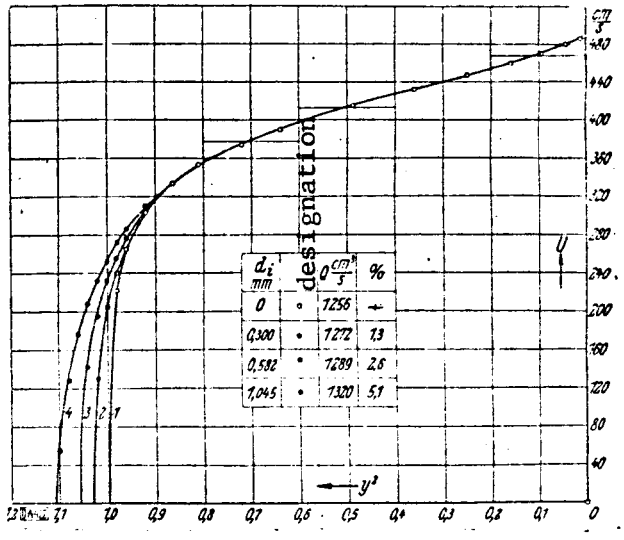


Fig. 15. $100\left(\frac{Q-Q_0}{Q}\right)=f(d_i)$

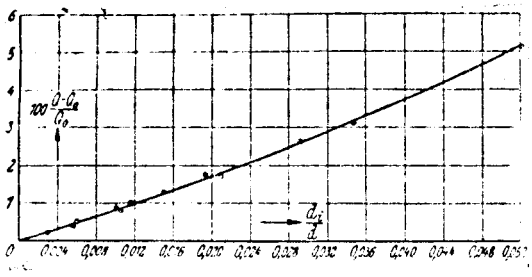

Fig. 16. $100\left(\frac{Q-Q_0}{Q}\right)=f\left(\frac{d_i}{d}\right)$

In order to determine the percentage error of the throughput that is obtained by integration of the uncorrected velocity distribution, the measured velocities that were obtained by measurement with various pitot tube openings were plotted in Fig. 15 as a function of the square of the distance from the pipe axis, and the throughput was calculated by graphic integration. The corrected velocity distribution is represented by curve 1 in this figure. Curves 2, 3, and 4 correspond to the velocity distribution determined with pitot tubes having openings d = 0.3 mm, 0.582 mm and 1.054 mm. /11

The numerical resume in Fig. 15 shows that the throughput of the corrected velocity distribution amounts to $Q_0$ = 1256 cc/sec. In addition it is observed that with increasing pitot tube opening the throughput that has been determined graphically increases in contrast to measured throughput (which agrees with the

graphically determined throughput of the corrected curve). The velocity distributions represented in Fig. 15 were measured in a pipe with diameter d = 2 cm. Similar tests were made in pipes with diameter d = 3 cm, d = 5 cm and d = 10 cm and the results represented in Fig. 16. Here the dimensionless pitot tube opening $\frac{d_i}{d}$ which is formed by dividing the diameter of the pitot tube tip by the tube diameter, is plotted as abscissa and the percentage error of the throughput $100\left(\frac{Q1 - Qo}{Qo}\right)$ is plotted as ordinate. This diagram makes it possible to state the occurring errors by a certain relationship $\frac{d_i}{d}$.

4. Execution of the Experiments

Carrying out the experiments with overflow was very simple, because the constancy of the throughput had been taken care of. If measurements of the velocity distribution were to be made, the throttle cone dk (Fig. 5) [i.e. 4] of the velocity measuring apparatus was set at a certain position corresponding to the desired throughput (the dependence of the throughput on the position of the throttle in the velocity measuring apparatus was known through preliminary experiments). Then so much water was let into the water tank through the feed pipe that only very little water flowed out through the overflow. When micromanometer I, which served for the pressure drop measurements, and micromanometer II, which served for the velocity measurements, had been checked as to the correctness of their indications, the pipe axis was determined by velocity measurements, which axis served as reference point for the actual measurements. Then the measurements were started, consisting in taking up measurements of pressure drop, temperature and throughput in addition to velocity measurements.

The experiments with water circulation were more difficult insofar as current fluctuations in the power network caused changes in the rpm of the drive motor and thereby changes in the throughput in the test pipe. It was therefore necessary to keep the pressure drop on a uniform level through precise adjustment of the throttle cone dk.

The execution of the measurements in the shock tests were made as follows: first the connection between water tank wk (Fig. 1) and compressed air tank dk was interrupted and the compressed air present in the water tank from the preceding experiment was permitted to escape through safety valve ksv of the water tank. While the air in the compressed air tank dk was brought to about 10 atm by means of a compressor for all experiments, the connection between rotary pump kp and water tank wk was established and the latter filled to a certain level with water. In the meantime the discharge cross section of the test pipe was sealed with oiled paper, which was between the flange of the test pipe and a ring flange fitting the pipe cross section, and now the feed pipe zr and the test pipe vr were filled with water by means of a diversion at the quick closing valve sh. The air that was present in the feed pipe could escape through the opened relief valve sv. Now the connection between the compressed air tank dk and the water tank wk was reestablished through Arca regulator, which had been set in advance for a certain pressure. With that the preparations were completed and the actual experiment could begin. On a signal from

the manometer observer the quick closing valve sh was opened; the oiled paper was ruptured by the water pressure. After a state of equilibrium of the flow had set in, the observer would establish the limit of the manometer deflection by means of a runner which was easily movable on the leg of the manometer (Fig. 3). The quick closing valve remained open until the water level in the water tank had dropped to about 40-50 cm above the discharge cross section. Then the manometer was read. Now the preparation for the next experiment could be started.

## II. Evaluation of the experiment

### 1. Velocity distribution

Velocity distributions were measured in pipes with d = 1cm, 2 cm, 3 cm, 5 cm and 10 cm diameter at low Reynolds number Re = $4 \cdot 10^3$, to the highest Reynolds number investigated, namely Re = $3240 \cdot 10^3$. As will be seen from further evaluations of the velocity distribution, exact knowledge of it is important not only in the vicinity of the wall where a sharp drop in velocity exists, but also in the vicinity of the center of the pipe where there is a slight drop in velocity. On this account the measuring points near the wall and near the pipe center were especially close together (the velocity distribution over the pipe radius in general contains 18 measurement points). The velocity distribution was symmetrical and showed no difference, or only slight differences, for a specific distance from each side of the pipe axis. About 150 velocity profiles were measured, of which however only 16 were used for the complete evaluations. Because of the perfect symmetry of the velocity profile, only half of the profile was used for the evaluation. The numerical values of these 16 velocity distributions over the pipe radius are summarized in Table 2. In order to determine velocity distributions at the lowest possible Reynolds numbers, the intake of the 10 mm diameter pipe was centrally covered with a plate having a 6 mm diameter opening. The plate caused strong turbulence in the intake, /12 so that at the Reynolds number Re = $4 \cdot 10^3$ the turbulent flow was fully established. Measurements with this arrangement were made for only the three lowest Reynolds numbers.

In order to follow the change of form of the velocity distribution as a function of the Reynolds number, velocity distributions were made dimensionless, in that the velocity distributions in question were referred to maximum velocities and corresponding wall distances on the pipe radius. Thus there was obtained equation

$$\frac{u}{U} = f\left(\frac{\eta}{r}\right), \qquad (6)$$

which is represented in Fig. 17 for six profiles, at Reynolds numbers Re = $4 \cdot 10^3$ to $3240 \cdot 10^3$. This representation shows very clearly that with increasing Reynolds number the configuration of the velocity distribution is more and more /13 full. This fact leads to the assumption that at infinitely high Reynolds number the layer affected by friction becomes infinitesimally small. In Fig. 18 the velocity distributions are shown in such a way that $\frac{u}{U}$ is ordinate, $\log\left(\frac{\bar{u}d}{\nu}\right)$ is abscissa and y/r is parameter of the dimensionless wall distance. The

Table 2. u as a function of y /12

| | | | | | | | | | | | |
|---|---|---|---|---|---|---|---|---|---|---|---|
| $d_p$ dyn / $d_x$ cm³ | 0,0395 | 0,1210 | 0,245 | 0,723 | 1,255 | — | 0,365 | — | 0,495 | — | 0,247 |
| $\bar{u}$ cm/s | 54,5 | 81,8 | 123,5 | 225,5 | 3[illegible] | — | 258,2 | — | 400 | — | [illegible] |
| $\nu$ cm²/s | 0,0135 | 0,0135 | 0,0135 | 0,0135 | 0,0[illegible]5 | | 0,0119 | — | 0,0114 | — | 0,0086 |
| $10^{-3}$ *Re* | 4,0 | 6,1 | 9,2 | 16,7 | 23,3 | — | 43,4 | — | 105 | — | 205 |
| *y* cm | *u* cm/s | *u* cm/s | *u* cm/s | *u* cm/s | *u* cm/s | *y* cm | *u* cm/s | *y* cm | *u* cm/s | *y* cm | *u* cm/s |
| 0 | 20,2 | 35,0 | 47,0 | 112,0 | 1[illegible]9 | 0,00 | 102,0 | 0,00 | 204,0 | 0,00 | 1[illegible]8,0 |
| [illegible] | 28,0 | 46,0 | 72,0 | 140,0 | 17[illegible]0 | 0,01 | 155,0 | 0,015 | 258,0 | 0,025 | 258,0 |
| [illegible] | 35,0 | 53,0 | 81,5 | 163,0 | 214,0 | 0,02 | 183,0 | 0,030 | 280,0 | 0,050 | 284,0 |
| [illegible] | 39,8 | 60,2 | 92,0 | 179,0 | 242,0 | 0,04 | 203,0 | 0,060 | 313,0 | 0,100 | 312,0 |
| [illegible]35 | 44,4 | 67,2 | 102,0 | 193,0 | 263,0 | 0,07 | 220,0 | 0,105 | 339,0 | 0,175 | 335,0 |
| [illegible],050 | 47,0 | 71,2 | 108,0 | 202,5 | 277,0 | 0,10 | 230,0 | 0,150 | 356,0 | 0,250 | 352,0 |
| [illegible],075 | 50,2 | 76,1 | 116,0 | 214,5 | 294,0 | 0,15 | 242,5 | 0,225 | 375,0 | 0,375 | 371,0 |
| 0,10 | 52,7 | 79,7 | 121,0 | 223,0 | 306,0 | 0,20 | 252,0 | 0,30 | 390,0 | 0,500 | 387,0 |
| 0,15 | 56,6 | 85,2 | 128,5 | 236,5 | 326,0 | 0,30 | 267,0 | 0,45 | 415,0 | 0,750 | 407,0 |
| 0,20 | 59,5 | 89,2 | 134,5 | 247,0 | 341,0 | 0,40 | 278,5 | 0,60 | 433,0 | 1,00 | 422,0 |
| 0,25 | 61,7 | 92,5 | 139,0 | 255,0 | 353,0 | 0,50 | 287,0 | 0,75 | 446,0 | 1,25 | 434,0 |
| 0,30 | 63,5 | 95,0 | 142,5 | 261,5 | 362,0 | 0,60 | 294,5 | 0,90 | 458,0 | 1,50 | 444,0 |
| 0,35 | 65,0 | 97,3 | 146,0 | 267,0 | 370,0 | 0,70 | 300,0 | 1,05 | 466,0 | 1,75 | 453,0 |
| 0,40 | 66,4 | 99,2 | 148,5 | 271,6 | 376,0 | 0,80 | 304,5 | 1,20 | 473,0 | 2,00 | 459,0 |
| 0,45 | 67,4 | 100,7 | 151,0 | 275,5 | 381,0 | 0,90 | 308,7 | 1,35 | 479,0 | 2,25 | 464,5 |
| 0,48 | 67,9 | 101,4 | 152,0 | 277,2 | 382,7 | 0,96 | 309,6 | 1,44 | 481,0 | 2,40 | 467,0 |
| 0,49 | 68,0 | 101,7 | 152,3 | 277,5 | 383,1 | 0,98 | 310,0 | 1,47 | 481,5 | 2,45 | 467,5 |
| 0,50 | 68,1 | 101,8 | 152,5 | 278,0 | 383,5 | 1,00 | 310,5 | 1,50 | 482,0 | 2,50 | 468,0 |
| $d_p$ dyn / $d_x$ cm³ | 0,755 | — | 0,48 | 0,91 | 1,59 | 2,45 | 1,90 | 2,262 | 2,82 | | |
| $\bar{u}$ cm/s | 732 | — | 875 | 1245 | 1690 | 2150 | 1928 | 2145 | 2430 | | |
| $\nu$ cm²/s | 0,00925 | — | 0,0121 | 0,01125 | 0,011 | 0,011 | 0,0082 | 0,0077 | 0,0075 | | |
| $10^{-3}$ *Re* | 396 | — | 725 | 1110 | 1536 | 1959 | 2350 | 2790 | 3240 | | |
| *y* cm | *u* cm/s | *y* cm | *u* cm/s | *u* cm/s | *u* cm/s | *u* cm/s | *u* cm/s | *u* cm/s | *u* cm/s | | |
| 0,00 | 360 | 0,000 | 505 | 705 | 9[illegible]0 | 1310 | 1310 | 1423 | 1510 | | |
| 0,025 | 490 | 0,05 | 617 | 847 | 1160 | 1598 | 1426 | 1578 | 1794 | | |
| 0,05 | 546 | 0,10 | 654 | 918 | 1260 | 1685 | 1496 | 1666 | 1890 | | |
| 0,10 | 597 | 0,20 | 717 | 1026 | 1380 | 1805 | 1604 | 1758 | 2026 | | |
| 0,175 | 632 | 0,35 | 765 | 1084 | 1480 | 1896 | 1700 | 1890 | 2142 | | |
| 0,250 | 660 | 0,50 | 794 | 1133 | 1539 | 1966 | 1772 | 1967 | 2230 | | |
| 0,375 | 690 | 0,75 | 833 | 1190 | 1613 | 2050 | 1845 | 2060 | 2326 | | |
| 0,500 | 714 | 1,00 | 859 | 1229 | 1668 | 2110 | 1900 | 2122 | 2396 | | |
| 0,75 | 751 | 1,5 | 899 | 1284 | 1744 | 2204 | 1980 | 2212 | 2492 | | |
| 1,00 | 778 | 2,0 | 929 | 1325 | 1799 | 2270 | 2040 | 2272 | 2566 | | |
| 1,25 | 799 | 2,5 | 954 | 1359 | 1840 | 2325 | 2088 | 2322 | 2622 | | |
| 1,50 | 816 | 3,0 | 973 | 1386 | 1876 | 2370 | 2128 | 2362 | 2670 | | |
| 1,75 | 831 | 3,5 | 988 | 1407 | 1902 | 2410 | 2156 | 2392 | 2706 | | |
| 2,00 | 842 | 4,00 | 1000 | 1424 | 1925 | 2437 | 2181 | 2418 | 2736 | | |
| 2,25 | 851 | 4,5 | 1010 | 1436 | 1940 | 2456 | 2198 | 2436 | 2755 | | |
| 2,40 | 854 | 4,8 | 1014 | 1441 | 1946 | 2463 | 2202 | 2445 | 2762 | | |
| 2,45 | 855 | 4,9 | 1015 | 1442 | 1948 | 2465 | 2203 | 2448 | 2764 | | |
| 2,50 | 856 | 5,0 | 1015,5 | 1443 | 1948 | 2466 | 2204 | 2449 | 2766 | | |

u = actual velocity

y = distance from the wall

Re = Reynolds number

$\bar{u}$ = average velocity

d = pipe diameter

v = kinematic viscosity

velocities $\frac{u}{U}$ referring to a specific wall distance y/r are interconnected by a curve on which the pertinent y/r value is written. This diagram shows that for the velocities in the vicinity of the wall there is a notable scatter. If it is desired to have a dimensionless velocity within the measured range, then above the corresponding Raynolds number on the curve the value for $\frac{u}{U}$ as a function of y/r is read off and the desired velocity distribution is obtained. To test, to what extent our velocity distributions correspond with those measured by other investigators, the following comparison was made.

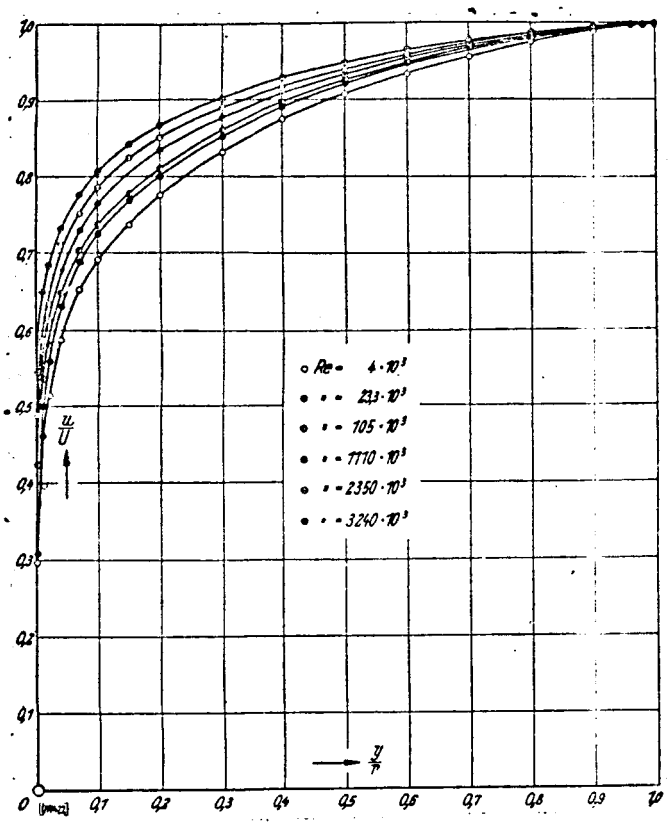


Fig. 17. $\frac{u}{U}$ as a function of y/r. /13

The most reliable measurement of velocity distribution in a circular pipe made so far was by T. E. Stanton (ref. 16) because first he undertook the measurements with a very fine 0.33 mm diameter pitot tube and secondly because he had a starting zone of adequate length x = 72 d (x = pipe length, d = pipe diameter = 7.4 cm), so that the measurements were in the range in which

distribution of velocity is no longer altered. A comparison of our measurements with those of Stanton seemed so much the more necessary, because Stanton measured the velocity distributions in the experimental pipe just ahead of the outlet end (2 to 3 d) while our average measurement was 0.1 to 0.2 mm behind the outlet end. For this reason the velocity distributions which refer approximately to the same Reynolds numbers were applied in such a way that the relationship of local velocities u to maximum velocity U were taken as a function of the dimensionless wall distance y/r (y = distance from the wall, r = pipe radius). The Stanton measurements were made at Reynolds numbers $37.6 \cdot 10^3$, $56.10^3$ and $89.3 \cdot 10^3$. Our measurements at approximately the same Reynolds numbers were in good agreement with Stanton's velocity distribution. Fig. 19 shows the comparison of Stanton's velocity distribution ($Re = 56 \cdot 10^3$) with ours $Re = 59 \cdot 10^3$). In addition there is also to be noted that data concerning average velocity u and kinematic viscosity v are lacking in Stanton's figures. On this account we have determined the average velocity u = 1235 cm/2 from the throughput quantity which is determined by integration of the velocity distribution. Since Stanton's measurements were made with air, in which the variation in kinematic viscosity with temperature is very slight, we have assumed he kinematic viscosity at an average laboratory temperature of 18° C.

For very high Reynolds numbers it appeared advisable to us to make a comparison with the velocity distributions of Bazin (ref. 17). The starting zone

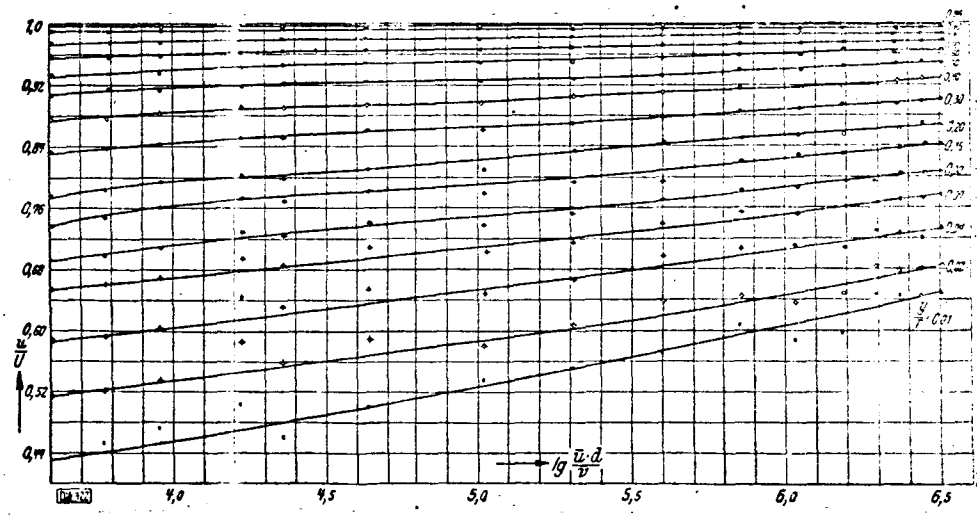


Fig. 18. $\frac{u}{U}$ as a function of $\log\left(\frac{\bar{u}.d}{\nu}\right)$

amounted to about x = 75 d (d = 80 cm). Data on temperature and average velocity are absent from Bazin's figures also. For this reason we determined the average velocity u = 164.9 cm/sec by integration of the velocity distribution. Bazin's measurements were done with water in the outside air, with temperature deviations of 10° to 20°. In this temperature range the kinematic viscosity is /14

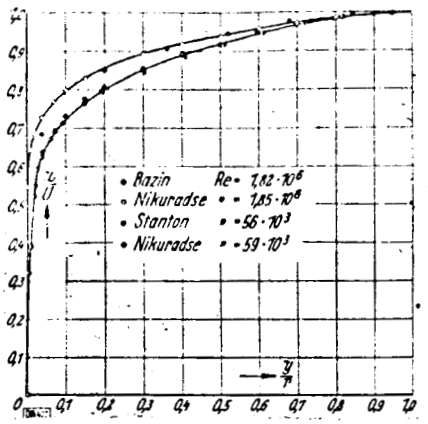


Fig. 19. Comparison of velocity distributions of Stanton, Bazin and Nikuradse.

very pronouncedly dependent upon the temperature, and on the other hand the change of velocity distribution with the Reynolds number at such high Re as those involved here is very slight. For these reasons we set the kinematic viscosity at 15° C (v = 0.0113 cm /sec).

The comparison of the velocity distribution of Bazin with ours is also shown in Fig. 19. Aside from the last points measured by Bazin, in the vicinity of the wall, there is good agreement of velocity distributions at approximately the same Reynolds numbers.

2) Expotential Law

Prandtl (ref. 18) determined from the Blasius law of resistance that velocity u of a turbulent flow in the vicinity of the wall changes by the exponent 1/7 the distance from the wall i.e.

$$u = a\,y^{1/7}, \qquad (7)$$

wherein a is a constant for one and the same velocity profile. The calculation can be developed as follows. In the equation for the drag coefficient:

$$\lambda = \frac{dp}{dx}\cdot\frac{2d}{\rho\,\bar{u}^2} \qquad (8)$$

$\frac{dp}{dx}$ instead of pressure drop there is introduced the shear stress at the wall $\tau_0$. The condition of equilibrium for a fluid cylinder with radius r and length dx yields

$$\frac{dp}{dx} = \frac{2\tau_0}{r} \qquad (9)$$

and therefore

$$\lambda = \frac{2\tau_0}{r}\cdot\frac{2d}{\rho\,\bar{u}^2}. \qquad (8a)$$

From this it follows that $\frac{\tau_0}{\rho} = \frac{\lambda\,\bar{u}^2}{8}$. If for drag coefficient $\lambda$ the Blasius value is introduced, we obtain

$$\lambda_B = 0{,}316\ Re^{-1/4}$$

$$\frac{\tau_0}{\rho} = \text{no.}\cdot\bar{u}^2\left(\frac{\bar{u}\cdot 2r}{\nu}\right)^{-1/4} \qquad (10)$$

or

$$\frac{\tau_0}{\rho} = \text{no.}\ \bar{u}^{7/4}\,r^{-1/4}\,\nu^{1/4}. \qquad (10a)$$

The solution of this equation for u produces

$$\left(\frac{\tau_0}{\rho}\right)^{4/7}\left(\frac{r}{\nu}\right)^{1/7} \qquad (11)$$

According to the Prandtl hypothesis, neither the pipe radius nor the velocity in the middle is in immediate relationship to the wall friction, but both are determined primarily by the velocity distribution in the vicinity of the wall.

If the ratio $\frac{u}{U}$ of the average velocity at the maximum is assumed as constant, then from equation (11) also

$$u = \text{number} \left(\frac{\tau_0}{\varrho}\right)^{6/7} \left(\frac{r}{\nu}\right)^{1/7}. \qquad (12)$$

This can be rewritten in as required if y is substituted for r and correspondingly the velocity u associated with y is substituted for U

$$u = \text{number} \left(\frac{\tau_0}{\varrho}\right)^{6/7} \left(\frac{y}{\nu}\right)^{1/7}. \qquad (13)$$

Since the velocity distribution is measured at a fixed value of $\frac{\tau_0}{\varrho}$ and $\nu = \frac{\mu}{\varrho}$ g there is obtained from equation (13)

$$\text{or} \quad \begin{aligned} u &= \text{const}\, y^{1/7} \\ u &= a y^{1/7}. \end{aligned} \qquad (14)$$

As is readily verified, in the velocity distribution as in (13), equation (11) is also satisfied, i.e. the Blasius law. This law of resistance

$$\lambda_B = \frac{0{,}316}{\sqrt[4]{Re}},$$

according to which therefore the drag coefficient is inversely proportional to the 4th root of the Reynolds number, is valid up to Re = $100 \cdot 10^3$. Since in the development of the 1/7 exponential law, the Blasius law was made the basis, it is not to be anticipated that this exponential law will also be valid for higher Reynolds numbers. In the range of validity of the Blasius law of resistance the gradient of the logarithmic $\lambda$curve = . For higher Reynolds numbers this gradient is less steep and in the range investigated by us it is almost 1/6. If for example $\lambda$ is made proportional to $Re^{-}$ , the calculation method as above yields U = ay 1/9. This signifies that the exponent n = 1/7 diminishes to 1/8, 1/9 etc. at increasingly high Reynolds numbers. At Re = $3240 \cdot 10^3$ the exponent is approximately n = 1/10. The change of the exponents with increasing Reynolds number is constantly diminishing. Naturally such a law of exponentials with changeable exponents is to be regarded only as a formula of approximation. In the Blasius range also it appears that the 1/7 law is only an approximation as calculations show. If the exponential law is written in the form

$$u = a y^n \qquad (15)$$

and the log of the measured velocity is dependent upon the log of the wall distance, the n values are obtained from the gradient of the curve. In Fig. 20 the exponent 1/n of the velocity as a function of wall distance is plotted for various Reynolds numbers. It is to be observed that in the range of the lowest Reynolds numbers the exponent has the value 1/n = 6 at about Re = $4 \cdot 10^3$. From about Re = $10 \cdot 10^3$ to $100 \cdot 10^3$ where the Blasius formula is valid, we have /15

1/n = 7 and at Re $3240 \cdot 10^3$ the exponent increases to 1/n = 10.

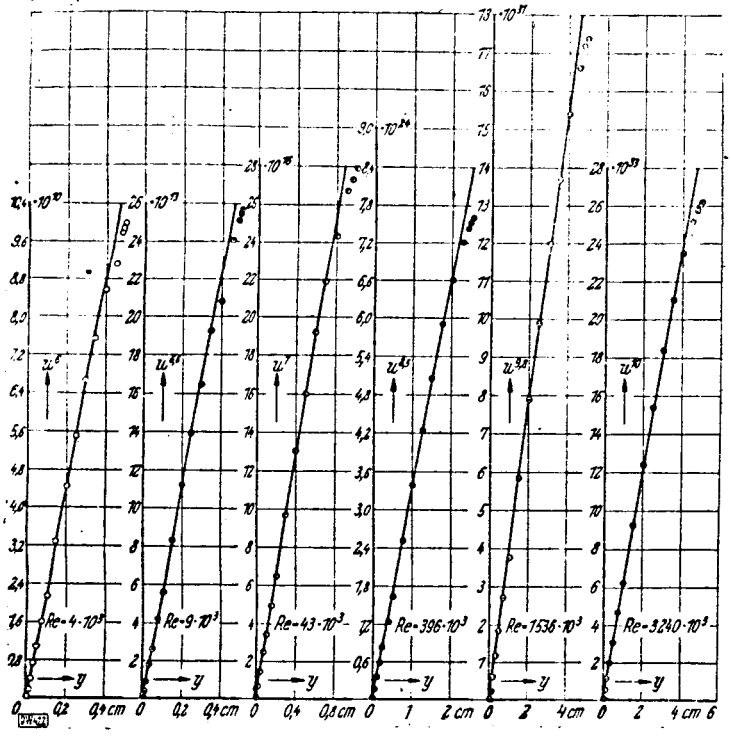


Fig. 20. 1/n exponent of velocity as a function of wall distance.

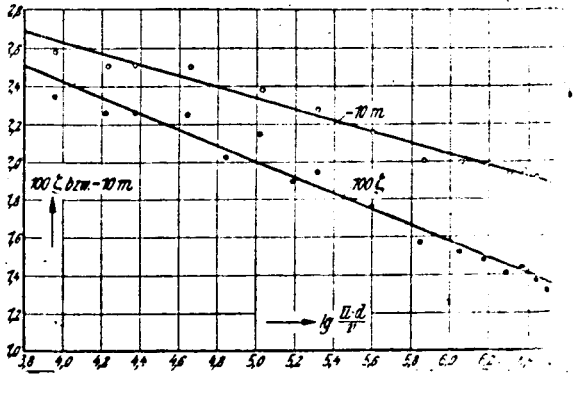


Fig. 21. 100 ζ or 10 m as a function of $\log \left(\frac{U \cdot d}{\nu}\right)$

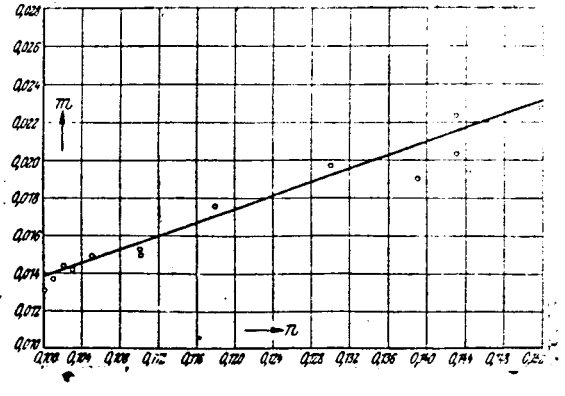


Fig. 22. m as a function of n

If the assumption is made that between the sheer stress $\tau_0$ at the wall, distance from the wall y and velocity u an unequivocal relationship exists, then in equation (9) we obtain

$$\frac{\tau_0}{\rho u^2} = f\left(\frac{u \cdot y}{\nu}\right). \qquad (16)$$

The magnitude $\frac{u \cdot y}{\nu}$ is a kind of Reynolds number which is related to the wall distance y. If the velocity distribution is expressed in the form of the Prandtl law of exponentials, we obtain

$$\frac{\tau_0}{\rho u^2} = \zeta\left(\frac{u \cdot y}{\nu}\right)^m, \qquad (17)$$

where $\zeta$ is a dimensionless number that can be determined from the measured velocity distribution in connection with the related wall shear stress. Then $m = \frac{2n}{1+n}$. If we take the log of equation (17)

$$\lg\left(\frac{\tau_0}{\rho u^2}\right) = \lg \zeta + m \lg\left(\frac{u \cdot y}{\nu}\right). \qquad (18)$$

If the magnitude $\log \left(\frac{\tau_0}{\rho u^2}\right)$ is determined from the measured velocity distribution and plotted as a function of $\log \left(\frac{u \cdot y}{\nu}\right)$, then the dimensionless constant $\zeta$ can be read from the ordinate at $\log \left(\frac{u \cdot d}{\nu \cdot n}\right) = 0$, so long as the obtained points are connected by a straight line.
The constant m which occurs as exponent of the dimensionless wall distance (equation 15) and corresponds to the exponent in the Blasius resistance law can be determined from our experiments. By solution of equation (18) for m we obtain

$$m = \frac{\lg\left(\frac{\tau_0}{\rho u^2}\right) - \lg \zeta}{\lg\left(\frac{u \cdot y}{\nu}\right)}. \qquad (19)$$

the constant $\zeta$ obtained in the experiments and exponent m are plotted in Fig. 21 as a function of $\log \left(\frac{u \cdot d}{\nu}\right)$. In Fig. 22 m is plotted as a function of exponent n.

3. Universal velocity distribution

In a new statement of his ides, Prandtl lays down no exponential law at all, but assumes only that the velocity in the vicinity of the wall is dependent only upon the physical magnitudes that are valid near the wall ($\tau_0$ = shear stress at the wall, $\mu$ = viscosity constant and $\rho$ = density) while it is independent of the distance of the opposite wall and of the average or maximum velocity. We now establish a magnitude characterizing friction according to Prandtl (ref. 19) from the shear stress $\tau_0$ at the wall and density : this friction state characterizing magnitude has the dimension of the velocity

$v_* = \sqrt{\frac{\tau_0}{\rho}}$. With this magnitude the "dimensionless velocity " can be established, in that the velocity u is divided by $v_*$: $\varphi = \frac{v}{v_*}$. /16

Similarly from the distance y from the wall, velocity $v_*$ and kinematic (viscosity $\nu = \frac{\mu}{\rho}$ in the manner of the Reynolds number we establish a "dimensionless wall distance" $\eta = \frac{v_* y}{\nu}$. Thus in the vicinity of the wall we obtain a universal velocity distribution $\varphi = \varphi(\eta)$ (ref. 20). This dependency is illustrated in Table 3, (Fig. 23).

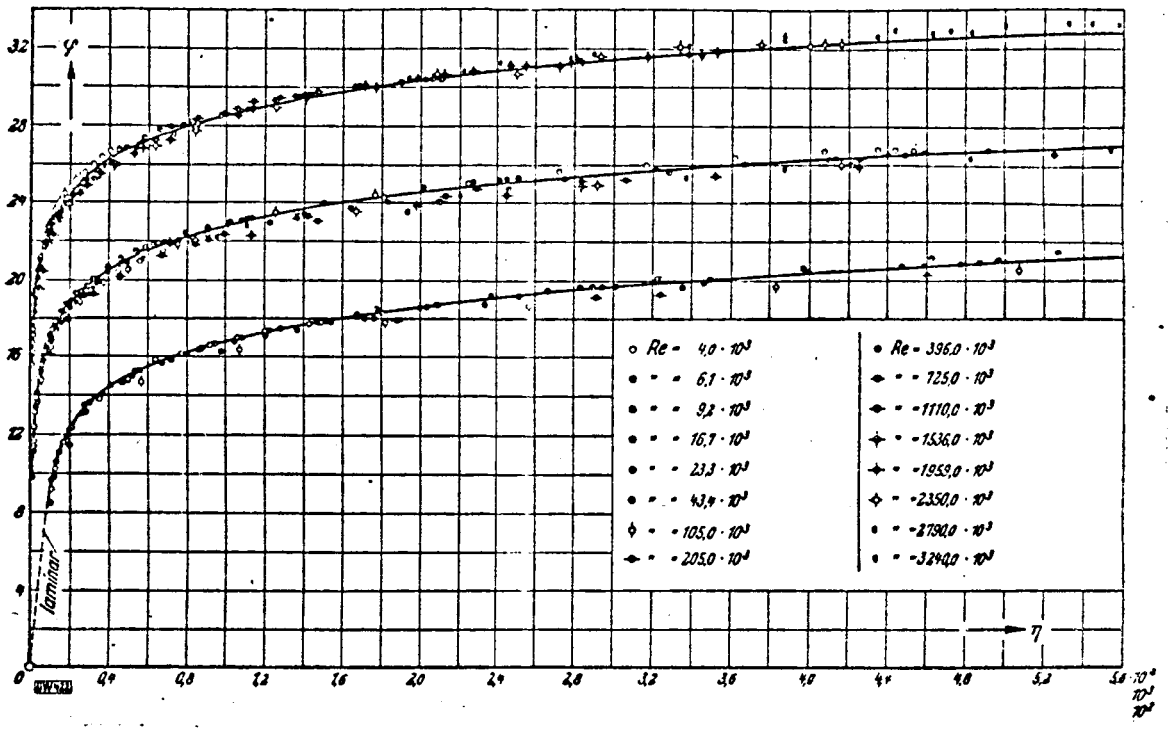


Fig. 23. Universal Velocity Distribution ( = [n])

In this figure dimensionless velocities are presented for a series of Reynolds numbers from the lowest $4 \cdot 10^3$ to the highest $3240 \cdot 10^3$. Because of the large abscissa range $\eta = \frac{v_* y}{\nu}$ three different scales are used. The points drawn in are measurement data.

The universal velocity distribution is still more clearly evident if instead of $\eta$ the magnitude $\log \eta$ is used as abscissa, as in Fig. 24. It is clear there that the experimental points lie within certain limits of scatter on a straight line. With closer scrutiny, we see that experimental points belonging to a specific Reynolds number do not lie exactly on a straight line but rather that they present a systematic trend upward from below. It should be noted in this connection that the experimental points extend to the middle of the pipe while according to the Prandtl hypotehsis only the points adjacent to the wall should lie on a continuous curve. This latter condition is met rather well. For $\log \eta < 1.0$ there is a determinable systematic deviation from the straight line. From Fig. 24 if we specially consider the points near the pipe axis, we

Table 3 /16

| $\eta$ | $\varphi$ | $\eta$ | $\varphi$ | $\eta$ | $\varphi$ | $\eta$ | $\varphi$ | $\eta$ | $\varphi$ | $\eta$ | $\varphi$ | $\eta$ | $\varphi$ | $\eta$ | $\varphi$ |
|---|---|---|---|---|---|---|---|---|---|---|---|---|---|---|---|
| $Re = 4 \cdot 10^3$ | | $Re = 6{,}1 \cdot 10^3$ | | $Re = 9{,}2 \cdot 10^3$ | | $Re = 16{,}7 \cdot 10^3$ | | $Re = 23{,}3 \cdot 10^3$ | | $Re = 43{,}4 \cdot 10^3$ | | $Re = 105 \cdot 10^3$ | | $Re = 205 \cdot 10^3$ | |
| 10 | 9,16 | 11 | 9,75 | 13 | 10,50 | 17 | 12,28 | 20 | 12,20 | 30 | 13,6 | 57 | 14,70 | 98 | 16,31 |
| 13 | 10,41 | 15 | 11,08 | 19 | 11,85 | 27 | 13,45 | 33 | 13,86 | 52 | 15,1 | 107 | 16,42 | 188 | 17,90 |
| 17 | 11,60 | 21 | 12,35 | 27 | 13,15 | 41 | 14,50 | 52 | 15,00 | 86 | 16,35 | 182 | 17,80 | 321 | 19,25 |
| 21 | 12,30 | 27 | 13,08 | 36 | 13,92 | 56 | 15,20 | 72 | 15,79 | 120 | 17,10 | 257 | 18,70 | 460 | 20,21 |
| 28 | 13,13 | 37 | 14,00 | 50 | 14,95 | 80 | 16,11 | 105 | 16,75 | 176 | 18,00 | 383 | 19,70 | 687 | 21,30 |
| 35 | 13,80 | 47 | 14,65 | 65 | 15,60 | 105 | 16,79 | 137 | 17,40 | 233 | 18,70 | 507 | 20,50 | 913 | 22,22 |
| 50 | 14,58 | 68 | 15,65 | 93 | 16,65 | 154 | 17,80 | 202 | 18,60 | 346 | 19,83 | 759 | 21,80 | 1367 | 23,40 |
| 64 | 15,58 | 87 | 16,40 | 122 | 17,32 | 203 | 18,56 | 267 | 19,41 | 459 | 20,72 | 1007 | 22,75 | 1817 | 24,23 |
| 78 | 16,15 | 108 | 17,00 | 151 | 17,90 | 252 | 19,18 | 332 | 20,10 | 572 | 21,32 | 1258 | 23,40 | 2267 | 24,96 |
| 92 | 16,61 | 128 | 17,47 | 180 | 18,35 | 301 | 19,68 | 397 | 20,60 | 685 | 21,90 | 1511 | 24,05 | 2727 | 25,50 |
| 106 | 17,00 | 148 | 17,88 | 208 | 18,70 | 349 | 20,09 | 462 | 21,10 | 798 | 22,30 | 1761 | 24,50 | 3177 | 26,00 |
| 120 | 17,38 | 168 | 18,21 | 237 | 19,12 | 399 | 20,40 | 527 | 21,40 | 911 | 22,62 | 2007 | 24,80 | 3627 | 26,10 |
| 134 | 17,62 | 188 | 18,49 | 266 | 19,45 | 447 | 20,70 | 592 | 21,70 | 1024 | 22,95 | 2267 | 25,15 | 4082 | 26,61 |
| 143 | 17,77 | 201 | 18,56 | 283 | 19,60 | 477 | 20,82 | 631 | 21,80 | 1092 | 23,00 | 2412 | 25,30 | 4357 | 26,80 |
| 146 | 17,79 | 205 | 18,66 | 289 | 19,63 | 487 | 20,85 | 643 | 21,81 | 1116 | 23,03 | 2467 | 25,33 | 4447 | 26,85 |
| 149 | 17,80 | 209 | 18,70 | 294 | 19,65 | 497 | 21,00 | 657 | 21,83 | 1137 | 23,10 | 2511 | 25,36 | 4537 | 26,90 |

$\varphi = \frac{u}{v_*}$ = dimensionless velocity; u = actual velocity; $v_* = \sqrt{\frac{\tau_o}{\varrho}}$ shear stress velocity; $n = \frac{v_* y}{\nu}$ = dimensionless wall distance; y = distance from the wall; $\varrho$ = density; Re = Reynolds number, $\tau_o$ = sheer stress.

/17

| $\eta$ | $\varphi$ | $\eta$ | $\varphi$ | $\eta$ | $\varphi$ | $\eta$ | $\varphi$ | $\eta$ | $\varphi$ | $\eta$ | $\varphi$ | $\eta$ | $\varphi$ | $\eta$ | $\varphi$ |
|---|---|---|---|---|---|---|---|---|---|---|---|---|---|---|---|
| $Re = 396 \cdot 10^3$ | | $Re = 725 \cdot 10^3$ | | $Re = 1110 \cdot 10^3$ | | $Re = 1536 \cdot 10^3$ | | $Re = 1959 \cdot 10^3$ | | $Re = 2350 \cdot 10^3$ | | $Re = 2790 \cdot 10^3$ | | $Re = 3240 \cdot 10^3$ | |
| 171 | 17,98 | 299 | 19,08 | 427 | 17,91 | 580 | 20,20 | 700 | 21,72 | 830 | 21,92 | 967 | 22,40 | 1 110 | 22,75 |
| 335 | 19,65 | 573 | 20,92 | 847 | 19,45 | 1 140 | 22,10 | 1 410 | 23,27 | 1 670 | 23,50 | 1 934 | 23,60 | 2 220 | 24,40 |
| 581 | 20,80 | 997 | 22,32 | 1 477 | 21,70 | 1 980 | 23,70 | 2 460 | 24,45 | 2 920 | 24,90 | 3 380 | 25,40 | 3 880 | 25,80 |
| 827 | 21,70 | 1426 | 23,16 | 2 107 | 24,00 | 2 830 | 24,80 | 3 520 | 25,35 | 4 160 | 26,00 | 4 835 | 26,38 | 5 550 | 26,82 |
| 1237 | 22,70 | 2129 | 24,30 | 3 160 | 25,20 | 4 250 | 25,85 | 5 270 | 26,45 | 6 250 | 27,00 | 7 250 | 27,70 | 8 330 | 28,00 |
| 1647 | 23,45 | 2842 | 25,06 | 4 210 | 26,00 | 5 660 | 26,70 | 7 040 | 27,22 | 8 340 | 27,80 | 9 670 | 28,50 | 11 100 | 28,82 |
| 2467 | 24,76 | 4257 | 26,23 | 6 310 | 27,20 | 8 500 | 27,95 | 10 540 | 28,42 | 12 510 | 29,00 | 14 500 | 29,65 | 16 650 | 30,00 |
| 3287 | 25,60 | 5667 | 27,10 | 8 410 | 28,05 | 11 300 | 28,80 | 14 080 | 29,28 | 16 680 | 29,90 | 19 340 | 30,50 | 22 200 | 30,90 |
| 4107 | 26,22 | 7087 | 27,92 | 10 510 | 28,75 | 14 150 | 29,50 | 17 580 | 30,00 | 20 850 | 30,60 | 24 200 | 31,20 | 27 740 | 31,60 |
| 4927 | 26,82 | 8507 | 28,35 | 12 600 | 29,35 | 17 000 | 30,07 | 21 120 | 30,60 | 25 020 | 31,20 | 29 000 | 31,74 | 33 300 | 32,17 |
| 5752 | 27,40 | 9907 | 28,53 | 14 700 | 29,80 | 19 800 | 30,50 | 24 620 | 31,10 | 29 190 | 31,60 | 33 800 | 32,10 | 38 800 | 32,58 |
| 6567 | 27,70 | 11327 | 29,17 | 16 800 | 30,20 | 20 600 | 30,84 | 28 160 | 31,40 | 33 360 | 32,00 | 38 680 | 32,40 | 44 400 | 32,90 |
| 7727 | 28,00 | 12757 | 29,46 | 18 910 | 30,40 | 25 500 | 31,10 | 31 620 | 31,60 | 37 530 | 32,20 | 43 500 | 32,70 | 50 000 | 33,10 |
| 7877 | 28,05 | 13610 | 29,58 | 20 210 | 30,53 | 27 200 | 31,18 | 33,750 | 31,79 | 40 000 | 32,28 | 46 420 | 32,80 | 53 300 | 33,21 |
| 8057 | 28,15 | 13910 | 29,59 | 20 610 | 30,57 | 27 800 | 31,20 | 34,450 | 31,80 | 40 900 | 32,30 | 47 400 | 32,86 | 54 400 | 33,24 |
| 8217 | 28,20 | 14200 | 29,60 | 21 000 | 30,60 | 28 300 | 31,21 | 35 200 | 31,82 | 41 700 | 32,31 | 48 400 | 32,90 | 55 500 | 33,30 |

obtain graphically the straight line (1) with equation

$$\varphi = 5{,}5 + 5{,}75 \lg \eta. \qquad (20)$$

Here we have calculated the n values for a series of $\varphi$ values and drawn the curve passing through the experimental points as in Fig. 23.

For further approximations it is advantageous however to lend preference to the points near the wall. The straight line (2) laid through these points is represented by the equation

$$\varphi = 5{,}84 + 5{,}52 \lg \eta \qquad (20a)$$

In laminar flow, if velocity u is dependent only upon y, we have for shear stress the equation

$$\tau_0 = \mu \left(\frac{du}{dy}\right)_0,$$

where $\left(\frac{du}{dy}\right)_0$ is the value of $\frac{du}{dy}$ near the wall and u is the viscosity constant or /18

$$du = \frac{\tau_0}{\mu} dy.$$

After integration of this equation we obtain

$$u = \frac{\tau_0}{\mu} y.$$

If we introduce $\tau_0 = \rho v_*^2$ and $\mu = \rho \nu$, we can immediately write

$$\frac{u}{v_*} = \frac{v_* y}{\nu}$$

or

$$\varphi = \eta.$$

According to an estimate this equation as a consequence of the introduction of the turbulent mixing process amounts to about $\eta = 10$. This laminar range is shown in Fig. 21 and is drawn in dashed lines in the lower curve. If equation (13) is divided by $v_* = \sqrt{\frac{\tau_0}{\rho}}$ and $\frac{u}{v_*}$ is divided by $\varphi$ and if $\eta$ is substituted for $\frac{v_* y}{\nu}$ and the number factor calculated, we obtain

$$\varphi = 8{,}74\, \eta^{1/7} \qquad (13a)'$$

The curve corresponding to this equation is shown in Fig. 24 in dashed lines. It is to be observed that the validity is limited to the range of log $\eta$ = 1.6 to 2.6.

Using this straight line law, it is possible to calculate the velocity distribution with very good approximation for any Reynolds number, if the physical magnitudes $\tau_0$, $\nu = \frac{\mu}{\rho}$ and pipe radius r are established. From the equation of the obtained straight lines, the appropriate $\varphi$ for different distances from the wall can be calculated and by multiplication by the velocity $v_*$ the velocity u can be determined, $u = \varphi v_*$. From the dimensionless distance $\eta$ the related distances from the wall $y = \frac{n\nu}{v^*}$ can be determined. We thus obtain the velocity distribution u = f(y) for a specific Reynolds number.

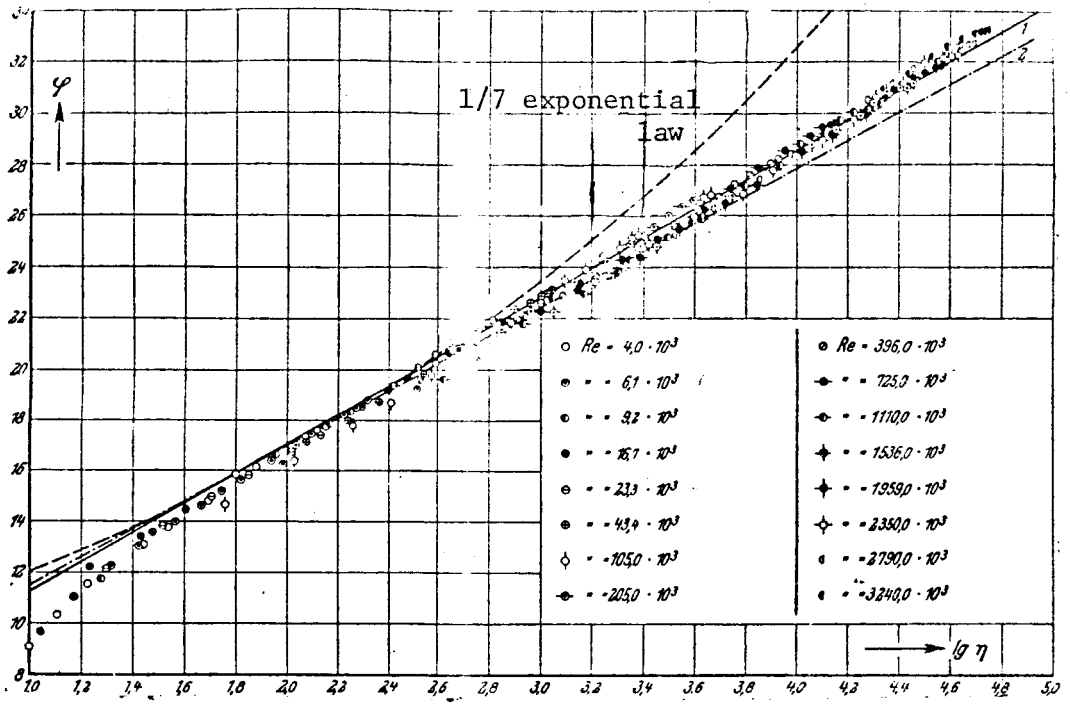


Fig. 24. $\varphi$ as a function of log n

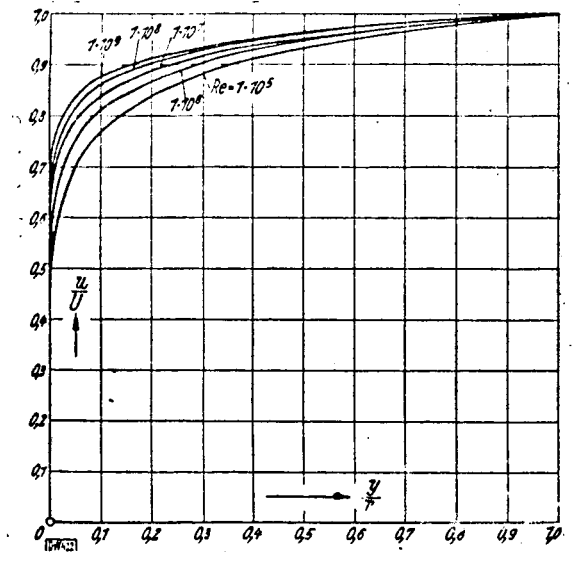


Fig. 25. Calculated velocity distributions for very high Reynolds numbers.

It naturally appears somewhat risky to calculate velocity in the middle of the pipe but the rule specifically intended for velocities in the vicinity of the wall. However, the differences in the central part of the pipe are not greater per se, and on the other hand, the results of Fig. 24 favor this method. Naturally the value in the middle is itself nonetheless inexact. The actual velocity distributions here present a perpendicular tangent, while the formula used here on the contrary has a finite though slight inclination. For the throughput volume this device is of very slight importance, however.

## 4. MIXING LENGTH AND EXCHANGE MAGNITUDE

In laminar flow, if the velocity u depends only upon y, for the shearing stress we have the equation

$$\tau = \mu \frac{du}{dy}, \tag{21}$$

where μ indicates the viscosity constant. Also, according to Boussinesq (ref. 21) in turbulent flow for the "apparent" shearing stress developed by the turbulent impulse exchange, we write

$$\tau' = A \frac{d\bar{u}}{dy}, \tag{22}$$

where $\bar{u}$ is the temporal mean value of velocity and A is the exchange magnitude which is the turbulent analog to the viscosity constant. The exchange magnitude is not constant, however; rather, it is different from place to place in the fluid. The essential now is to bring exchange magnitude A into correlation with the velocity distribution. For this we conceive of the velocity as decomposed, according to Reynolds, into a temporal mean value and deviations therefrom. We therefore write

$$u = \bar{u} + u', \qquad v = \bar{u} + v',$$

where u' and v' are the fluctuations of the x-component or of the y-component of the velocity. The fluctuations of velocity are the cause of an apparent state of stress that is described by the equations

$$\sigma_x = -\rho \overline{u'^2}; \quad \tau_{xy} = -\rho \overline{u'v'}; \quad \sigma_y = -\rho \overline{v'^2}. \tag{23}$$

It is now suggested that we describe the fluctuations of velocity u' and v' in terms of the "main flow" $\bar{u}$, $\bar{v}$. Prandtl succeeded in doing this by the following. We assume as above in Equations (21) and (22) for the sake of simplicity that the main flow runs parallel to the x-axis and that a drop in velocity prevails perpendicular to the direction of principal flow. A length ℓ is characteristic for the turbulent state of the flow, designated as mixing length by Prandtl. The physical significance of mixing length ℓ is that in turbulent flow small masses of fluid have an individual motion and are displaced consequently by a certain amount, exactly that of mixing length ℓ, transversely to the direction of flow before they mix with the new ambiency. If now a small mass of fluid originating at a locus with mean velocity $\bar{u}$ is displaced perpendicularly to the principal flow by length ℓ, its velocity is differentiated from the mean velocity of the new locus in first approximation by the

quantity $l \frac{d\bar{u}}{dy}$. It is therefore possible to introduce for the absolute value

of the fluctuation of the x-component of velocity: /19

$$|u'| = l\left|\frac{d\bar{u}}{dy}\right|. \qquad (24)$$

The fluctuations of the y-component of velocity v' occur because fluid masses that have a velocity of different magnitude in the x-direction collide and consequently are deflected laterally. For this reason it is possible to make v' proportional to u', thus

$$|v'| = l\left|\frac{d\bar{u}}{dy}\right|. \qquad (25)$$

Thereby for the shearing stress according to Equation (23), if the constant of proportionality is included in the still unknown $l$, we have the expression:

$$\tau = \varrho l^2 \left|\frac{d\bar{u}}{dy}\right| \cdot \frac{d\bar{u}}{dy}. \qquad (26)$$

Because one factor is with and the other without indication of quantity, it is provided that $\tau$ changes sign with $\frac{d\bar{u}}{dy}$. Comparison of the Prandtl formula for shearing stress with Equation (22) shows for the exchange magnitude the formula:

$$A = \varrho l^2 \left|\frac{d\bar{u}}{dy}\right|. \qquad (27)$$

This Prandtl formula which yields a penetrating analysis of turbulent flows, has already in many cases (ref. 22) led to a quite good calculation of turbulent flow. For flows in circular pipes satisfactory mathematical relationships can be found by means of it.

If Equation (22) is divided by the density, we obtain

$$\frac{\tau}{\varrho} = \frac{A}{\varrho} \cdot \frac{du}{dy}.$$

If we introduce $\frac{A}{\varrho} = \varepsilon$ here, where $\varepsilon$ is a kinematic measure for the turbulent impulse exchange, then

$$\frac{\tau}{\varrho} = \varepsilon \cdot \frac{du}{dy} \qquad (28)$$

$$\text{or} \quad \varepsilon = \frac{\tau}{\varrho} : \frac{du}{dy}.$$

The kinematic exchange magnitude $\varepsilon$ is therefore obtained by dividing the "kinematic shearing stress " $\frac{\tau}{\varrho}$ by the differential quotient of velocity $\frac{du}{dy}$. The magnitude of this differential quotient over the pipe radius was graphically determined from the measured velocity distributions. Since $\frac{du}{dy}$ and

$\frac{\tau}{\varrho} = \frac{r - y}{2\varrho} \frac{dp}{dx}$, (deduction as in Equation (9)) both tend toward zero in approaching the pipe axis and therefore the determination of the impulse

exchange magnitudes in this region is inexact. For this reason the measuring points for determination of velocity distribution in the pipe axis were placed closer together. In order to plot a velocity characteristic of the measured velocity values in such a way that they would yield a smooth characteristic of the $\frac{du}{dy}$ value, the differential quotients are formed at the measured points and connected by a smooth curve. Now backward from this curve the characteristic of velocity distribution is determined for small distances from the pipe center.

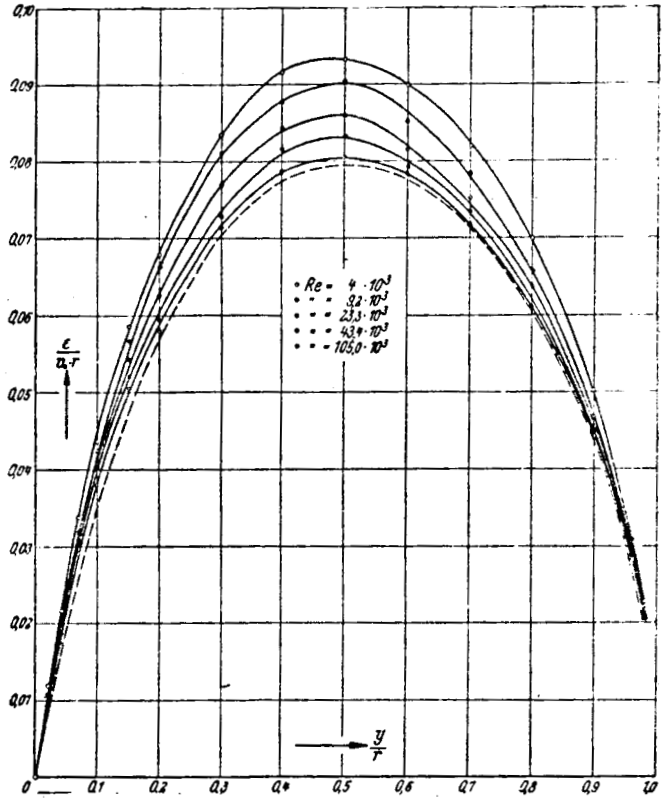


Fig. 26. $\frac{\varepsilon}{v_* r}$ as a function of y/r for low Reynolds numbers.

It was possible by this method to calculate the $\varepsilon$ values near the pipe axis more precisely. In this way the values in the measured range of Reynolds numbers (from $4 \cdot 10^3$ to $3240 \cdot 10^3$) were determined for the above described 16 velocity profiles which are shown in Table 4. In order to make the distribution of $\varepsilon$ values over the pipe radius comparable for all ranges of the Reynolds numbers, since $\varepsilon$ has the dimension of velocity x length, these values are divided by $v_* r$, where $v_* = \sqrt{\frac{\tau_0}{\varrho}}$ i.e., the dimension of a velocity. The actual distances from the wall are taken on the pipe radius. The relationship (29)

is shown in Figures 26 and 27. If we observe this dependency in Fig. 26, we see that the $\frac{\varepsilon}{v_* r}$ values decline with increasing Reynolds numbers to a constant value which in this figure is indicated by a broken-line curve. /21

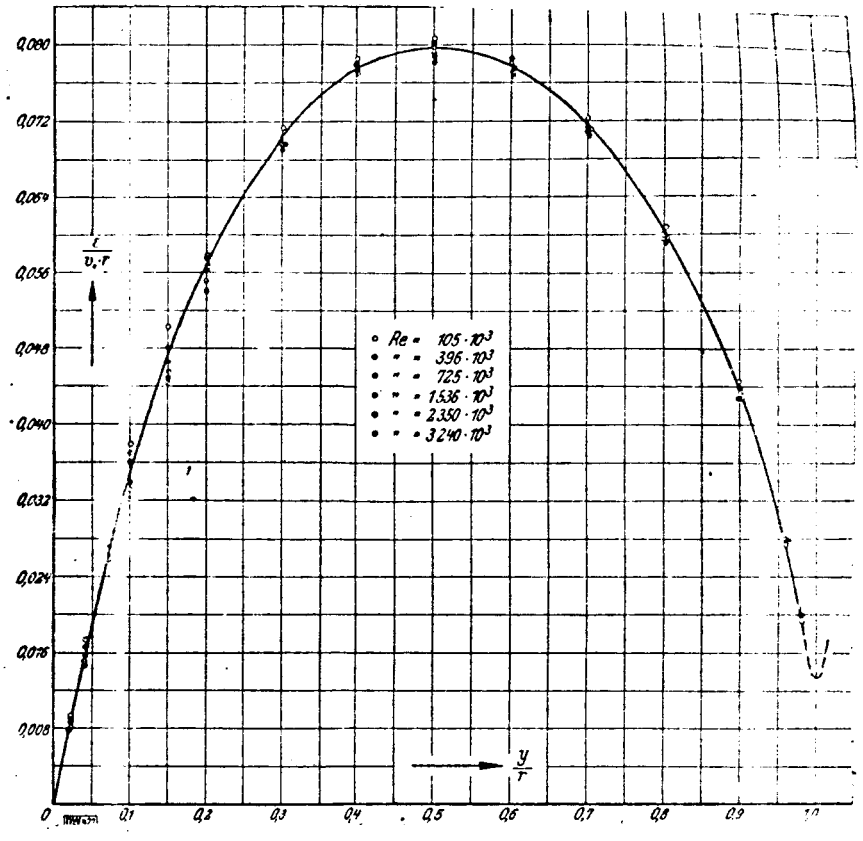


Fig. 27. $\frac{\varepsilon}{v*r}$ as a function of y/r for high Reynolds numbers.

In Fig. 27 the $\frac{\varepsilon}{v_* r}$ values are plotted for Reynolds numbers Re > $100 \cdot 10^3$. Within a certain range of scatter they yield a curve that is independent of the Reynolds number. This curve corresponds to the broken-line curve in Fig. 26. The broken line curve in Fig. 27, which represents the $\frac{\varepsilon}{v_* r}$ values near the pipe axis was determined by extrapolation. It is characteristic of the course of this value that the exchange magnitude at the wall is zero because here no exchange can take place; with increasing wall distance $\frac{\varepsilon}{v_* r}$ increases rapidly, linearly at first, and reaches a maximum at y = r/2. In approaching the pipe axis $\frac{\varepsilon}{v_* r}$ drops again to a very low value. In the increase in the vicinity of the wall a more pronounced scatter of $\frac{\varepsilon}{v_* r}$ values is observed

Table 4 $\frac{\varepsilon}{v_* \cdot r}$ as a function of $\frac{y}{r}$

| $\frac{y}{r}$ | $\frac{\tau}{\varrho}$ | $\frac{du}{dy}$ | $\frac{\varepsilon}{v_* \cdot r}$ | $\frac{\tau}{\varrho}$ | $\frac{du}{dy}$ | $\frac{\varepsilon}{v_* \cdot r}$ | $\frac{\tau}{\varrho}$ | $\frac{du}{dy}$ | $\frac{\varepsilon}{v_* \cdot r}$ | $\frac{\tau}{\varrho}$ | $\frac{du}{dy}$ | $\frac{\varepsilon}{v_* \cdot r}$ |
|---|---|---|---|---|---|---|---|---|---|---|---|---|
| | $Re = 4 \cdot 10^3$; $v_* = 3{,}82$ cm/s $r = 0{,}5$ cm | | | $Re = 6{,}1 \cdot 10^3$; $v_* = 5{,}44$ cm/s $r = 0{,}5$ cm | | | $Re = 9{,}2 \cdot 10^3$; $v_* = 7{,}76$ cm/s $r = 0{,}5$ cm | | | $Re = 16{,}7 \cdot 10^3$; $v_* = 13{,}3$ cm/s $r = 0{,}5$ cm | | |
| 0,02 | 14,30 | 631,0 | 0,0119 | 29,0 | 945,0 | 0,01135 | 59,0 | 1392 | 0,0108 | 173,7 | 2540 | 0,01025 |
| 0,04 | 14,00 | 340,0 | 0,0216 | 28,4 | 501,0 | 0,01042 | 57,8 | 738 | 0,0202 | 170,0 | 1322 | 0,01035 |
| 0,07 | 13,55 | 210,0 | 0,0338 | 27,5 | 318,0 | 0,0320 | 56,0 | 454 | 0,0318 | 164,6 | 782 | 0,01170 |
| 0,10 | 13,12 | 157,0 | 0,0437 | 26,0 | 231,0 | 0,0427 | 54,1 | 331 | 0,0422 | 159,2 | 583 | 0,0140 |
| 0,15 | 12,40 | 111,0 | 0,0585 | 25,2 | 163,0 | 0,0572 | 51,1 | 233 | 0,0565 | 150,4 | 405 | 0,0160 |
| 0,20 | 11,68 | 90,0 | 0,0680 | 23,6 | 129,0 | 0,0678 | 48,1 | 187 | 0,0662 | 141,5 | 330 | 0,0145 |
| 0,30 | 10,21 | 64,0 | 0,0835 | 20,7 | 93,0 | 0,0825 | 42,1 | 134 | 0,0812 | 124,0 | 232 | 0,0804 |
| 0,40 | 8,75 | 50,0 | 0,0916 | 17,75 | 73,0 | 0,0905 | 36,1 | 106 | 0,0878 | 106,2 | 184 | 0,0869 |
| 0,50 | 7,30 | 41,0 | 0,0933 | 14,80 | 59,0 | 0,0930 | 30,1 | 86 | 0,0904 | 88,5 | 152 | 0,0876 |
| 0,60 | 5,84 | 34,0 | 0,0900 | 11,82 | 50,0 | 0,0875 | 24,1 | 73 | 0,0852 | 70,8 | 129 | 0,0825 |
| 0,70 | 4,38 | 29,0 | 0,0820 | 8,88 | 41,0 | 0,0804 | 18,1 | 59 | 0,0788 | 53,1 | 104 | 0,0767 |
| 0,80 | 2,95 | 22,0 | 0,0700 | 5,92 | 32,0 | 0,0685 | 12,0 | 47,0 | 0,0659 | 35,4 | 83 | 0,0641 |
| 0,90 | 1,46 | 15,2 | 0,0502 | 2,96 | 22,0 | 0,0500 | 6,0 | 33 | 0,0469 | 17,7 | 58 | 0,0459 |
| 0,96 | 0,584 | 9,5 | 0,0322 | 1,183 | 13,8 | 0,0317 | 2,4 | 20 | 0,0310 | 7,08 | 35,5 | 0,0301 |
| 0,98 | 0,292 | 6,7 | 0,0228 | 0,592 | 9,8 | 0,0224 | 1,2 | 14 | 0,0221 | 3,54 | 25 | 0,0212 |
| | $Re = 23{,}3 \cdot 10^3$; $v_* = 17{,}55$ cm/s $r = 0{,}5$ cm | | | $Re = 43{,}4 \cdot 10^3$; $v_* = 13{,}44$ cm/s $r = 0{,}5$ cm | | | $Re = 105 \cdot 10^3$; $v_* = 19{,}05$ cm/s $r = 1{,}5$ cm | | | $Re = 205 \cdot 10^3$; $v_* = 17{,}4$ cm/s $r = 2{,}5$ cm | | |
| 0,02 | 302,0 | 3410 | 0,0101 | 177,0 | 1348 | 0,0098 | 356 | 1338 | 0,0093 | 297,0 | 755 | 0,0091 |
| 0,04 | 296,0 | 1760 | 0,0192 | 173,5 | 693 | 0,0186 | 350 | 698 | 0,0175 | 291,0 | 390 | 0,0172 |
| 0,07 | 286,0 | 1040 | 0,0313 | 168,0 | 411 | 0,0304 | 338 | 407 | 0,0290 | 282,0 | 232 | 0,0280 |
| 0,10 | 277,0 | 778 | 0,0406 | 162,6 | 302 | 0,0401 | 328 | 302 | 0,0380 | 273,0 | 170 | 0,0369 |
| 0,15 | 262,0 | 550 | 0,0542 | 153,6 | 229 | 0,0520 | 310 | 215 | 0,0504 | 258,0 | 121 | 0,0496 |
| 0,20 | 246,0 | 448 | 0,0625 | 144,6 | 181 | 0,0594 | 290,5 | 175 | 0,0580 | 242,0 | 96 | 0,0580 |
| 0,30 | 215,0 | 318 | 0,0770 | 126,5 | 129 | 0,0730 | 255 | 125 | 0,0714 | 212,0 | 69 | 0,0707 |
| 0,40 | 185,0 | 250 | 0,0844 | 108,5 | 99 | 0,0816 | 218 | 97 | 0,0787 | 182,0 | 53 | 0,0790 |
| 0,50 | 154,0 | 204 | 0,0860 | 90,4 | 81 | 0,0832 | 182 | 79 | 0,0805 | 151,5 | 44 | 0,0791 |
| 0,60 | 123,0 | 172 | 0,0815 | 72,4 | 68 | 0,0795 | 145,6 | 65 | 0,0784 | 121,0 | 36,3 | 0,0768 |
| 0,70 | 92,5 | 140 | 0,0753 | 54,2 | 55 | 0,0735 | 109,2 | 53,3 | 0,0718 | 90,9 | 29,2 | 0,0715 |
| 0,80 | 61,5 | 110 | 0,0638 | 36,2 | 44 | 0,0612 | 72,8 | 41,6 | 0,0610 | 60,6 | 22,9 | 0,0610 |
| 0,90 | 30,8 | 77 | 0,0455 | 18,1 | 30 | 0,0450 | 36,4 | 28,8 | 0,0443 | 30,3 | 15,8 | 0,0441 |
| 0,96 | 12,3 | 47,8 | 0,0293 | 7,24 | 18,5 | 0,0292 | 14,5 | 17,9 | 0,0284 | 12,1 | 9,9 | 0,0280 |
| 0,98 | 6,15 | 33,5 | 0,0210 | 3,62 | 13,0 | 0,0208 | 7,3 | 12,6 | 0,0210 | 6,05 | 7,0 | 0,0196 |

$\varepsilon$ = turbulent transfer magnitude: $v_* = \sqrt{\frac{\tau_0}{\varrho}}$ = shearing stress velocity

$r = \frac{d}{2}$ = pipe radius: y = distance from the wall: $\tau_0$ = shearing stress at the wall: $\varrho$ = density: $\frac{du}{dy}$ = differential velocity quotient: Re = Reynolds number: $\bar{u}$ = mean velocity. v = kinematic viscosity.

Table 4 continued on p. 42

Table 4 continued

| | $Re = 396 \cdot 10^3$; $v_* = 30{,}4$ cm/s $r = 2{,}5$ cm | | | $Re = 725 \cdot 10^3$; $v_* = 34{,}28$ cm/s $r = 5{,}0$ cm | | | $Re = 1110 \cdot 10^3$; $v_* = 47{,}2$ cm/s $r = 5{,}0$ cm | | | $Re = 1536 \cdot 10^3$; $v_* = 62{,}1$ cm/s $r = 5{,}0$ cm | | |
|---|---|---|---|---|---|---|---|---|---|---|---|---|
| 0,02 | 906 | 1370 | 0,0087 | 1151 | 795 | 0,0085 | 2185 | 1117 | 0,0083 | 3830 | 1506 | 0,0082 |
| 0,04 | 887 | 704 | 0,0166 | 1129 | 410 | 0,0160 | 2140 | 576 | 0,0157 | 3750 | 770 | 0,0156 |
| 0,07 | 860 | 416 | 0,0272 | 1092 | 237 | 0,0269 | 2075 | 337 | 0,0261 | 3630 | 460 | 0,0254 |
| 0,10 | 832 | 304 | 0,0360 | 1058 | 174 | 0,0354 | 2007 | 243 | 0,0350 | 3510 | 333 | 0,0339 |
| 0,15 | 785 | 215 | 0,0480 | 998 | 124 | 0,0470 | 1898 | 173 | 0,0465 | 3320 | 230 | 0,0465 |
| 0,20 | 740 | 169 | 0,0577 | 940 | 97 | 0,0565 | 1785 | 134,5 | 0,0562 | 3122 | 179 | 0,0561 |
| 0,30 | 647 | 123 | 0,0692 | 823 | 68 | 0,0705 | 1560 | 94,0 | 0,0705 | 2730 | 127 | 0,0691 |
| 0,40 | 555 | 92,5 | 0,0790 | 705 | 53,5 | 0,0770 | 1340 | 72,3 | 0,0785 | 2340 | 97,5 | 0,0771 |
| 0,50 | 462 | 76 | 0,0802 | 587 | 43,7 | 0,0782 | 1115 | 59,2 | 0,0796 | 1950 | 80,0 | 0,0785 |
| 0,60 | 370 | 62 | 0,0785 | 470 | 35,7 | 0,0766 | 893 | 48,4 | 0,0781 | 1560 | 64,8 | 0,0775 |
| 0,70 | 277 | 51,7 | 0,0705 | 352 | 29,0 | 0,0710 | 670 | 39,2 | 0,0725 | 1170 | 53,1 | 0,0709 |
| 0,80 | 185 | 41,0 | 0,0595 | 235 | 23,0 | 0,0596 | 446 | 31,2 | 0,0606 | 780 | 41,9 | 0,0600 |
| 0,90 | 92,5 | 27,8 | 0,0438 | 117,5 | 16,0 | 0,0428 | 223 | 21,5 | 0,0439 | 390 | 28,8 | 0,0435 |
| 0,96 | 37,0 | 17,5 | 0,0278 | 47,0 | 9,9 | 0,0277 | 89,3 | 13,5 | 0,0280 | 156 | 18,0 | 0,0279 |
| 0,98 | 18,5 | 12,3 | 0,0189 | 23,5 | 7,0 | 0,0196 | 44,6 | 9,6 | 0,0197 | 78 | 12,8 | 0,0196 |
| | $Re = 1959 \cdot 10^3$; $v_* = 77{,}5$ cm/s $r = 5{,}0$ cm | | | $Re = 2350 \cdot 10^3$; $v_* = 68{,}3$ cm/s $r = 5{,}0$ cm | | | $Re = 2790 \cdot 10^3$; $v_* = 74{,}5$ cm/s $r = 5{,}0$ cm | | | $Re = 3240 \cdot 10^3$; $v_* = 83{,}1$ cm/s $r = 5{,}0$ cm | | |
| 0,02 | 5900 | 1890 | 0,0081 | 4567 | 1670 | 0,0080 | 5460 | 1860 | 0,0079 | 6760 | 2080 | 0,0078 |
| 0,04 | 5770 | 977 | 0,0154 | 4474 | 872 | 0,0151 | 5345 | 968 | 0,0148 | 6620 | 1085 | 0,0147 |
| 0,07 | 5595 | 575 | 0,0251 | 4330 | 514 | 0,0248 | 5172 | 573 | 0,0242 | 6412 | 645 | 0,0243 |
| 0,10 | 5410 | 414 | 0,0338 | 4194 | 370 | 0,0332 | 5000 | 414 | 0,0324 | 6210 | 466 | 0,0321 |
| 0,15 | 5110 | 288 | 0,0459 | 3870 | 254 | 0,0447 | 4730 | 280 | 0,0454 | 5860 | 319 | 0,0442 |
| 0,20 | 4810 | 223 | 0,0558 | 3730 | 198,5 | 0,0551 | 4450 | 221 | 0,0540 | 5515 | 246 | 0,0540 |
| 0,30 | 4210 | 157 | 0,0692 | 3265 | 138 | 0,0693 | 3900 | 151 | 0,0692 | 4882 | 168 | 0,0697 |
| 0,40 | 3604 | 118 | 0,0790 | 2800 | 106 | 0,0775 | 3360 | 114,7 | 0,0787 | 4140 | 128 | 0,0775 |
| 0,50 | 3005 | 98 | 0,0792 | 2330 | 86,2 | 0,0791 | 2780 | 95,0 | 0,0786 | 3450 | 104 | 0,0797 |
| 0,60 | 2404 | 81 | 0,0767 | 1865 | 70,2 | 0,0780 | 2224 | 76,7 | 0,0780 | 2760 | 86,7 | 0,0765 |
| 0,70 | 1803 | 65,6 | 0,0710 | 1400 | 57,0 | 0,0721 | 1669 | 63,2 | 0,0708 | 2068 | 69,5 | 0,0714 |
| 0,80 | 1202 | 52,0 | 0,0596 | 932 | 45,5 | 0,0600 | 1112 | 50,5 | 0,0591 | 1380 | 55,7 | 0,0595 |
| 0,90 | 601 | 35,6 | 0,0435 | 466 | 31,7 | 0,0431 | 556 | 34,5 | 0,0433 | 690 | 38,8 | 0,0427 |
| 0,96 | 240 | 22,3 | 0,0278 | 186,4 | 19,8 | 0,0276 | 222 | 21,4 | 0,0278 | 276 | 23,7 | 0,0280 |
| 0,98 | 120 | 15,9 | 0,0195 | 93,2 | 13,9 | 0,0196 | 111 | 15,1 | 0,0197 | 138 | 16,8 | 0,0197 |

than in the vicinity of the pipe axis. This is to be explained by the fact that in the vicinity of the wall there is a greater influence exerted by the viscosity.

From $\varepsilon = \frac{A}{\varrho} = l^2 \frac{du}{dy}$ it follows that the mixing length is

$$l = \sqrt{\varepsilon : \frac{du}{dy}} \qquad (30)$$

The course of the mixing length over the pipe diameter at different Reynolds numbers is calculated according to this formula and presented in Table 5. $\ell/r = f(y/r)$ shows the dependence of mixing length $\ell$ upon wall distance y in nondimensional representation (Figs. 28 & 29). It is to be observed that the mixing length in the immediate vicinity of the wall (to about y/r = 0.07) increases linearly from zero. Von Karman assumes this linear increase to be $\ell = xy$ wherein y is the distance from the wall and x a proportionality constant. This has the value x = 0.38 from Re = $100 \cdot 10^3$ upward (Fig. 29). Below Re $100 \cdot 10^3$ we obtain x = 0.40 (Fig. 28). Above the value y/r = 0.07 the

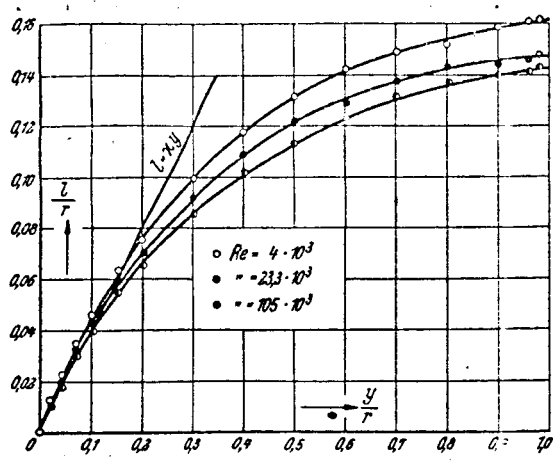


Fig. 28. ℓ/r as a function of y/r for low Reynolds numbers.

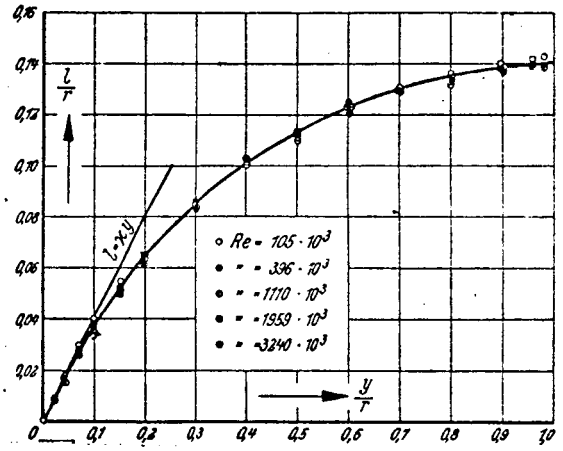


Fig. 29. ℓ/r as a function of y/r for high Reynolds numbers.

mixing length increases more slowly and in the pipe axis it reaches a fixed value of about $l/r = 0.14$ (Fig. 29). In this illustration the values of the dimensionless mixing length for the five Reynolds numbers Re = $105 \cdot 10^3$ to $3240 \cdot 10^3$ are plotted. With a very narrow range of scatter they yield the same characteristic. From this diagram it can be recognized that at further increasing Reynolds numbers the values of the dimensionless mixing length $l/r$ do not decrease further at a specific dimensionless wall distance y/r. This is true because at Reynolds numbers indicated in Fig. 29, the influence of viscosity is no longer present. Below Re = $100 \cdot 10^3$ as a result of the effect of viscosity there is observed the change of the dimensionless mixing length $l/r$ with the Reynolds number, $l/r$ increasing with decreasing Reynolds number. Hence we obtain different $l/r$ curves for different Re numbers in Fig. 28. The dependency $l/r$ as a function of y/r as shown in Fig. 29 can be obtained by the following Prandtl interpolation formula /22

$$l/r = 0{,}14 - 0{,}08\,(1 - y/r)^2 - 0{,}06\,(1 - y/r)^4, \qquad (31\,a)$$

from which

$$\varkappa = \left[\frac{d\,l}{d\,y}\right]_{y=0} = 0{,}40$$

is obtained.

When viscosity is also taken into consideration, a dimensionless equation results for the dependence of the mixing length upon wall distance from the following operation. The flow ratios in the vicinity of the wall are of course determined by the physical magnitudes $\tau_0, \varrho, \mu$ and y alone.

From these magnitudes the above mentioned dimensionless magnitude $\frac{\varrho\, y}{\mu}\sqrt{\frac{\tau_0}{\varrho}} = \frac{v_* y}{\nu}$ is formed. For the mixing length we thus have the equation (ref. 23)

$$l = y\, f\left(\frac{v_* y}{\nu}\right) = y\, f(\eta). \qquad (32)$$

$\eta = \frac{v_* y}{\nu}$ can be regarded as a (variable) Reynolds number in the vicinity of the wall. Function f is to be determined empirically. Since

$$v_* = \sqrt{\frac{\tau_0}{\varrho}} = l\left|\frac{d\,\bar{u}}{d\,y}\right|, \qquad (33)$$

$$\frac{d\,\bar{u}}{d\,y} = \frac{v_*}{l} = \frac{v_*}{y \cdot f(\eta)} \qquad (34)$$

or after integration

$$|\bar{u}| = \int_{y_0}^{y} \frac{v_*\, d\,y}{y \cdot f(\eta)}, \qquad (35)$$

This formula obviously links the velocity distribution to the law of resistance. The lower limit of the integral that is here designated $y_0$, assuming an adequately exact formulation for $f(\eta)$ in the vicinity of the wall, is equal to zero in a smooth pipe and in a rough pipe it is equal to a length characteristic

for the roughness. The determination of the f-function follows from the measured velocity distribution, in that first $\ell$ is calculated and then $\ell/y = f(\eta)$. This relationship is presented in Fig. 30 (Table 6) in logarithmic scale. Each curve from top to bottom corresponds to a specific Reynolds number that is set down as a parameter. The uppermost points of the curve are in the immediate vicinity of the wall. The curves from left to right connect points of equal y/r value. In addition the diagram shows that for a specific y/r curve above $Re = 100 \cdot 10^3$ the log ($\ell$/y) values are equal for all Reynolds numbers. /23

Table 5

$\frac{\ell}{r}$ as a function of $\frac{y}{r}$

$\ell$ = Mixing length; r = pipe radius; y = distance from the wall; Re = Reynolds number; $\bar{u}$ = mean velocity; v = kinematic viscosity.

| y/r | l/r | l/r | l/r | l/r | l/r | l/r | l/r | l/r |
|---|---|---|---|---|---|---|---|---|
| | $Re = 4{,}0 \cdot 10^3$ $r = 0{,}5$ cm | $Re = 6{,}1 \cdot 10^3$ $r = 0{,}5$ cm | $Re = 9{,}2 \cdot 10^3$ $r = 0{,}5$ cm | $Re = 16{,}7 \cdot 10^3$ $r = 0{,}5$ cm | $Re = 23{,}3 \cdot 10^3$ $r = 0{,}5$ cm | $Re = 43{,}4 \cdot 10^3$ $r = 1{,}0$ cm | $Re = 105 \cdot 10^3$ $r = 1{,}5$ cm | $Re = 205 \cdot 10^3$ $r = 2{,}5$ cm |
| 0,02 | 0,0120 | 0,0114 | 0,0110 | 0,0104 | 0,0102 | 0,0099 | 0,0094 | 0,0092 |
| 0,04 | 0,0220 | 0,0212 | 0,0206 | 0,0197 | 0,0195 | 0,0190 | 0,0179 | 0,0175 |
| 0,07 | 0,0351 | 0,0340 | 0,0330 | 0,0328 | 0,0325 | 0,0315 | 0,0300 | 0,0290 |
| 0,10 | 0,0460 | 0,0446 | 0,0444 | 0,0432 | 0,0428 | 0,0423 | 0,0400 | 0,0389 |
| 0,15 | 0,0634 | 0,0616 | 0,0614 | 0,0606 | 0,0588 | 0,0564 | 0,0546 | 0,0532 |
| 0,20 | 0,0758 | 0,0752 | 0,0742 | 0,0720 | 0,0700 | 0,0665 | 0,0652 | 0,0649 |
| 0,30 | 0,0996 | 0,0978 | 0,0968 | 0,0960 | 0,0922 | 0,0872 | 0,0850 | 0,0845 |
| 0,40 | 0,1180 | 0,1156 | 0,1132 | 0,1120 | 0,1088 | 0,1049 | 0,1015 | 0,1016 |
| 0,50 | 0,1320 | 0,1304 | 0,1276 | 0,1218 | 0,1216 | 0,1173 | 0,1136 | 0,1120 |
| 0,60 | 0,1422 | 0,1372 | 0,1344 | 0,1304 | 0,1288 | 0,1250 | 0,1236 | 0,1210 |
| 0,70 | 0,1492 | 0,1454 | 0,1440 | 0,1400 | 0,1374 | 0,1346 | 0,1310 | 0,1305 |
| 0,80 | 0,1520 | 0,1520 | 0,1472 | 0,1432 | 0,1428 | 0,1383 | 0,1367 | 0,1360 |
| 0,90 | 0,1590 | 0,1564 | 0,1486 | 0,1450 | 0,1440 | 0,1417 | 0,1398 | 0,1395 |
| 0,96 | 0,1608 | 0,1574 | 0,1548 | 0,1500 | 0,1466 | 0,1454 | 0,1418 | 0,1411 |
| 0,98 | 0,1614 | 0,1572 | 0,1564 | 0,1540 | 0,1480 | 0,1464 | 0,1430 | 0,1400 |
| | $Re = 396 \cdot 10^3$ $r = 2{,}5$ cm | $Re = 725 \cdot 10^3$ $r = 2{,}5$ cm | $Re = 1110 \cdot 10^3$ $r = 5{,}0$ cm | $Re = 1536 \cdot 10^3$ $r = 5{,}0$ cm | $Re = 1959 \cdot 10^3$ $r = 5{,}0$ cm | $Re = 2350 \cdot 10^3$ $r = 5{,}0$ cm | $Re = 2790 \cdot 10^3$ $r = 5{,}0$ cm | $Re = 3240 \cdot 10^3$ $r = 5{,}0$ cm |
| 0,02 | 0,0088 | 0,0086 | 0,0084 | 0,0082 | 0,0081 | 0,0081 | 0,0080 | 0,0079 |
| 0,04 | 0,0169 | 0,0164 | 0,0161 | 0,0158 | 0,0156 | 0,0154 | 0,0151 | 0,0150 |
| 0,07 | 0,0282 | 0,0279 | 0,0270 | 0,0262 | 0,0260 | 0,0256 | 0,0251 | 0,0248 |
| 0,10 | 0,0370 | 0,0374 | 0,0368 | 0,0356 | 0,0355 | 0,0350 | 0,0342 | 0,0338 |
| 0,15 | 0,0520 | 0,0509 | 0,0505 | 0,0500 | 0,0496 | 0,0490 | 0,0492 | 0,0481 |
| 0,20 | 0,0645 | 0,0631 | 0,0628 | 0,0624 | 0,0622 | 0,0615 | 0,0607 | 0,0604 |
| 0,30 | 0,0830 | 0,0845 | 0,0840 | 0,0820 | 0,0827 | 0,0829 | 0,0826 | 0,0833 |
| 0,40 | 0,1020 | 0,0994 | 0,1011 | 0,0990 | 0,1017 | 0,1000 | 0,1010 | 0,1000 |
| 0,50 | 0,1130 | 0,1110 | 0,1130 | 0,1101 | 0,1120 | 0,1120 | 0,1110 | 0,1130 |
| 0,60 | 0,1240 | 0,1218 | 0,1238 | 0,1220 | 0,1211 | 0,1230 | 0,1230 | 0,1211 |
| 0,70 | 0,1290 | 0,1294 | 0,1319 | 0,1290 | 0,1294 | 0,1312 | 0,1291 | 0,1310 |
| 0,80 | 0,1329 | 0,1330 | 0,1353 | 0,1337 | 0,1330 | 0,1340 | 0,1320 | 0,1332 |
| 0,90 | 0,1382 | 0,1359 | 0,1389 | 0,1340 | 0,1377 | 0,1360 | 0,1368 | 0,1359 |
| 0,96 | 0,1390 | 0,1389 | 0,1400 | 0,1390 | 0,1391 | 0,1380 | 0,1390 | 0,1400 |
| 0,98 | 0,1400 | 0,1381 | 0,1390 | 0,1380 | 0,1380 | 0,1390 | 0,1390 | 0,1400 |

The equality of these values offers new support for the hypothesis that in this range of Reynolds numbers, aside from the immediate vicinity of the wall, there is no effect exerted by viscosity.

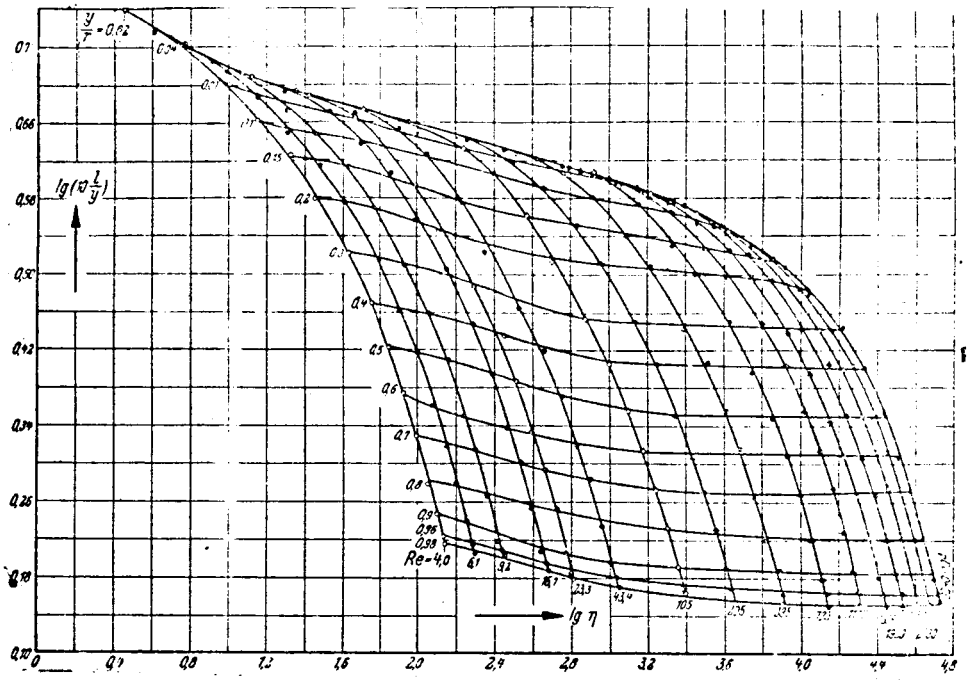


Fig. 30. $\ell g\ (10\ \ell/y)$ as a function of $\ell g\ \eta$

/24

## 5. CONSIDERATIONS ON SIMILARITY

Recently von Kármán (ref. 24) succeeded in basing another viewpoint on the Prandtl law of mixing length.

Concerning the character of the dependence of turbulent stresses upon the flow field, two basically different assumptions can be made. It can be hypothesized that the turbulent stresses can only be explained by an "integral law" from the total flow field with its boundary conditions, or that the turbulent stresses at a given locus are already determined by the behavior of the next neighborhood in the same way as by a differential law. For the stresses developed by the molecular motion, i.e., for laminar friction, a differential law is valid of course: the laminar stresses can be expressed by the prevalent velocity gradients at the locus in question and the constant of internal friction:

$$\tau = \mu \frac{du}{dy}. \qquad (36)$$

Von Kármán tests the hypothesis of a differential law for turbulent flows. In order that such a law can stand, obviously the secondary motions insofar as they are coherent, must have no great spatial extent and furthermore they must

Table 6

$l$= mixing length; y = distance from the wall; $\eta = \frac{v_* y}{\nu}$ dimensionless wall distance; $v_* = \sqrt{\frac{\tau_0}{\varrho}}$ = shearing stress velocity; $\nu$ = kinematic viscosity; r = pipe radius; Re = Reynolds number; $\bar{u}$ = mean velocity.

| y/r | $\eta$ | $l/y$ | $\eta$ | $l/y$ | $\eta$ | $l/y$ | $\eta$ | $l/y$ | $\eta$ | $l/y$ | $\eta$ | $l/y$ | $\eta$ | $l/y$ | $\eta$ | $l/y$ |
|---|---|---|---|---|---|---|---|---|---|---|---|---|---|---|---|---|
| | $Re = 4 \cdot 10^3$ $r = 0{,}5$ cm | | $Re = 6{,}1 \cdot 10^3$ $r = 0{,}5$ cm | | $Re = 9{,}2 \cdot 10^3$ $r = 0{,}5$ cm | | $Re = 16{,}6 \cdot 10^3$ $r = 0{,}5$ cm | | $Re = 23{,}3 \cdot 10^3$ $r = 0{,}5$ cm | | $Re = 43{,}4 \cdot 10^3$ $r = 1{,}0$ cm | | $Re = 105 \cdot 10^3$ $r = 1{,}5$ cm | | $Re = 205 \cdot 10^3$ $r = 2{,}5$ cm | |
| 0,02 | 2,83 | 0,600 | 4,03 | 0,569 | 5,75 | 0,552 | 9,8 | 0,518 | 13 | 0,510 | 22,6 | 0,495 | 50 | 0,470 | 90,5 | 0,457 |
| 0,04 | 5,66 | 0,550 | 8,10 | 0,531 | 11,5 | 0,515 | 19,6 | 0,493 | 26 | 0,488 | 45,2 | 0,475 | 100 | 0,447 | 181 | 0,437 |
| 0,07 | 9,90 | 0,501 | 14,1 | 0,485 | 20,1 | 0,470 | 34,2 | 0,468 | 46 | 0,464 | 79,1 | 0,450 | 175 | 0,430 | 317 | 0,415 |
| 0,10 | 14,14 | 0,460 | 20,2 | 0,446 | 28,7 | 0,443 | 49,0 | 0,433 | 65 | 0,429 | 113,0 | 0,423 | 250 | 0,400 | 453 | 0,389 |
| 0,15 | 21,20 | 0,422 | 30,2 | 0,410 | 43,1 | 0,409 | 73,4 | 0,404 | 98 | 0,392 | 169,4 | 0,376 | 376 | 0,364 | 680 | 0,355 |
| 0,20 | 28,30 | 0,379 | 40,3 | 0,376 | 57,5 | 0,371 | 98,0 | 0,360 | 130 | 0,350 | 226,0 | 0,333 | 500 | 0,326 | 906 | 0,324 |
| 0,30 | 42,50 | 0,333 | 60,5 | 0,326 | 86,3 | 0,323 | 147 | 0,320 | 195 | 0,307 | 339 | 0,291 | 752 | 0,284 | 1360 | 0,282 |
| 0,40 | 56,60 | 0,295 | 80,5 | 0,289 | 115,0 | 0,288 | 196 | 0,280 | 260 | 0,272 | 452 | 0,262 | 1000 | 0,254 | 1810 | 0,254 |
| 0,50 | 70,70 | 0,264 | 101,0 | 0,261 | 143,8 | 0,256 | 245 | 0,248 | 325 | 0,243 | 565 | 0,2346 | 1251 | 0,227 | 2260 | 0,224 |
| 0,60 | 85,00 | 0,237 | 121,0 | 0,229 | 172,5 | 0,224 | 294 | 0,217 | 390 | 0,215 | 678 | 0,2083 | 1504 | 0,206 | 2720 | 0,202 |
| 0,70 | 99,00 | 0,213 | 141,0 | 0,208 | 201,0 | 0,206 | 342 | 0,200 | 455 | 0,1965 | 791 | 0,1920 | 1754 | 0,187 | 3170 | 0,186 |
| 0,80 | 113,00 | 0,190 | 161,0 | 0,190 | 230,0 | 0,184 | 392 | 0,179 | 520 | 0,1785 | 904 | 0,1716 | 2000 | 0,171 | 3620 | 0,170 |
| 0,90 | 127,30 | 0,1765 | 181,2 | 0,1735 | 258,5 | 0,165 | 440 | 0,161 | 585 | 0,160 | 1017 | 0,1574 | 2260 | 0,1555 | 4075 | 0,155 |
| 0,96 | 136,0 | 0,1675 | 193,5 | 0,164 | 276,0 | 0,1615 | 470 | 0,1563 | 624 | 0,153 | 1085 | 0,1515 | 2405 | 0,1478 | 4350 | 0,147 |
| 0,98 | 138,8 | 0,1645 | 197,5 | 0,1603 | 282,0 | 0,1595 | 480 | 0,1535 | 636 | 0,1512 | 1109 | 0,1480 | 2460 | 0,146 | 4440 | 0,143 |
| | $Re = 396 \cdot 10^3$ $r = 2{,}5$ cm | | $Re = 725 \cdot 10^3$ $r = 2{,}5$ cm | | $Re = 1110 \cdot 10^3$ $r = 5{,}0$ cm | | $Re = 1536 \cdot 10^3$ $r = 5{,}0$ cm | | $Re = 1959 \cdot 10^3$ $r = 5{,}0$ cm | | $Re = 2350 \cdot 10^3$ $r = 5{,}0$ cm | | $Re = 2790 \cdot 10^3$ $r = 5{,}0$ cm | | $Re = 3240 \cdot 10^3$ $r = 5{,}0$ cm | |
| 0,02 | 0,164 | 0,439 | 0,284 | 0,427 | 0,42 | 0,418 | 0,566 | 0,411 | 0,704 | 0,406 | 0,834 | 0,404 | 0,967 | 0,398 | 1,11 | 0,395 |
| 0,04 | 0,328 | 0,423 | 0,566 | 0,410 | 0,84 | 0,401 | 1,13 | 0,394 | 1,41 | 0,389 | 1,668 | 0,384 | 1,934 | 0,378 | 2,22 | 0,375 |
| 0,07 | 0,574 | 0,404 | 0,990 | 0,399 | 1,47 | 0,386 | 1,98 | 0,375 | 2,46 | 0,372 | 2,92 | 0,366 | 3,380 | 0,358 | 3,88 | 0,355 |
| 0,10 | 0,820 | 0,389 | 1,419 | 0,375 | 2,10 | 0,367 | 2,83 | 0,356 | 3,52 | 0,355 | 4,16 | 0,350 | 4,835 | 0,332 | 5,55 | 0,335 |
| 0,15 | 1,230 | 0,347 | 2,122 | 0,339 | 3,15 | 0,336 | 4,25 | 0,334 | 5,27 | 0,331 | 6,25 | 0,327 | 7,25 | 0,328 | 8,33 | 0,32 |
| 0,20 | 1,64 | 0,322 | 2,835 | 0,316 | 4,20 | 0,314 | 5,66 | 0,312 | 7,04 | 0,311 | 8,34 | 0,308 | 9,67 | 0,304 | 11,10 | 0,30 |
| 0,30 | 2,46 | 0,277 | 4,250 | 0,282 | 6,30 | 0,281 | 8,50 | 0,274 | 10,54 | 0,276 | 12,51 | 0,276 | 14,50 | 0,276 | 16,65 | 0,27 |
| 0,40 | 3,28 | 0,255 | 5,66 | 0,249 | 8,40 | 0,253 | 11,30 | 0,248 | 14,08 | 0,254 | 16,68 | 0,250 | 19,34 | 0,253 | 22,20 | 0,27 |
| 0,50 | 4,10 | 0,227 | 7,08 | 0,222 | 10,50 | 0,226 | 14,15 | 0,221 | 17,58 | 0,224 | 20,85 | 0,224 | 24,20 | 0,222 | 27,74 | 0,22 |
| 0,60 | 4,92 | 0,207 | 8,50 | 0,203 | 12,60 | 0,206 | 17,00 | 0,203 | 21,12 | 0,202 | 25,02 | 0,205 | 29,00 | 0,205 | 33,29 | 0,20 |
| 0,70 | 5,745 | 0,184 | 9,90 | 0,185 | 14,70 | 0,188 | 19,80 | 0,184 | 24,62 | 0,185 | 29,19 | 0,188 | 33,80 | 0,185 | 38,80 | 0,18 |
| 0,80 | 6,56 | 0,166 | 11,32 | 0,166 | 16,80 | 0,169 | 22,60 | 0,167 | 28,16 | 0,166 | 33,36 | 0,138 | 38,68 | 0,165 | 44,40 | 0,1 |
| 0,90 | 7,72 | 0,154 | 12,75 | 0,151 | 18,90 | 0,154 | 25,50 | 0,152 | 31,62 | 0,153 | 37,53 | 0,151 | 43,50 | 0,152 | 50,0 | 0,15 |
| 0,96 | 7,87 | 0,145 | 13,60 | 0,145 | 20,20 | 0,146 | 27,20 | 0,145 | 33,75 | 0,145 | 40,00 | 0,144 | 46,42 | 0,145 | 53,3 | 0,14 |
| 0,98 | 8,05 | 0,143 | 13,90 | 0,141 | 20,60 | 0,142 | 27,80 | 0,141 | 34,45 | 0,141 | 40,90 | 0,142 | 47,40 | 0,1422 | 54,40 | 0,143 |

run similarly in the individual points of the flow field. Since the hypothesis is only valid for high Reynolds numbers, the influence of viscosity can in general be neglected.

The mathematical formulation is now simple. Von Kármán now makes the not absolutely required assumption for the following operation that the secondary motion in a system of coordinates which participate in the principal motion of the locus under consideration is stationary. The entire motion is considered to be two-dimensional, principal motion U in the x-direction being dependent only upon the transverse coordinate y. The point of origin of the above coordinate system we allow to coincide with the point on which we focus, so that the principal velocity in the neighborhood of the point in question will be

$$U = U_0' y + \frac{U_0''}{2} y^2 + \dots \qquad (37)$$

The total flow function $\Psi$ with $\psi$ as flow function of the secondary motion is

$$\Psi(x, y) = \frac{U_0' y^2}{2} + \frac{U_0'' y^3}{6} + \dots + \psi(x, y). \qquad (38)$$

Since $\psi$ in the transition to another point will change similarly, it will change only by a factor A which is a measure of the intensity of fluctuation movement, and a length measure $\ell$ for the spatial measurements of the flow field, i.e., if we write

$$x = l\xi, \quad y = l\eta, \quad \psi = A f(\xi, \eta) \qquad (39)$$

$f(\xi,\eta)$ will be independent of the choice of the locus investigated.

If we eliminate pressure p from the Euler differential equations for smooth, stationary frictionless flow

$$u\frac{\partial u}{\partial x} + v\frac{\partial u}{\partial y} = -\frac{1}{\varrho}\frac{\partial p}{\partial x}, \quad u\frac{\partial v}{\partial x} + v\frac{\partial v}{\partial y} = -\frac{1}{\varrho}\frac{\partial p}{\partial y}$$

in differentiating the first equation with reference to y and the second with reference to x and then introduce the flow function by

$$u = U + u' = \frac{\partial \Psi}{\partial y} \quad \text{and} \quad v = v' = -\frac{\partial \Psi}{\partial x},$$

where u' and v' are velocity components of the secondary motion, we obtain

$$\frac{\partial \Psi}{\partial y}\cdot\frac{\partial \Delta \Psi}{\partial x} - \frac{\partial \Psi}{\partial x}\cdot\frac{\partial \Delta \Psi}{\partial y} = 0, \qquad (40)$$

where $\Delta$ is the Laplace operator

$$\Delta = \frac{\partial^2}{\partial x^2} + \frac{\partial^2}{\partial y^2}$$

After introduction of the above equation (38) in the next neighborhood of the point in question we obtain

$$\left(U_0' y + \frac{\partial \psi}{\partial y}\right)\frac{\partial \Delta \psi}{\partial x} - \frac{\partial \psi}{\partial x}\left(U_0'' + \frac{\partial \Delta \psi}{\partial y}\right) = 0, \qquad (41)$$

and in the dimensionless magnitudes f, $\xi$ and $\eta$

$$U_0' l \eta \frac{A}{l^3} \frac{\partial \Delta f}{\partial \xi} - \frac{A}{l} \frac{\partial f}{\partial \xi} U_0'' + \frac{A^2}{l^4} \left( \frac{\partial f}{\partial \eta} \cdot \frac{\partial \Delta f}{\partial \xi} - \frac{\partial f}{\partial \xi} \cdot \frac{\partial \Delta f}{\partial \eta} \right) = 0. \quad (42)$$

where the differentiation of f now is referred to the new variables $\xi$ and $\eta$. The prime at U indicates differentiation with reference to y, however. In order that f may be independent of the locus in question, that is form A, $\ell$, $U_o'$ and $U_o''$, the coefficients of this differential equation for f must be constant. After division of Equation (42) by $\frac{A^2}{\ell^4}$ we obtain

$$\frac{U_0'}{A} l^2 \eta \frac{\partial \Delta f}{\partial \xi} - U_0'' \frac{l^3}{A} + \left( \frac{\partial f}{\partial y} \cdot \frac{\partial \Delta f}{\partial \xi} - \frac{\partial f}{\partial \xi} \cdot \frac{\partial \Delta f}{\partial \eta} \right) = 0. \quad (43)$$

Therefore $$U_0' \frac{l^2}{A} = \text{const}, \qquad U_0'' \frac{l^3}{A} = \text{const}$$

must be true, or $$U_0' \sim \frac{A}{l^2}, \qquad U_0'' \sim \frac{A}{l^3}$$ ($\sim$ means proportional)

or $$l \sim \frac{U_0'}{U_0''}, \qquad A \sim \frac{U_0'^3}{U_0''^2} \sim l^2 U_0'. \quad (44)$$

For this result the following very clear operation can also be effected according to Betz (ref. 25):

The fluctuations of velocity of the u-component of a specific layer of the principal flow with mean velocity $U_o$ develop in that as a result of turbulent transverse motion particles of adjacent layers with greater or less velocity penetrate into layer $U_o$, retaining their original velocity. If these particles originate in areas which are removed from the layer under consideration by length $\ell_1$ their velocity $U_o + \ell_1 U_o'$ and the fluctuation of the u-component in layer $U_o$ is therefore equal to $$u' = \pm l_1 U_0'. \quad (45)$$

This concept can be still further extended. In addition to their velocity $U_o + \ell_1 U_o'$ the particles in the transverse motion also bring along their mean rotation

$$\zeta = \text{rot}\, U = U'$$

$\xi_o$ = rotation $U_o$ = $U_o'$ is the mean rotation in layer $U_o$ under consideration and

$$\zeta = \zeta_0 \pm l_1 \zeta_0' \quad = \zeta_0 \pm l_1 U_0''$$

are the mean rotations in the layers at a distance of $\pm \ell_1$. The rotation of the particles that penetrate into layer $U_o$ by the transverse motion deviates thus from the mean rotation here present by the amount

$$\zeta - \zeta_0 = l_1 U_0''$$

These particles thus constitute a system of dextrorotary and levorotary vortices, and the turbulent flow velocities can now be regarded as the field of these vortices. If $\ell_2$ is the average distance of the dextro and levorotary particles, their diameter is $\sim \ell_2$, For flow velocity v = v' between two vortices we then obtain

$$v' \sim l_2 (\zeta - \zeta_0) \sim l_2 l_1 U_0''. \qquad (46)$$

/25

By virtue of the assumed similarity of the turbulent fluctuating movement, u' $\sim$v' and $\ell_1 \sim \ell_2$ so that instead of $\ell_1$ and $\ell_2$ we can introduce a common length measurement $\ell$. Then from (45) and (46) we have

$$l U_0' \sim l^2 U_0''$$

or

$$l \sim \frac{U_0'}{U_0''} \qquad (47)$$

in agreement with the Von Kármán result.

Earlier, for turbulent shearing stress $\tau$ we had the equation

$$\tau = -\rho \overline{u'v'},$$

wherein u' and v' are the components of velocity fluctuations. Therefore

$$\tau = \rho \frac{\partial \psi}{\partial x} \cdot \frac{\partial \psi}{\partial y} = \rho \frac{A^2}{l^2} \frac{\partial f}{\partial \xi} \cdot \frac{\partial f}{\partial \eta}$$

or

$$\tau = \rho l^2 U_0'^2 \frac{\partial f}{\partial \xi} \cdot \frac{\partial f}{\partial \eta}; \qquad (48)$$

since f is independent of x and y we have confirmation of the Prandtl expression for the mixing length

$$\tau = \rho l^2 \left| \frac{dU}{dy} \right|^2 \qquad (49)$$

From this we obtain an explicit formula for $\ell$

$$l = \varkappa \frac{dU}{dy} \Big/ \frac{d^2U}{dy^2} \qquad (50)$$

with a universal dimensionless constant $\chi$.

It can immediately be said with reference to the range of validity of the above hypothesis that it breaks off where U' and U'' disappear, because then $\Psi$ in the neighborhood of the point under consideration can no longer be approximated as in the above described defect equation (41). It is also immediately appreciated that the point in which the differential quotient of the principal motion changes its sign (in the center of the channel) so that on both sides there is more weakly moved fluid, is distinguished from the other points. Naturally the whole hypothesis is incomplete so long as there is no actual solution of the above defect equation of the required type.

Deduction of the velocity distribution in pipe and channel

It is possible readily to calculate the velocity distribution in the

channel or pipe using formulas (49) and (50) for the shearing stress and the mixing length, since the shearing stress is linearly distributed here, so that with $\tau_0$ as shearing stress at the wall and y as distance from the middle of the pipe and r as pipe radius we have $\tau = \tau_0 \frac{y}{r}$.

On the other hand according to Equation (49) and (50);

$$\tau_0 \frac{y}{r} = \varrho l^2 \left(\frac{dU}{dy}\right)^2 = \varrho \varkappa^2 \frac{\left(\frac{dU}{dy}\right)^4}{\left(\frac{d^2U}{dy^2}\right)^2}$$

or

$$\frac{U''}{U'^2} = \varkappa \frac{\sqrt{r}}{v_*} \cdot \frac{1}{\sqrt{y}},$$

with

$$v_* = \sqrt{\frac{\tau_0}{\varrho}}.$$

This equation can be immediately integrated

$$-\frac{1}{U'} = 2\varkappa \frac{\sqrt{r}}{v_*} (\sqrt{y} - a),$$

where a is an integration constant or

$$U' = \frac{1}{2\varkappa} \frac{v_*}{\sqrt{r}} \frac{1}{(a - \sqrt{y})}$$

The integration constant a is determined for U' from the limiting conditions. For very high Reynolds numbers $\frac{dU}{dy}$ near the wall is very large and approaches the laminar value $\frac{dU}{dy} = \frac{\tau_0}{\mu}$ which is very large because of the low value of $\mu$. Without commiting a sizeable error, we can allow the point where $\frac{dU}{dy}$ becomes infinite to coincide with the wall (y = r). Thus we obtain the integration constant as $a = \sqrt{r}$

$$\frac{dU}{dy} = -\frac{1}{2\varkappa} \frac{v_*}{\sqrt{r}} \frac{1}{(\sqrt{r} - \sqrt{y})}$$

and by integration between the limits 0 and y

$$\frac{U_{max} - U}{v_*} = -\frac{1}{\varkappa} \left[\ln\left(1 - \sqrt{\frac{y}{r}}\right) + \sqrt{\frac{y}{r}}\right]. \qquad (51)$$

The mixing length increases linearly from the wall according to this solution which we can demonstrate to ourselves in the following manner. In this neighborhood the shearing stress is still approximately $\tau_0$ so that here the equation

$$\tau_0 = \varrho \varkappa^2 \frac{U'^2}{U''^2}$$

is valid. Consequently with $y_1$ as wall distance

$$-\int_{r}^{r-y}\frac{U''}{U'^2}dy=\left[\frac{1}{U'}\right]_{r-y}=\int_{r}^{r-y}v_*\,dy=\frac{\varkappa y_1}{v_*},$$

whereby the integration constant on condition of the later refinement (see section on law of resistance) can be written approximately as zero since U' at the wall is actually very great. Hence

$$U''=-\varkappa v_*\cdot\frac{1}{y_1^2}$$

and

$$l=\varkappa\left(\frac{U'}{U''}\right)=\varkappa y_1, \qquad (52)$$

as stated. In what range this relationship is supported by our experiments is indicated in Figs. 30 and 31.

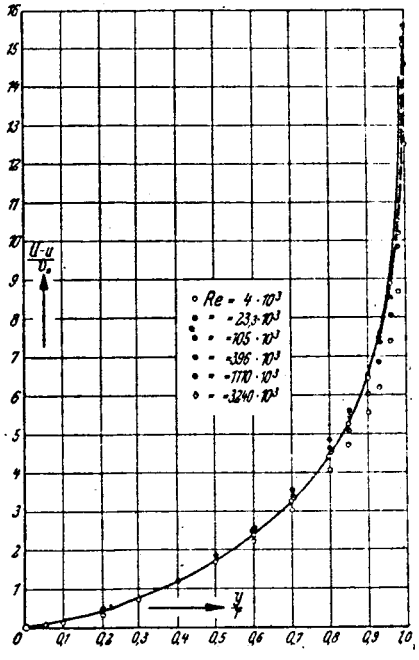


Fig. 31. $\frac{U_{max}-u}{v_*}$ as a function of y/r.

/26

Law of resistance

Independently of this theory von Kármán has given a most satisfactory explanation of the law of resistance in smooth and rough pipes.

He only assumes with reference to the mixing length that it increases outward from the wall ($l = \varkappa y$ where y now again indicates the wall distance) and in other respects independently of the character of the wall and of the viscosity it has a similar course: $\frac{l}{r}=\varkappa\frac{y}{r}f\left(\frac{y}{r}\right)$

or $$l = \varkappa \cdot y \cdot f\left(\frac{y}{r}\right); \qquad (53)$$

a zone immediately at the wall where laminar flow prevails must of course be excluded. The condition of equilibrium is

$$\tau_0 = \varrho\, l^2 \left(\frac{dU}{dy}\right)^2 = \tau_0 \left(1 - \frac{y}{r}\right)$$

or because of Equation (53)

$$\varkappa \cdot y \cdot f\left(\frac{y}{r}\right) \cdot \left(\frac{dU}{dy}\right) = v_* \sqrt{\left(1 - \frac{y}{r}\right)};$$

and if we integrate between limits y and r, we obtain

$$U_{max} - U = v_* \int_y^r \frac{\sqrt{(1 - y/r)}}{\varkappa \cdot y \cdot f(y/r)} \cdot dy$$

$$U_{max} - U = v_* g\left(\frac{y}{r}\right),$$

where g is the same function for all smooth pipes. The equation $\frac{U_{max} - U}{v_*} = f(y/r)$ has been computed according to our experiments and is presented in Table 7.

Table 7

$\frac{U-u}{v_*}$ as a function of v/r

| *Re* | 4 | 6,1 | 9,2 | 16,7 | 23,3 | 43,4 | 105 | 205 | 396 | 725 | 1110 | 1596 | 1959 | 2350 | 2790 | 3240 |
|---|---|---|---|---|---|---|---|---|---|---|---|---|---|---|---|---|
| *y/r* | $\frac{U-u}{v_*}$ | $\frac{U-u}{v_*}$ | $\frac{U-u}{v_*}$ | $\frac{U-u}{v_*}$ | $\frac{U-u}{v_*}$ | $\frac{U-u}{v_*}$ | $\frac{U-u}{v_*}$ | $\frac{U-u}{v_*}$ | $\frac{U-x}{v_*}$ | $\frac{U-u}{v_*}$ | $\frac{U-u}{v_*}$ | $\frac{U-u}{v_*}$ | $\frac{U-u}{v_*}$ | $\frac{U-u}{v_*}$ | $\frac{U-u}{v_*}$ | $\frac{U-u}{v_*}$ |
| 1,00 | 12,52 | 12,92 | 13,48 | 12,50 | 15,20 | 15,50 | 14,60 | 16,65 | 16,30 | 14,90 | 15,60 | 16,00 | 14,90 | 13,09 | 13,80 | 15,30 |
| 0,98 | 8,66 | 8,98 | 9,15 | 8,65 | 9,65 | 9,48 | 10,60 | 10,59 | 10,20 | 10,54 | 11,06 | 11,05 | 10,09 | 10,36 | 10,50 | 10,50 |
| 0,96 | 7,40 | 7,65 | 7,80 | 7,45 | 8,06 | 8,00 | 8,88 | 8,95 | 8,50 | 8,71 | 8,83 | 9,11 | 8,54 | 8,79 | 9,30 | 8,98 |
| 0,93 | 6,20 | 6,36 | 6,76 | 6,39 | 6,86 | 6,74 | 7,51 | 7,64 | 7,35 | 7,31 | 7,59 | 7,51 | 7,35 | 7,39 | 7,51 | 7,50 |
| 0,90 | 5,53 | 5,63 | 5,74 | 5,67 | 6,06 | 5,99 | 6,62 | 6,66 | 6,45 | 6,45 | 6,55 | 6,41 | 6,45 | 6,33 | 6,47 | 6,45 |
| 0,85 | 4,69 | 4,73 | 4,70 | 4,77 | 5,10 | 5,05 | 5,61 | 5,56 | 5,45 | 5,33 | 5,35 | 5,49 | 5,37 | 5,25 | 5,23 | 5,29 |
| 0,80 | 4,04 | 4,06 | 4,07 | 4,14 | 4,42 | 4,35 | 4,84 | 4,65 | 4,66 | 4,56 | 4,52 | 4,50 | 4,60 | 4,45 | 4,40 | 4,45 |
| 0,70 | 3,02 | 3,05 | 3,10 | 3,20 | 3,28 | 3,24 | 3,52 | 3,50 | 3,45 | 3,40 | 3,36 | 3,28 | 3,38 | 3,28 | 3,18 | 3,30 |
| 0,60 | 2,26 | 2,32 | 2,32 | 2,33 | 2,42 | 2,38 | 2,58 | 2,64 | 2,58 | 2,52 | 2,50 | 2,40 | 2,53 | 2,40 | 2,38 | 2,46 |
| 0,50 | 1,68 | 1,71 | 1,74 | 1,73 | 1,74 | 1,75 | 1,89 | 1,95 | 1,87 | 1,80 | 1,77 | 1,75 | 1,82 | 1,70 | 1,71 | 1,73 |
| 0,40 | 1,21 | 1,23 | 1,29 | 1,24 | 1,23 | 1,19 | 1,26 | 1,38 | 1,31 | 1,24 | 1,20 | 1,17 | 1,24 | 1,11 | 1,17 | 1,56 |
| 0,30 | 0,81 | 0,83 | 0,84 | 0,83 | 0,77 | 0,78 | 0,84 | 0,86 | 0,82 | 0,80 | 0,76 | 0,75 | 0,72 | 0,70 | 0,77 | 0,72 |
| 0,20 | 0,39 | 0,48 | 0,52 | 0,48 | 0,43 | 0,45 | 0,47 | 0,57 | 0,46 | 0,45 | 0,40 | 0,39 | 0,37 | 0,34 | 0,42 | 0,36 |
| 0,10 | 0,13 | 0,20 | 0,19 | 0,19 | 0,143 | 0,134 | 0,158 | 0,20 | 0,16 | 0,16 | 0,15 | 0,14 | 0,13 | 0,09 | 0,17 | 0,1 |
| 0,04 | 0,05 | 0,07 | 0,065 | 0,06 | 0,046 | 0,067 | 0,052 | 0,03 | 0,07 | 0,04 | 0,04 | 0,05 | 0,04 | 0,03 | 0,05 | 0,0 |
| 0,02 | 0,03 | 0,02 | 0,026 | 0,04 | 0,023 | 0,037 | 0,026 | 0,02 | 0,03 | 0,02 | 0,02 | 0,02 | 0,01 | 0,02 | 0,01 | 0,0 |
| 0,00 | 0,00 | 0,00 | 0,000 | 0,00 | 0,000 | 0,000 | 0,000 | 0,00 | 0,00 | 0,00 | 0,00 | 0,00 | 0,00 | 0,00 | 0,00 | 0,0 |

U = maximum velocity; u = actual velocity; $v_* = \sqrt{\frac{\tau_0}{\varrho}}$ = shearing stress velocity; $\tau_0$ = shearing stress at the wall; $q = \varrho \frac{U^2}{2} =$ pressure head of

maximum velocity; $\varrho$ = density; y = distance from middle of the pipe; r = pipe radius.

This dependency is illustrated in Fig. 31. The solid line of this figure is the velocity curve according to equation (51) with $\chi = 0.36$. The dashed curve is drawn through the experimental points. It is to be noted that in the vicinity of the wall the calculated velocity curve shows a deviation from the measured one. This is true because the hypothesis of similarity is not fulfilled in the vicinity of the wall where an effect is exerted by viscosity.

Friction or roughness consequently has an influence only on the interior in the form of a limiting condition. This is found by von Kármán in smooth pipes in the following way. In a thin layer at the wall, of density $\delta$ the velocity is determined only by the viscosity. Thereby the velocity distribution calculated according to the above formula, using the mixing length, is conformed to. This is of course a very simplified description of the effect of viscosity. $\ell$ must therefore be assumed only up to the value $\chi\delta$. According to the known concept that led according to Prandtl and von Kármán to the law of velocity in the vicinity of the wall (1/7 exponential law, etc.) on the other hand, $\delta$ can depend only upon the physical magnitudes in the vicinity of the wall $\tau_0$, $\varrho$, $\mu$. We therefore write

$$\delta = \frac{\alpha}{\varkappa} \cdot \frac{\nu}{v_*},$$

where $\alpha$ again is a dimensionless constant that is independent of the Reynolds number. In the laminar layer $\tau_0 = \mu \frac{du}{dy}$; at the boundary we have the velocity

$$U_1 = \frac{\alpha}{\varkappa} v_*.$$

Velocity outside the laminar layer becomes

$$U = \int_{\delta}^{y} v_* \sqrt{\left(1 - \frac{y}{r}\right)} \frac{1}{\varkappa \cdot y f(y/r)} dy + U_1. \qquad /27$$

Since the essential increase in velocity occurs very near the wall, it is sufficient to carry out the integration with f(y/r) = 1. Thereby, with new constants c and $\beta$, there will be in approximation

$$U_{max} = \frac{1}{\varkappa} v_* \left[c - \ln \frac{\delta}{\varkappa} + \alpha\right] = \frac{1}{\varkappa} v_* \left[\ln \frac{r \cdot v_*}{\nu} + \beta\right]. \quad (55)$$

If we introduce the resistance coefficient derived from maximum velocity

$$\psi = \frac{2}{U_{max}^2} v_*^2$$

and correspondingly the Reynolds number

$$Re_{max} = \frac{U_{max} \cdot r}{\nu}$$

then

$$\frac{1}{\sqrt{\psi}} = \alpha + \frac{1}{\varkappa\sqrt{2}} \ln \left(Re_{max} \sqrt{\psi}\right). \quad (56)$$

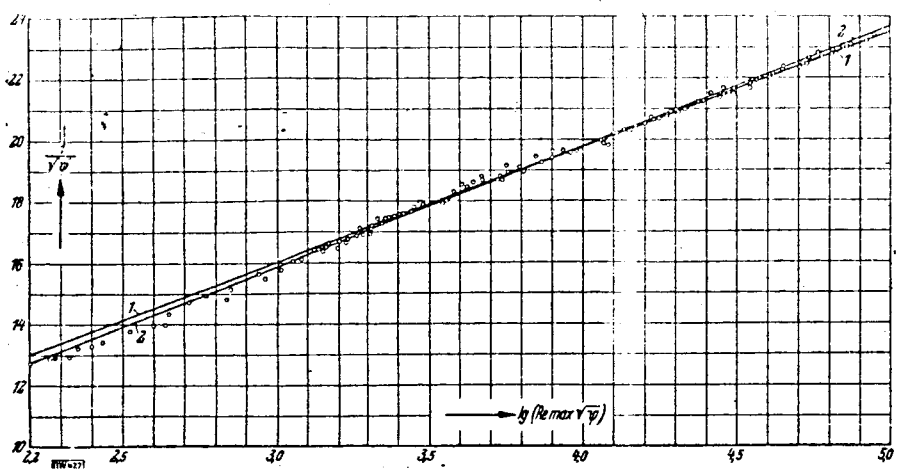


Fig. 32 $\frac{1}{\sqrt{\psi}}$ as a function of $(Re_{max}\sqrt{\psi})$

The values for this equation as determined by experiment are presented in Table 8 and illustrated in Fig. 32. $\frac{1}{\sqrt{\psi}}$ is plotted as ordinate and the usual log of $Re_{max}\sqrt{\psi}$ as abscissa. Since the similarity hypothesis strictly speaking refers to frictionless fluids, and for this reason for the comparison with the experiment only flows are involved in which the effect of viscosity in the pipe interior is very slight, we have plotted a straight line (1) through these points in which the effect of viscosity is practically no longer present. Fig. 32 shows that below log $(Re_{max}\sqrt{\psi})$ ). This signifies that effect of viscosity with declining Reynolds number is increasingly strong. The straight line is described by the equation

$$\frac{1}{\sqrt{\psi}} = A + B \lg (Re_{max}\sqrt{\psi}) \qquad (56a)$$

Constants A and B were determined from this figure and yielded A = 4.75; B = 3.77. As the hypothesis indicates, the equation of this straight line is valid for all flows that are not influenced by viscosity. For this reason we are justified in extrapolating the dependence $\frac{1}{\sqrt{\psi}}$ of log $(Re_{max}\sqrt{\psi})$ for any magnitude of $Re_{max}$.

We also plotted a second straight line (2) for the following calculation of approximation, referring especially to the points in the middle range: the equation is

$$\frac{1}{\sqrt{\psi}} = 4{,}16 + 3{,}90 \lg (Re_{max}\sqrt{\psi}). \qquad (56b)$$

Similarity hypothesis according to Prandtl

The basic concept of the above minutely described von Kármán hypothesis of similarity is the assumption of the geometric and mechanical similarity of the

turbulent transfer mechanism. Through the hypothesis that the turbulent fluctuation motion in different loci of the principal flow is distinguished only by a length and time scale, von Kármán came to his law of universal velocity distribution for channel and pipe flows.

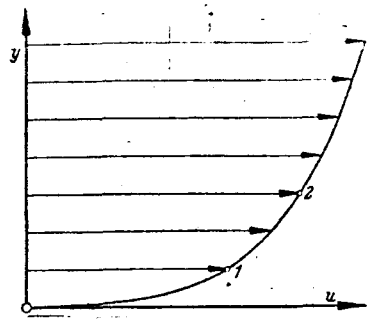


Fig. 33. Definition sketch.

Only the first and second differential quotient $\frac{du}{dy}$ and $\frac{d^2u}{dy^2}$ of the main flow $u = u(y)$ are taken into consideration. Prandtl (ref. 26) takes the view that such a similarity of the secondary motion can strictly speaking only be anticipated if the same similarity satisfies the principal motion.

Let (1) and (2) be two points of the profile of the main flow, then at the transition from (1) to (2) we have to change the scale of length such as y and the time scale such as $\frac{y}{u}$ (y = distance from the axis of similarity).

The most general velocity distribution u(y) which fulfills the similarity hypothesis, i.e., whose curve upon change of the y- and u-scale coincides with the former curve, is represented by the equation

$$u = a\,y^n + b, \tag{57}$$

where a and b are constants. Earlier we introduced the characteristic magnitude $v_* = \sqrt{\frac{\tau_0}{\varrho}}$ for a turbulent flow ( $\tau_0 = \varrho\, v_*^2$ ). The magnitude $v_*$ defined in this way by turbulent shearing stress $\tau_0$, which magnitude has the dimension of a velocity, can be considered as a measure for the turbulent defect motion. Because of the equality of two systems of coordinates which move toward each other with constant velocity, the turbulent fluctuation velocity at any point of the flow cannot depend upon velocity, u, of the main flow but only upon the values of the differential quotients $\frac{du}{dy}$, $\frac{d^2u}{dy^2}$ ...at the point in question and additionally upon distance y of the point from the axis of similarity. Prandtl establishes a simple equation with at first undetermined exponents p and q

$$v_* \sim y^p \left(\frac{d\,u}{d\,y}\right)^q. \tag{58}$$

The sole possible value for which this formula is dimensionally correct is p = 1; q = 1, so that we have

$$v_* = \varkappa \cdot y \frac{d\,u}{d\,y},$$

where $\chi$ signifies a universal constant. Prandtl now takes $\tau$ = const and also $v_*$ = const as the simplest case. It is then possible to integrate the last equation, to obtain

$$u = \frac{v_*}{\varkappa} \ln y + \text{const} = \frac{v_*}{\varkappa} \ln \left(\frac{y}{y_0}\right). \tag{59}$$

It can be stated concerning constant $y_0$ that it has length as a dimension. It is a measure of the density of the laminar layer in the immediate vicinity of

Table 8

$\frac{1}{\sqrt{\varphi}}$ as a function of $\lg(Re_{max}\sqrt{\varphi})$

| Nr. | $U_{max}$ cm/s | $Re_{max}\cdot 10^{-3}$ | $\tau_0$ Dyn/cm² | $Re_{max}\sqrt{\varphi}\cdot 10^{-3}$ | $\frac{1}{\sqrt{\varphi}}$ |
|---|---|---|---|---|---|
| | | **d = 1 cm** | ○ | | |
| 1 | 56,2 | 2,01 | 0,00995 | 0,159 | 12,72 |
| 2 | 63,4 | 2,35 | 0,01240 | 0,183 | 12,88 |
| 3 | 66,6 | 2,46 | 0,01375 | 0,192 | 12,82 |
| 4 | 74,6 | 2,76 | 0,0169 | 0,213 | 12,95 |
| 5 | 80,4 | 2,97 | 0,0190 | 0,225 | 13,18 |
| 6 | 90,0 | 3,33 | 0,0234 | 0,250 | 13,30 |
| 7 | 98,5 | 3,65 | 0,0275 | 0,272 | 13,42 |
| 8 | 125,7 | 4,65 | 0,0425 | 0,337 | 13,77 |
| 9 | 150,8 | 6,14 | 0,0595 | 0,440 | 13,97 |
| 10 | 152,5 | 5,65 | 0,0612 | 0,405 | 13,95 |
| 11 | 174 | 6,44 | 0,0753 | 0,450 | 14,34 |
| 12 | 206 | 7,63 | 0,1000 | 0,518 | 14,71 |
| 13 | 237,8 | 8,80 | 0,1300 | 0,590 | 14,93 |
| 14 | 226 | 10,20 | 0,1806 | 0,690 | 14,79 |
| 15 | 311 | 14,22 | 0,3140 | 0,920 | 15,48 |
| | | **d = 2 cm** | □ | | |
| 16 | 143,5 | 10,62 | 0,0460 | 0,705 | 15,12 |
| 17 | 184,0 | 13,62 | 0,0710 | 0,870 | 15,62 |
| 18 | 218,0 | 16,14 | 0,0983 | 1,030 | 15,74 |
| 19 | 263,0 | 19,48 | 0,1370 | 1,210 | 16,10 |
| 20 | 294,0 | 21,78 | 0,1645 | 1,325 | 16,40 |
| 21 | 265,0 | 22,2 | 0,134 | 1,355 | 16,40 |
| 22 | 290,0 | 24,3 | 0,1552 | 1,463 | 16,60 |
| 23 | 317,0 | 26,6 | 0,184 | 1,595 | 16,69 |
| 24 | 317,3 | 26,6 | 0,186 | 1,598 | 16,65 |
| 25 | 337 | 28,27 | 0,207 | 1,690 | 16,70 |
| 26 | 384 | 32,2 | 0,257 | 1,870 | 17,10 |
| 27 | 424 | 35,5 | 0,311 | 2,070 | 17,18 |
| 28 | 450 | 37,7 | 0,340 | 2,160 | 17,42 |
| 29 | 475 | 39,9 | 0,379 | 2,29 | 17,41 |
| 30 | 512 | 43,0 | 0,437 | 2,460 | 17,50 |
| 31 | 547 | 46,0 | 0,495 | 2,6160 | 17,58 |
| 32 | 596 | 50,0 | 0,580 | 2,825 | 17,65 |
| 33 | 644 | 54,0 | 0,662 | 3,015 | 17,91 |
| 34 | 768 | 64,4 | 0,925 | 3,575 | 18,00 |
| 35 | 827 | 69,4 | 1,032 | 3,775 | 18,35 |
| 36 | 901 | 75,5 | 1,2025 | 4,060 | 18,55 |
| 37 | 975 | 82,6 | 1,3915 | 4,430 | 18,60 |
| 38 | 1040 | 88,1 | 1,5800 | 4,710 | 18,69 |
| 39 | 1155 | 99,5 | 1,9400 | 5,310 | 18,71 |
| 40 | 1254 | 108,2 | 2,2200 | 5,700 | 18,95 |
| | | **d = 3 cm** | △ | | |
| 41 | 483 | 63,5 | 0,371 | 3,54 | 17,94 |
| 42 | 530 | 69,8 | 0,428 | 3,81 | 18,31 |
| 43 | 592 | 78,0 | 0,525 | 4,22 | 18,48 |
| 44 | 657 | 88,8 | 0,652 | 4,70 | 18,80 |
| 45 | 754 | 99,4 | 0,820 | 5,38 | 18,80 |
| 46 | 819 | 108,0 | 0,935 | 5,64 | 19,15 |
| 47 | 901 | 118,6 | 1,140 | 6,20 | 19,08 |
| 48 | 1045 | 137,0 | 1,480 | 7,06 | 19,42 |
| 49 | 1198 | 156,0 | 1,910 | 7,96 | 19,60 |
| 50 | 1304 | 169,0 | 2,245 | 8,60 | 19,62 |
| | | **d = 5 cm** | × | | |
| 51 | 112,5 | 22,8 | 0,0245 | 1,400 | 16,25 |
| 52 | 151,5 | 30,7 | 0,0414 | 1,825 | 16,84 |
| 53 | 210,0 | 42,6 | 0,0736 | 2,340 | 17,48 |
| 54 | 247,0 | 50,2 | 0,0985 | 2,820 | 17,80 |
| 55 | 286,0 | 58,1 | 0,1300 | 3,240 | 17,92 |
| 56 | 87,5 | 18,0 | 0,01520 | 1,125 | 16,04 |
| 57 | 111,8 | 23,0 | 0,0238 | 1,405 | 16,36 |
| 58 | 125,4 | 25,7 | 0,0296 | 1,562 | 16,45 |
| 59 | 142,3 | 28,0 | 0,0373 | 1,680 | 16,65 |
| 60 | 171,0 | 35,2 | 0,0511 | 2,06 | 17,10 |
| 61 | 187,0 | 38,5 | 0,0600 | 2,23 | 17,25 |
| 62 | 218,0 | 44,8 | 0,0788 | 2,55 | 17,55 |
| 63 | 260,0 | 53,5 | 0,1075 | 2,99 | 17,90 |
| 64 | 126,0 | 23,5 | 0,0300 | 1,43 | 16,48 |
| 65 | 172,0 | 32,4 | 0,0529 | 1,92 | 16,88 |
| 66 | 236,0 | 46,1 | 0,0876 | 2,56 | 18,02 |
| 67 | 503,0 | 101,7 | 0,370 | 5,44 | 18,70 |
| 68 | 468,0 | 121,5 | 0,360 | 6,43 | 18,95 |
| 69 | 671,0 | 130,0 | 0,610 | 7,00 | 19,42 |
| 70 | 770,0 | 155,8 | 0,800 | 8,00 | 19,50 |
| 71 | 856,0 | 232,0 | 0,946 | 11,70 | 19,84 |
| 72 | 858,0 | 232,0 | 0,940 | 11,60 | 20,00 |
| 73 | 1068,0 | 285,0 | 1,425 | 14,10 | 20,25 |
| 74 | 1256,0 | 388,0 | 1,850 | 18,70 | 20,82 |
| | | **d = 10 cm** | + | | |
| 75 | 405 | 187,0 | 0,217 | 9,52 | 19,60 |
| 76 | 442 | 204,5 | 0,250 | 10,25 | 19,95 |
| 77 | 458 | 211,5 | 0,273 | 10,70 | 19,80 |
| 78 | 545 | 552,0 | 0,373 | 12,50 | 20,21 |
| 79 | 562 | 261,0 | 0,396 | 12,92 | 20,21 |
| 80 | 596 | 276,0 | 0,440 | 13,60 | 20,32 |
| 81 | 622 | 288,0 | 0,480 | 14,20 | 20,29 |
| 82 | 666 | 309,0 | 0,544 | 15,15 | 20,42 |
| 83 | 693 | 324,0 | 0,585 | 15,80 | 20,50 |
| 84 | 770 | 346,0 | 0,710 | 16,75 | 20,65 |
| 85 | 813 | 366,5 | 0,790 | 17,70 | 20,65 |
| 86 | 896 | 404,0 | 0,943 | 19,36 | 20,85 |
| 87 | 1015 | 420,0 | 1,200 | 20,04 | 20,22 |
| 88 | 948 | 430,5 | 1,055 | 20,60 | 20,88 |
| 89 | 976 | 450,0 | 1,110 | 21,48 | 20,96 |
| 90 | 1085 | 500,0 | 1,340 | 23,60 | 21,19 |
| 91 | 915 | 594,0 | 0,930 | 27,80 | 21,35 |
| 92 | 1443 | 640,0 | 2,270 | 29,80 | 21,50 |
| 93 | 1015 | 660,0 | 1,138 | 30,70 | 21,59 |
| 94 | 1084 | 613,0 | 1,305 | 28,60 | 21,45 |
| 85 | 1155 | 760,0 | 1,440 | 34,80 | 21,80 |
| 96 | 1120 | 780,0 | 1,350 | 35,70 | 21,82 |
| 97 | 1170 | 825,0 | 1,240 | 37,50 | 21,98 |
| 98 | 1045 | 746,0 | 1,176 | 34,20 | 21,82 |
| 99 | 793 | 555,0 | 0,695 | 25,80 | 21,70 |
| 100 | 882 | 617,0 | 0,850 | 28,50 | 21,65 |
| 101 | 958 | 671,0 | 1,000 | 31,00 | 21,65 |
| 102 | 1108 | 775,0 | 1,305 | 35,40 | 21,92 |
| 103 | 306 | 141,0 | 0,1284 | 7,33 | 19,26 |
| 104 | 336 | 155,0 | 0,1530 | 7,98 | 19,42 |
| 105 | 364 | 168,0 | 0,177 | 8,59 | 19,57 |
| 106 | 384 | 177,0 | 0,197 | 9,05 | 19,55 |
| 107 | 846 | 347,0 | 0,850 | 16,75 | 20,71 |
| 108 | 937 | 387,5 | 1,040 | 18,70 | 20,76 |
| 109 | 1168 | 519,0 | 1,557 | 24,55 | 21,25 |
| 110 | 1528 | 670,0 | 2,540 | 31,00 | 21,65 |
| 111 | 1949 | 885,0 | 4,000 | 40,3 | 22,00 |
| 112 | 2020 | 920,0 | 4,170 | 41,6 | 22,13 |
| 113 | 1620 | 978,0 | 2,675 | 44,75 | 22,38 |
| 114 | 2212 | 1005,0 | 5,000 | 45,2 | 22,25 |
| 115 | 1869 | 1169,0 | 3,550 | 52,0 | 22,42 |
| 116 | 1870 | 1183,0 | 3,540 | 52,9 | 22,44 |
| 117 | 2019 | 1220,0 | 4,030 | 54,0 | 22,65 |
| 118 | 2207 | 1318,0 | 4,780 | 57,6 | 22,82 |
| 119 | 2208 | 1345,0 | 4,850 | 59,2 | 22,68 |
| 120 | 2465 | 1135,0 | 6,250 | 51,0 | 22,31 |
| 121 | 2306 | 1470,0 | 5,200 | 64,2 | 22,80 |
| 122 | 2446 | 1650,0 | 5,800 | 71,5 | 23,0 |
| 123 | 2463 | 1610,0 | 5,86 | 70,0 | 23,0 |
| 124 | 2525 | 1701,0 | 6,04 | 73,5 | 23,1 |
| 125 | 2756 | 1930,0 | 7,20 | 83,2 | 23,2 |

Key for Table 8:

$\psi = \frac{\tau_0}{q}$ = Coefficient of resistance with reference to maximum velocity; $\tau_0$ = shearing stress at the wall; $q = \varrho \frac{U^2}{2}$ = pressure lead of maximum velocity; $\varrho$ = density; $Re = \frac{U \cdot r}{\nu}$ = Reynolds number of maximum velocity; r = pipe radius; $\nu$ = kinematic viscosity.

the wall. The sole possible length that can be formed from the characteristic constant of turbulent flow is $\frac{\nu}{v_*}$. We therefore write

$$y_0 = \text{Zahl} \cdot \frac{\nu}{v_*} = m \frac{\nu}{v_*}; \qquad (60)$$

Therewith from (59) $u = \frac{v_*}{\varkappa} \left\{ \ln \frac{y \cdot v_*}{\nu} - \ln m \right\}$

or $$\frac{u}{v_*} = \frac{1}{\varkappa} \left\{ \ln \frac{y \cdot v_*}{\nu} - \ln m \right\}, \qquad (61)$$

and with $\frac{u}{v_*} = \varphi$ und $\frac{y \cdot v_*}{\nu} = \eta$

we have $$\varphi = A + B \ln \eta. \qquad (62)$$

The measurements produce $A = -\frac{1}{\varkappa} \ln m = 5{,}5$, $B = \frac{1}{\varkappa} = 2{,}5$, $\varkappa = 0{,}40$ and $m = \frac{1}{9}$.

The density $\delta$ of the laminar layer is therefore of the order of magnitude

$$y_0 = \frac{1}{9} \frac{\nu}{v_*},$$

whereby nothing can yet be stated concerning the numerical factor supervening at $y_0$. Equation (62) is exactly the same expression for velocity distribution that von Kármán arrives at with his hypothesis of similarity, which moreover was to be anticipated.

## 6. LAW OF RESISTANCE

The coefficient of resistance $\lambda = \frac{dp}{dx} \cdot \frac{d}{q}$ which has already been defined was determined as a function of the Reynolds number over a large range and is presented in logarithmic scale in Fig. 34. The plotted points (Table 9) represent the value log (1000 $\lambda$) beginning with very low Reynolds number of about $3 \cdot 10^3$ on to the upper limit. The measured values up to Re $100 \cdot 10^3$ (log Re = 5) are in good agreement with the Blasius formula $\lambda_B = \frac{0.316}{Re^{1/4}}$ which in this figure is represented by curve 1. Above this limit the measured $\lambda$-values deviate more and more from the Blasius line with increasing Reynolds

number. Lees (ref. 27) structured a formula $\lambda = a + \frac{b}{Re^n}$ from the measurements by Stanton and Pannell, which extended to Re $460 \cdot 10^3$ (log Re = 5.67), namely $\lambda = 0.0072 + \frac{0.6104}{\text{Re } 0.35.}$ Since our measurement results are in agreement with those of Stanton and Pannell, they are also represented in this area by the Lees formula. Outside this range our measurements deviate from the resistance values of the Lees curve, indicated by 2 in Fig. 34. As can be seen from this figure, the deviation is larger with increasing Reynolds number. Recently Schiller and Hermann (ref. 28) set up the formula of approximation

$$\psi = 0{,}00270 + \frac{0{,}161}{Re^{0{,}3}}$$

on the basis of their measurements and ours, according to the Lees formula $\lambda = \alpha + \frac{b}{Re^n}$. In the present formula $\Psi = \frac{\lambda}{2}$ and $Re = \frac{\bar{u} \cdot r}{\nu}$. Since it is common generally to relate the Reynolds number and the coefficient of resistance to the pipe diameter, we recalculated the Schiller (ref. 29) formula on this basis. This produces the formula

$$\lambda = 0{,}0054 + \frac{0{,}396}{Re^{0{,}3}}, \qquad (63)$$

which is represented in Fig. 34 by the dot-and-dash line 3. It is to be noted that the Schiller curve coincides with that of Stanton and Pannell up to Re $4.6 \cdot 10^5$ (log Re = 5.67). From there on the Schiller curve agrees with the values determined by us to about $Re = \frac{\bar{u} \cdot d}{\nu} = 2.5 \cdot 10^6$ or log Re = 6.4.

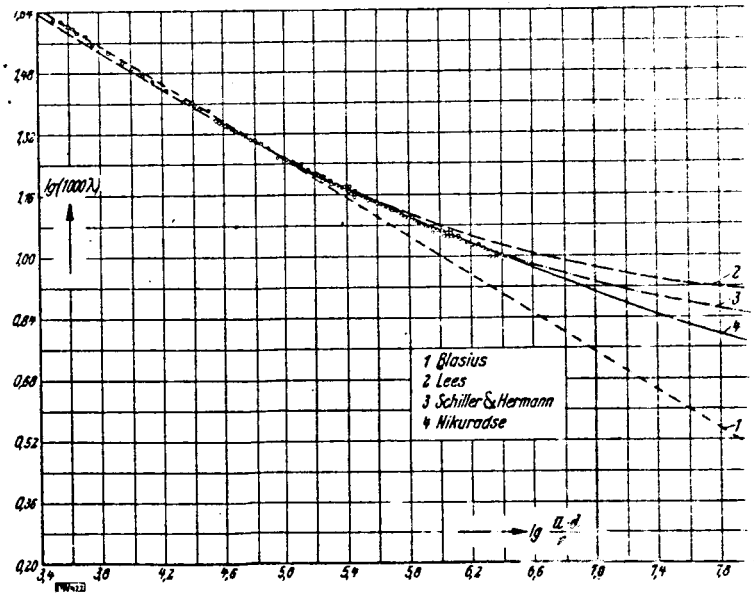


Fig. 34. lg (1000λ) as a function of $\left(\frac{\bar{u} \cdot d}{\nu}\right)$

Table 9.



log $\lambda$ or $\frac{u}{U_{max}}$ as a function of log Re and as a function of log $\frac{Re}{\sqrt{\lambda}}$

$\bar{u}$ = mean velocity

$\nu = \frac{\mu}{\varrho}$ = kinematic viscosity;

$\mu$ = viscosity constant;

$\varrho$ = density;

Re = Reynolds number;

d = pipe diameter

$\frac{dp}{dx}$ = pressure drop

$\lambda = \frac{dp}{dx} \cdot \frac{d}{q}$ = coefficient of resistance

$q = \varrho \frac{\bar{u}^2}{2}$ = head pressure of mean velocity;

$U_{max}$ = maximum velocity.

| Nr. | $u$ cm/s | $\nu$ cm²/s | $Re \cdot 10^{-3}$ | $\frac{dp}{dx}$ Dyn/cm³ | $\lambda$ | $Re\sqrt{\lambda} \cdot 10^{-3}$ | $\frac{1}{\sqrt{\lambda}}$ | $\frac{\bar{u}}{U_{max}}$ |
|---|---|---|---|---|---|---|---|---|
| | | | | **d = 1 cm** | | | | |
| 1 | 42,8 | 0,0140 | 3,07 | 0,0398 | 0,0426 | 0,634 | 4,85 | 0,760 |
| 2 | 48,5 | 0,0135 | 3,59 | 0,0496 | 0,0414 | 0,780 | 4,92 | 0,765 |
| 3 | 51,4 | 0,0135 | 3,81 | 0,0550 | 0,0408 | 0,770 | 4,95 | 0,770 |
| 4 | 57,6 | 0,0135 | 4,27 | 0,0676 | 0,0399 | 0,854 | 5,00 | 0,771 |
| 5 | 62,0 | 0,0135 | 4,60 | 0,0760 | 0,0388 | 0,906 | 5,08 | 0,771 |
| 6 | 70,2 | 0,0135 | 5,20 | 0,0936 | 0,0372 | 1,004 | 5,18 | 0,780 |
| 7 | 76,9 | 0,0135 | 5,70 | 0,1100 | 0,0363 | 1,086 | 5,25 | 0,780 |
| 8 | 98,5 | 0,0135 | 7,30 | 0,1700 | 0,0343 | 1,352 | 5,40 | 0,784 |
| 9 | 118,8 | 0,0135 | 8,80 | 0,238 | 0,0326 | 1,590 | 5,54 | 0,788 |
| 10 | 121,0 | 0,0135 | 8,97 | 0,245 | 0,0329 | 1,626 | 5,52 | 0,794 |
| 11 | 137,5 | 0,0135 | 10,9 | 0,3012 | 0,0311 | 1,800 | 5,67 | 0,791 |
| 12 | 163,3 | 0,0135 | 12,1 | 0,400 | 0,0294 | 2,075 | 5,83 | 0,793 |
| 13 | 189,0 | 0,0135 | 14,0 | 0,520 | 0,0285 | 2,362 | 5,92 | 0,795 |
| 14 | 226,0 | 0,0135 | 16,7 | 0,723 | 0,0278 | 2,785 | 6,00 | 0,811 |
| 15 | 311,0 | 0,0136 | 23,0 | 1,255 | 0,0254 | 3,665 | 6,28 | 0,815 |
| | | | | **d = 2 cm** | | | | |
| 16 | 114,6 | 0,0135 | 17,0 | 0,092 | 0,0274 | 2,81 | 6,04 | 0,800 |
| 17 | 148,4 | 0,0135 | 22,0 | 0,142 | 0,0253 | 3,50 | 6,29 | 0,807 |
| 18 | 175,5 | 0,0135 | 26,0 | 0,1966 | 0,0250 | 4,11 | 6,33 | 0,805 |
| 19 | 212,5 | 0,0135 | 31,5 | 0,274 | 0,0237 | 4,85 | 6,50 | 0,808 |
| 20 | 240,0 | 0,0135 | 35,6 | 0,329 | 0,0224 | 5,33 | 6,68 | 0,816 |
| 21 | 214,4 | 0,0119 | 36,0 | 0,264 | 0,02243 | 5,40 | 6,68 | 0,809 |
| 22 | 233,6 | 0,0119 | 39,2 | 0,3104 | 0,0223 | 5,85 | 6,70 | 0,806 |
| 23 | 258,0 | 0,0119 | 43,2 | 0,368 | 0,02274 | 6,51 | 6,64 | 0,814 |
| 24 | 259,6 | 0,0117 | 44,4 | 0,372 | 0,0216 | 6,53 | 6,80 | 0,818 |
| 25 | 275,8 | 0,0119 | 46,4 | 0,414 | 0,0212 | 6,76 | 6,86 | 0,818 |
| 26 | 315 | 0,0119 | 53,0 | 0,514 | 0,0196 | 7,42 | 7,14 | 0,820 |
| 27 | 349 | 0,0119 | 58,7 | 0,622 | 0,0201 | 8,33 | 7,06 | 0,823 |
| 28 | 370 | 0,0119 | 62,2 | 0,680 | 0,0188 | 8,52 | 7,30 | 0,822 |
| 29 | 392 | 0,0119 | 66,0 | 0,758 | 0,0194 | 9,19 | 7,18 | 0,825 |
| 30 | 425 | 0,0119 | 71,4 | 0,874 | 0,0190 | 9,84 | 7,26 | 0,830 |
| 31 | 454 | 0,0119 | 76,2 | 0,990 | 0,01885 | 10,45 | 7,28 | 0,830 |
| 32 | 495 | 0,0119 | 83,3 | 1,160 | 0,0188 | 11,41 | 7,29 | 0,831 |
| 33 | 533,6 | 0,0119 | 89,6 | 1,324 | 0,0183 | 12,11 | 7,40 | 0,829 |
| 34 | 638 | 0,0119 | 107,3 | 1,850 | 0,0178 | 14,33 | 7,50 | 0,831 |
| 35 | 687 | 0,0119 | 115,2 | 2,064 | 0,0172 | 15,12 | 7,62 | 0,831 |
| 36 | 752 | 0,0119 | 126,5 | 2,405 | 0,0167 | 16,35 | 7,74 | 0,835 |
| 37 | 811 | 0,0118 | 137,5 | 2,783 | 0,01665 | 17,74 | 7,76 | 0,832 |
| 38 | 863 | 0,0118 | 146,0 | 3,16 | 0,0166 | 18,80 | 7,77 | 0,830 |
| 39 | 972 | 0,0116 | 168,0 | 3,88 | 0,01614 | 21,32 | 7,88 | 0,842 |
| 40 | 1053 | 0,0116 | 182,0 | 4,44 | 0,0157 | 22,93 | 7,94 | 0,840 |
| | | | | **d = 3 cm** | | | | |
| 41 | 402 | 0,0114 | 106,0 | 0,495 | 0,0180 | 14,22 | 7,46 | 0,832 |
| 42 | 439 | 0,0114 | 115,5 | 0,570 | 0,0174 | 15,25 | 7,58 | 0,828 |
| 43 | 488 | 0,0114 | 128,5 | 0,700 | 0,0173 | 16,90 | 7,60 | 0,824 |
| 44 | 559 | 0,0114 | 147,0 | 0,870 | 0,01638 | 18,81 | 7,82 | 0,850 |
| 45 | 627 | 0,0114 | 165,0 | 1,092 | 0,01638 | 21,11 | 7,82 | 0,831 |
| 46 | 688 | 0,0114 | 181,0 | 1,246 | 0,01549 | 22,54 | 8,04 | 0,840 |
| 47 | 756 | 0,0114 | 199,0 | 1,520 | 0,01560 | 24,86 | 8,01 | 0,839 |
| 48 | 879 | 0,0114 | 231,0 | 1,970 | 0,01500 | 28,30 | 8,16 | 0,841 |
| 49 | 1010 | 0,0115 | 266,0 | 2,545 | 0,01470 | 32,30 | 8,24 | 0,843 |
| 50 | 1106 | 0,0115 | 288,0 | 2,990 | 0,01435 | 34,50 | 8,35 | 0,848 |
| | | | | **d = 5 cm** | | | | |
| 51 | 91,4 | 0,01233 | 37,0 | 0,0196 | 0,0230 | 5,61 | 6,59 | 0,812 |
| 52 | 124,4 | 0,01233 | 50,3 | 0,0331 | 0,02104 | 7,30 | 6,90 | 0,818 |
| 53 | 172,0 | 0,01230 | 70,0 | 0,0583 | 0,0195 | 9,78 | 7,16 | 0,819 |
| 54 | 203,5 | 0,01230 | 82,6 | 0,0787 | 0,0186 | 11,26 | 7,34 | 0,819 |
| 55 | 237,0 | 0,01230 | 96,2 | 0,1020 | 0,01815 | 12,96 | 7,44 | 0,829 |
| 56 | 71,2 | 0,01214 | 29,3 | 0,01215 | 0,0226 | 4,40 | 6,66 | 0,814 |

Table 9

lg λ or $\frac{u}{U_{max}}$ dependent on lg Re and $\frac{1}{\sqrt{\lambda}}$ dependent on lg Re $\sqrt{\lambda}$

| Nr. | $\bar{u}$ cm/s | $\bar{\nu}$ cm²/s | $Re \cdot 10^{-3}$ | $\frac{dp}{dx}$ Dyn/cm³ | $\lambda$ | $Re\sqrt{\lambda} \cdot 10^{-3}$ | $\frac{1}{\sqrt{\lambda}}$ | $\frac{\bar{u}}{U_{max}}$ |
|---|---|---|---|---|---|---|---|---|
| | | | | **d = 5 cm** (continuation) | | | | |
| 57 | 90,8 | 0,01214 | 37,4 | 0,0190 | 0,0226 | 5,62 | 6,66 | 0,812 |
| 58 | 102,5 | 0,0122 | 42,0 | 0,0237 | 0,0220 | 6,23 | 6,75 | 0,817 |
| 59 | 116,5 | 0,0122 | 47,7 | 0,0298 | 0,02146 | 6,98 | 6,83 | 0,819 |
| 60 | 140,0 | 0,01215 | 57,6 | 0,0409 | 0,02042 | 8,23 | 7,00 | 0,819 |
| 61 | 153,5 | 0,01215 | 63,2 | 0,0480 | 0,01990 | 8,92 | 7,09 | 0,821 |
| 62 | 179,5 | 0,01215 | 73,8 | 0,0630 | 0,01915 | 10,21 | 7,23 | 0,823 |
| 63 | 214,4 | 0,01214 | 88,3 | 0,0860 | 0,01830 | 11,95 | 7,40 | 0,825 |
| 64 | 103,0 | 0,0134 | 38,4 | 0,0240 | 0,0222 | 5,72 | 6,71 | 0,817 |
| 65 | 141,0 | 0,0133 | 53,0 | 0,0423 | 0,02085 | 7,65 | 6,93 | 0,820 |
| 66 | 194,5 | 0,0128 | 76,0 | 0,0701 | 0,0182 | 10,25 | 7,42 | 0,824 |
| 67 | 423,5 | 0,01235 | 171,5 | 0,296 | 0,01617 | 21,8 | 7,86 | 0,842 |
| 68 | 395,0 | 0,00925 | 213,4 | 0,250 | 0,01567 | 26,71 | 7,99 | 0,844 |
| 69 | 570,0 | 0,0097 | 294 | 0,488 | 0,01470 | 35,63 | 8,26 | 0,849 |
| 70 | 652,0 | 0,01235 | 264 | 0,640 | 0,01475 | 32,18 | 8,24 | 0,847 |
| 71 | 733 | 0,00925 | 396 | 0,757 | 0,0138 | 41,52 | 8,51 | 0,856 |
| 72 | 740,0 | 0,00925 | 400 | 0,752 | 0,01314 | 46,40 | 8,63 | 0,862 |
| 73 | 912,8 | 0,00925 | 493,4 | 1,140 | 0,01325 | 56,8 | 8,69 | 0,855 |
| 74 | 1082,0 | 0,0081 | 670 | 1,470 | 0,01229 | 74,3 | 9,02 | 0,861 |
| | | | | **d = 10 cm** | | | | |
| 75 | 345,9 | 0,01083 | 318,9 | 0,0868 | 0,01421 | 38,0 | 8,39 | 0,854 |
| 76 | 377,1 | 0,01080 | 348,6 | 0,1008 | 0,01388 | 41,06 | 8,49 | 0,853 |
| 77 | 392,7 | 0,01083 | 363,0 | 0,1092 | 0,01390 | 42,80 | 8,48 | 0,857 |
| 78 | 466,3 | 0,01080 | 431,5 | 0,1492 | 0,01342 | 50,00 | 8,62 | 0,856 |
| 79 | 482,8 | 0,01079 | 446,8 | 0,1582 | 0,01334 | 51,6 | 8,66 | 0,859 |
| 80 | 510,0 | 0,01079 | 472,0 | 0,1760 | 0,01328 | 54,40 | 8,67 | 0,855 |
| 81 | 533,2 | 0,01080 | 493,7 | 0,1920 | 0,01324 | 56,82 | 8,69 | 0,857 |
| 82 | 569,1 | 0,01079 | 562,6 | 0,2175 | 0,01320 | 60,50 | 8,71 | 0,855 |
| 83 | 602,0 | 0,01072 | 597,0 | 0,2340 | 0,01277 | 63,30 | 8,87 | 0,869 |
| 84 | 660,3 | 0,0110 | 600,0 | 0,2840 | 0,01277 | 67,80 | 8,86 | 0,858 |
| 85 | 704,0 | 0,0111 | 634 | 0,316 | 0,0125 | 70,90 | 8,95 | 0,866 |
| 86 | 769,8 | 0,0110 | 700 | 0,387 | 0,0129 | 79,50 | 8,80 | 0,859 |
| 87 | 876 | 0,0121 | 725 | 0,480 | 0,01228 | 80,40 | 9,02 | 0,863 |
| 88 | 810 | 0,0111 | 737 | 0,422 | 0,0126 | 82,80 | 8,91 | 0,854 |
| 89 | 843,4 | 0,01094 | 771 | 0,444 | 0,01227 | 85,42 | 9,02 | 0,864 |
| 90 | 940,0 | 0,01086 | 865 | 0,536 | 0,01188 | 94,24 | 9,18 | 0,866 |
| 91 | 790 | 0,0077 | 1025 | 0,372 | 0,01170 | 110,9 | 9,25 | 0,863 |
| 92 | 1248 | 0,01125 | 1108 | 0,92 | 0,01159 | 119,3 | 9,29 | 0,864 |
| 93 | 882 | 0,0077 | 1148 | 0,455 | 0,01146 | 123,0 | 9,34 | 0,869 |
| 94 | 944 | 0,0077 | 1225 | 0,522 | 0,01150 | 131,25 | 9,33 | 0,871 |
| 95 | 1005 | 0,0076 | 1320 | 0,576 | 0,01118 | 139,60 | 9,46 | 0,870 |
| 96 | 982 | 0,0072 | 1364 | 0,540 | 0,0110 | 143,20 | 9,53 | 0,877 |
| 97 | 1020 | 0,0071 | 1438 | 0,596 | 0,01122 | 152,3 | 9,45 | 0,872 |
| 98 | 900 | 0,0070 | 1285 | 0,471 | 0,01144 | 137,5 | 9,35 | 0,861 |
| 99 | 685 | 0,0070 | 979 | 0,278 | 0,01161 | 105,0 | 9,28 | 0,864 |
| 100 | 761 | 0,0070 | 1088 | 0,340 | 0,0115 | 116,7 | 9,33 | 0,862 |
| 101 | 830 | 0,0070 | 1185 | 0,400 | 0,0114 | 126,6 | 9,37 | 0,866 |
| 102 | 958 | 0,0070 | 1368 | 0,522 | 0,01115 | 144,4 | 9,47 | 0,865 |
| 103 | 259 | 0,01087 | 238,8 | 0,514 | 0,0150 | 29,25 | 8,17 | 0,846 |
| 104 | 286,8 | 0,01083 | 264,4 | 0,612 | 0,01459 | 31,92 | 8,29 | 0,854 |
| 105 | 309,5 | 0,01083 | 285,4 | 0,708 | 0,01446 | 34,30 | 8,32 | 0,850 |
| 106 | 325,4 | 0,01083 | 300,0 | 0,788 | 0,01457 | 36,24 | 8,28 | 0,847 |
| 107 | 726,0 | 0,0122 | 595 | 0,340 | 0,01265 | 66,90 | 8,90 | 0,858 |
| 108 | 806 | 0,0121 | 666 | 0,416 | 0,01255 | 74,60 | 8,93 | 0,860 |
| 109 | 1013 | 0,01125 | 900 | 0,623 | 0,0119 | 98,10 | 9,17 | 0,867 |
| 110 | 1325 | 0,01125 | 1178 | 1,015 | 0,0113 | 125,2 | 9,41 | 0,867 |
| 111 | 1691 | 0,0110 | 1539 | 1,600 | 0,01098 | 161,4 | 9,54 | 0,868 |
| 112 | 1765 | 0,0110 | 1600 | 1,670 | 0,0105 | 164,0 | 9,76 | 0,874 |
| 113 | 1410 | 0,0083 | 1700 | 1,070 | 0,01060 | 175,1 | 9,71 | 0,870 |
| 114 | 1926 | 0,0083 | 1850 | 2,000 | 0,01058 | 190,4 | 9,72 | 0,871 |
| 115 | 1630 | 0,0080 | 2038 | 1,420 | 0,01043 | 208,0 | 9,80 | 0,872 |
| 116 | 1630 | 0,0079 | 2062 | 1,415 | 0,01045 | 210,5 | 9,79 | 0,872 |
| 117 | 1758 | 0,00825 | 2130 | 1,615 | 0,01029 | 216,0 | 9,87 | 0,875 |
| 118 | 1940 | 0,0084 | 2310 | 1,910 | 0,00995 | 230,8 | 10,02 | 0,879 |
| 119 | 1930 | 0,0082 | 2351 | 1,94 | 0,01021 | 237,5 | 9,89 | 0,874 |
| 120 | 2150 | 0,0110 | 1964 | 2,199 | 0,0106 | 202,3 | 9,71 | 0,872 |
| 121 | 2010 | 0,0078 | 2580 | 2,050 | 0,00995 | 257,2 | 10,02 | 0,874 |
| 122 | 2150 | 0,0079 | 2722 | 2,317 | 0,0098 | 269,5 | 10,10 | 0,879 |
| 123 | 2162 | 0,0077 | 2810 | 2,345 | 0,00985 | 279,2 | 10,06 | 0,878 |
| 124 | 2220 | 0,0074 | 3000 | 2,470 | 0,00988 | 298,2 | 10,06 | 0,879 |
| 125 | 2425 | 0,0075 | 3230 | 2,88 | 0,00960 | 321,0 | 10,07 | 0,880 |

From log Re = 6.4 on the Schiller curve deviates from ours. This deviation increases with increasing Reynolds number. The deviations of the Lees and Schiller-Hermann formulas from the measured curves occur because the formulas are calculated directly from the measurements and therefore they are only correct to the extent of the experiments. We have now succeded by another method which is described below in establishing a formula of approximation which relates to the upper limit of the Blasius law, and whose validity to Re = $1 \cdot 10^8$ (log Re = 8.0) seems to be confirmed. This formula is represented by curve 4. It will be noted that this curve at the upper limit (log Re = 6.4) deviates downward from the Schiller Hermann curve, and at Re $1 \cdot 10^8$ it deviates more pronouncedly from the Schiller curve than the latter does from the Lees curve.

Previous methods only give us formulas for the range that has been tested experimentally. Von Kármán's formula on page 43 suggests a similarly constructed formula, however, namely /32

$$\frac{1}{\sqrt{\lambda}} = A + B \lg (Re\sqrt{\lambda}). \qquad (61)$$

The distinction lies in the fact that von Kármán relates the resistance and Reynolds number to maximum velocity and pipe radius, whereas we use the mean velocity and the pipe diameter. If we write $\frac{1}{\sqrt{\lambda}} = y$ and log (Re $\sqrt{\lambda}$)$= x$, )

the equation then takes the form

$$y = A + Bx$$

In Fig. 35, $y = \frac{1}{\sqrt{\lambda}}$ is plotted according to the measurements as a function of $x$ = log (Re $\sqrt{\lambda}$ ) (Table 9). We thus obtain straight line 1 and for constants

A and B we have the values A = -0.8 and B = 2.0. In Fig. 35, the experimental results of various investigators are plotted, whereby in laying down the straight lines less weight is placed on the Ombeck values because these experiments that were performed with air are somewhat less certain on account of the changes in volume of the air. From x = log (Re $\sqrt{\lambda}$ ) we calculated the value Re $\sqrt{\lambda}$, divided by $\frac{1}{y} = \sqrt{\lambda}$ and obtained the Reynolds number. Thus we have obtained a dependence of the coefficient of resistance upon the Reynolds number from the above equation $\lambda = f(Re)$.

It can be anticipated with a certain probability that we may extrapolate rather widely from this formula, even though not to R = ∞ as in the von Karman formula.

In Fig. 36 the relationship $\lambda = f(Re)$ is shown as it appears if extrapolation is carried out to high Reynolds numbers, to Re = $1 \cdot 10^8$ with the constants A and B as determined by measurement.

We can now apply this formula in a similar manner to obtain a more convenient formula of approximation for $\lambda$ than Lees and Schiller and Hermann have done on the basis of experiments. The range of the new formula is to begin where the Blasius formula leaves off. At the end of the range we establish Re = $1 \cdot 10^8$.

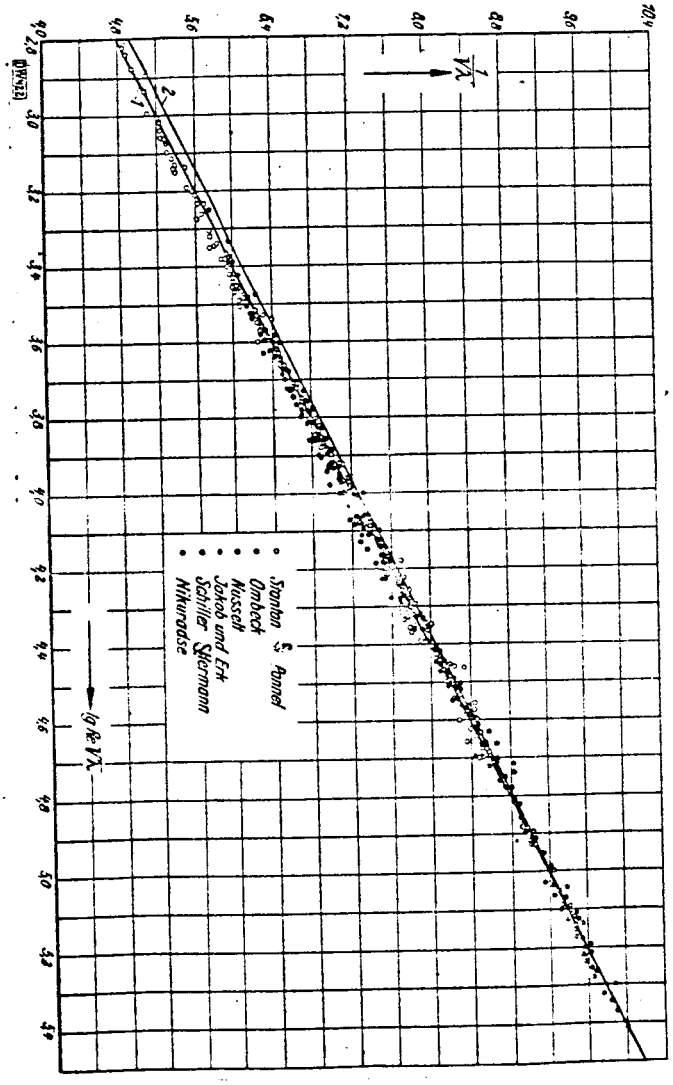


Fig. 35. $\frac{1}{\sqrt{\lambda}}$ as a function of lg (Re $\sqrt{\lambda}$ )

From curve 4 of Fig. 34 we find for the constants of the approximation formula $\lambda = a + \frac{b}{Re^n}$,

the values $a = 0.0032$ $b = 0.221$ $n = 0.237$;

and thereby $\lambda = 0{,}0032 + \frac{0{,}221}{Re^{0{,}237}}$. (65)

In order to test the above formulas of Blasius, Lees, Schiller, Hermann and ourselves, in Fig. 37 the relationship $\frac{1}{\sqrt{\lambda}} = f[\lg(Re\sqrt{\lambda})]$ was calculated and plotted according to the respective formulas. The plotted points are calculated from our measured values. Below log $Re\sqrt{\lambda}$ = 3.7 the values of $\frac{1}{\sqrt{\lambda}}$ are below the straight line. This is to be explained in that the effect of viscosity at these Reynolds numbers is substantial. Above the indicated limits the effect of viscosity is negligible and the experimental points lie on the straight line. Curve 1 calculated by the Blasius formula deviates from straight line 4 below log ( $Re\sqrt{\lambda}$ ) = 4.0 (corresponding to about Re $40 \cdot 10^3$). Above this indicated Reynolds number to about log ($Re\sqrt{\lambda}$) = 5.1 (Corresponding to a Reynolds number of about Re = $100 \cdot 10^3$) the curve is superimposed on straight line 4. In its further course, curve 1 deviates upward pronouncedly from straight line 4. In addition curve 1 shows, in agreement with earlier findings, that the Blasius law is only valid to log ( $Re\sqrt{\lambda}$ )/33 = 5.1 corresponding to a Reynolds number of Re = $100 \cdot 10^3$. Curves 2 and 3 are calculated according to the formulas of Lees and Schiller and deviate at log ($Re\sqrt{\lambda}$) = 4.7, (Re about $4.5 \cdot 10^5$), and at log ($Re\sqrt{\lambda}$) = 5.25 (Reynolds number about $1.9 \cdot 10^6$) from the straight lines. If we plot the resistance values of curve 4 for Re $> 1 \cdot 10^8$ a corresponding deviation occurs here also.

For the following calculations of approximation still another straight line (2, Fig. 35) is plotted with the equation

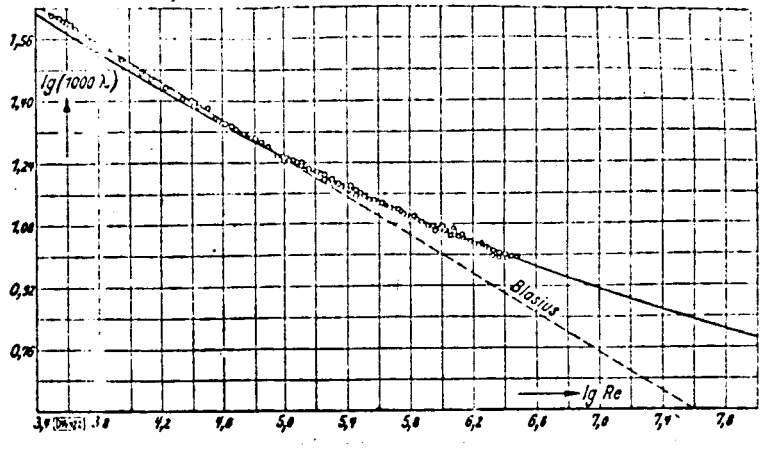


Fig. 36. lg (1000 $\lambda$) as a function of lg Re

7. Relation between the mean and the maximum velocity

a) According to a proposal of Prof. Prandtl the von Kármán law of resistance, Equation (56b) is correlated with our Equation (64b) by means of Equation (54):

$$\frac{U-u}{v_*}=f(y/r).$$

From this the mean velocity $\bar{u}$ can be determined by graphic integration, with $\frac{U-u}{v^*}$ as function of $(y/r)^2$, so that we obtain

$$\frac{U-\bar{u}}{v_*}=\text{number}=\beta. \qquad (66)$$

By developing the integration we obtained $\beta = 4.03$. With this relationship we obtained the connection between the von Kármán law of resistance and ours in the following manner. From von Kármán's Equation (56b), we introduce

$$Re_{max}=\frac{U\cdot r}{\nu} \text{ and } \sqrt{\psi}=1{,}414\,\frac{v_*}{U}$$

it follows that

$$\frac{U}{v_*}=A+B\lg\left[1{,}414\left(\frac{v_*\cdot r}{\nu}\right)\right]$$

or

$$\frac{U}{v_*}=A'+B\lg\left(\frac{v_*\,r}{\nu}\right). \qquad (67)$$

Analogously, from our Equation (64b), if we introduce

$$Re=\frac{\bar{u}\cdot 2r}{\nu} \text{ and } \sqrt{\lambda}=2{,}828\,\frac{v_*}{\bar{u}}$$

we obtain

$$\frac{\bar{u}}{v_*}=a+b\lg\left[2{,}828\left(\frac{v_*\,r}{\nu}\right)\right]$$

or

$$\frac{\bar{u}}{v_*} = a' + b \lg\left(\frac{v_* r}{\nu}\right). \qquad (68)$$

Equation (66) now requires that constants B and b in equations (67) and (68) be in agreement. This equation can be used by balancing between the different diagrams to derive the best value of B = b. From this balancing, reference is made to the previously mentioned straight line 2 in the figures. The optimum value of B = b was 5.52. With this we determine further

$$A = 5.87 \qquad a = -1.555$$

and hence

$$A' = 6.68 \qquad a' = 2.63$$

By introduction of these values and subtraction of Equation (67) and (68) it then follows that

$$\frac{U - \bar{u}}{v_*} = 4{,}08\,, \qquad (69)$$

which is in good agreement with the earlier result. In fig. 38 the experimental values $\frac{U}{v^*}$ and $\frac{\bar{u}}{v^*}$ are plotted as function of log $\frac{v^* r}{\nu}$. The last two straight lines laid down are parallel and the difference of the function value is on the average 4.03, as above. The equation for universal velocity

$$\varphi = c_1 + c_2 \lg \eta$$

distribution on theoretical grounds (ref. 30) ought to agree with equations (67) and (68) if the straight line $\varphi = \varphi(\eta)$ is plotted only through the points near the wall, insofar as $c_2 = b$. In fact the straight line

$$\varphi = 5{,}84 + 5{,}52 \lg \eta$$

is in good agreement with the experimental points near the wall. The value 5.52 corresponds to a value of von Karman's universal constants.

$$\varkappa = \frac{2{,}3025}{5{,}52} = 0{,}417\,.$$

b) By division of equation (67) and (68) $\frac{\bar{u}}{U}$ is obtained as function

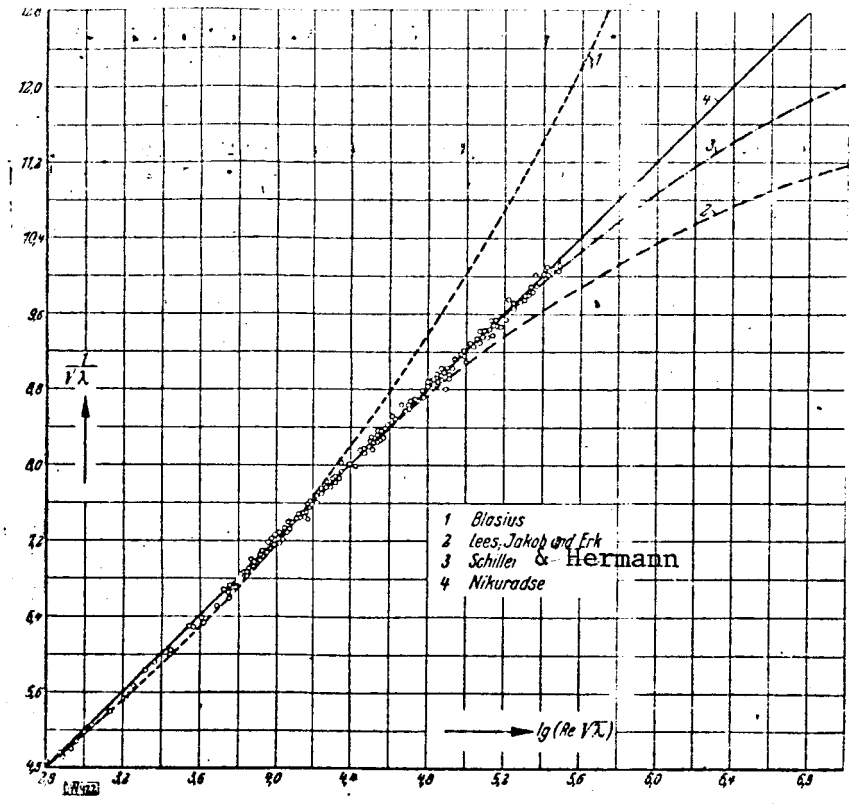


Fig. 37. $\frac{1}{\sqrt{\lambda}}$ as a function of log $(Re\sqrt{\lambda})$

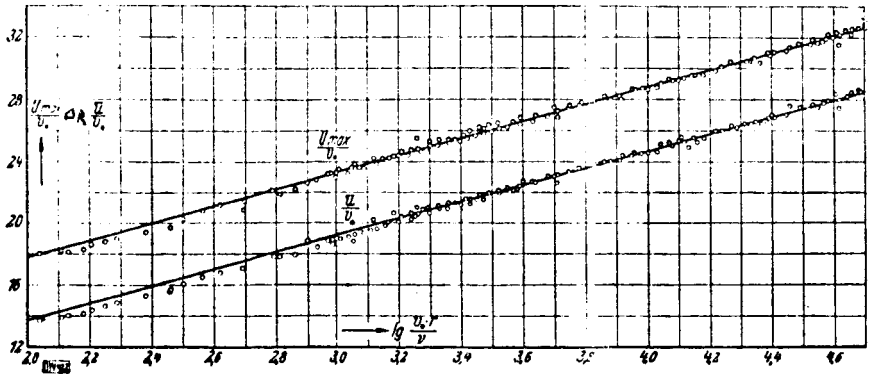


Fig. 38 $\frac{U_{max}}{v_*}$ & $\frac{\bar{u}}{v_*}$ as a function of log $\left(\frac{v_* \cdot r}{\nu}\right)$

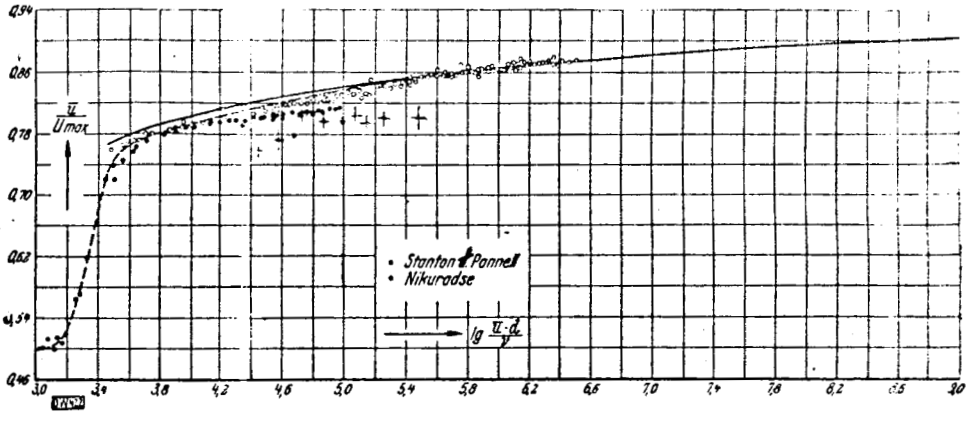


Fig. 39 $\frac{\bar{u}}{U_{max}}$ as a function of $\log\left(\frac{\bar{u}\cdot d}{\nu}\right)$

of $\frac{v^*r}{\nu}$ but therewith also as function of the Reynolds number that is expressed by $\frac{v^*r}{\nu}$ since

$$Re = \frac{2\bar{u}r}{\nu} = \frac{2\bar{u}}{v_*}\cdot\frac{v_*r}{\nu} = 2\cdot 2{,}828\left(\frac{v_*r}{\nu}\right)\frac{1}{\sqrt{\lambda}}.$$

$\frac{1}{\sqrt{\lambda}}$ can however also be expressed by means of equation (64a) by $\frac{v^*r}{\nu}$. In Fig. 39 the thus obtained equation

$$\frac{\bar{u}}{U} = f\left(\frac{\bar{u}\cdot d}{\nu}\right)$$

for Reynolds numbers $3\cdot10^3$ to $1\cdot10^8$ are drawn in. In addition, the experimental values of Stanton and Pannell and our own are plotted (table 9). In the zone of developed laminar flow $\frac{\bar{u}}{U} = 0.5$. The upper limit of laminar flow is at log Re = 3.1, corresponding to a Reynolds number of $Re = 12.6\cdot10^3$. It will be noted that the measured points up to Reynolds number $Re = 200\cdot10^3$ (log Re = 5.4) deviate from the calculated curve: they are connected by a broken line curve. This deviation is to be explained by the effect of viscosity which the formula does not show. In the further course above $Re = 200\cdot10^3$ the agreement is rather good. The measured values of Stanton and Pannell are in good agreement with ours to log Re = 4.2. Above this limit, there is an almost constant deviation. This deviation is certainly caused by the method of measurement. As mentioned on page we undertook supplementary measurements at different Reynolds numbers 20d upstream of the threshold cross section, which yielded the same values as our earlier measurements.

## SUMMARY

The object of the present study was to investigate the mathematical relationships of turbulent flows in smooth pipes in the greatest possible range of Reynolds numbers. For this purpose, an experimental setup was constructed for determination of turbulent water flows in circular pipes up to Reynolds number $3240 \cdot 10^3$. By evaluation of the measured velocity distributions and pressure gradients the following was established:

1. The form of the velocity distribution changes with the Reynolds number. With increasing Reynolds number the velocity distribution is fuller and fuller. Comparison of the velocity distributions measured by /35 and those of Stanton with our measurements produced good agreement.

2. The exponent n of the Prandtl law of exponentials ($u = ay^n$, if y = distance from the wall) has the fixed value of n = 1/7 in the Blasius resistance range up to $Re = 100 \cdot 10^3$. At very low Reynolds numbers, the exponent is greater than 1/7. Above Reynolds number $Re = 100 \cdot 10^3$, with increasing Reynolds number there is observed a decrease of exponent n. At the highest Reynolds number $Re = 3240 \cdot 10^3$, exponent n reaches the value of 1/10. Since characteristic magnitudes for turbulent flow in the vicinity of the wall are made dimensionless: $\tau_0$ = shearing stress at the wall, v = kinematic viscosity, $\varrho$ = density, there is a valid law of velocity distribution for all Reynolds numbers in the zone near the wall

$$\varphi = \varphi(\eta)$$

$$\text{where } \frac{u}{v_*} = \varphi, \quad \frac{v_* y}{\nu} = \eta, \quad v_* = \sqrt{\frac{\tau_0}{\varrho}}.$$

For sufficiently high values of $\eta$ (above $\eta = 10$)

$$\varphi = A + B \log \eta$$

is sufficiently exact (A and B are universal constants).

3. The turbulent exchange magnitude was determined as a function of wall distance. The dimensionless plotting of $\frac{\varepsilon}{v^* r}$ as a function of y/r shows that above Re $100 \cdot 10^3$ the distribution of exchange magnitudes over the cross-section is independent of the Reynolds number. Below this Reynolds number, this distribution is very pronouncedly dependent upon the Reynolds number. For the Prandtl mixing length that is related to the turbulent impulse exchange, it was found that the ratio l/r for each point of the cross-section decreases with increasing Reynolds number. If Re exceeds the value $100 \cdot 10^3$, the dimensionless mixing length distribution $l/r = f(y/r)$ is independent of the Reynolds number. The independence indicates that the effect of viscosity is no longer present above this Reynolds number.

4. The measured velocity distributions and the law of resistance were

compared with von Kármán's calculated distribution based on his hypothesis of similarity and were found to be in good agreement with this distribution in the range of highest Reynolds numbers where the effect of viscosity is absent.

In connection with the von Kármán similarity hypothesis, new theories of Prandtl and Betz are reported.

5. If $\lambda = \frac{dp}{dx}\frac{2d}{\rho \bar{u}^2}$ is the pipe coefficient of resistance, there is confirmation of the Blasius formula for resistance $\lambda_B = \frac{0.316}{\text{Re } 1/4}$ up to Reynolds number $100 \cdot 10^3$. For higher numbers there is the formula

$$\lambda = 0{,}0032 + \frac{0{,}221}{Re^{0{,}237}}.$$

In connection with the von Kármán resistance formula and ours, relationships between the mean velocity $\bar{u}$ and maximum velocity $\overline{U}$ were determined which indicated new correlations of the various formulas.

## REFERENCES


1. Blasius, H.: The law of similarity for friction processes in fluids. Forsch. Arb. Ing. Wis., Nr. 131, Berlin, 1913.
2. Saph, V. and E. H. Schoder: An experimental study of the resistance to the flow of water in pipes. Trans. Am. Soc. Civ. Engr. Pap. 944, Vol. 51, 1903.
3. Nusselt, W.: Heat transfer in pipelines. Forsch. Arb. Ing. Wis. Nr. 89, Berlin, 1910.
4. Ombeck, H.: Pressure loss of flowing air in straight cylindrical pipelines. Forsch. Arb. Ing. Wis., Nr. 158/159, Berlin, 1914.
5. Stanton, T. E. and J. R. Pannell: Similarity of motion in relation to the surface friction of fluids. Proc. Roy. Soc. Lond. (A) vol. 214, p. 199, 1914.
6. Lees, Ch. H.: On the flow of viscous fluids through smooth circular pipes. Proc. Roy. Soc. Lond. (A) vol. 91, p. 46, 1915.
7. Jakob, M. and S. Erk: The pressure drop in smooth pipes and the discharge coefficient of standard nozzles. Forsch. Arb. Ing. Wis., Nr. 267, Berlin, 1924.
8. Hermann, R.: Experimental investigations on the law of resistance in circular pipes at high Reynolds numbers and long starting zones. Diss. Leipzig and Akadem. Verlagsgesellschaft m.b.H. Leipzig, 1930.
9. Schiller, L.: Pipe resistance at high Reynolds numbers. Lecture from the field of aerodynamics and related subjects. Aachen 1929, pub. by A. Gilles, L. Hopf and Th. v. Kármán. Berlin, 1930, p. 69.
10. Prandtl, L.: Discussion remarks on the lecture by L. Schiller (footnote 9), Lectures...p. 78.
11. Stanton, T. E.: The mechanical viscosity of fluids. Proc. Roy. Soc., Lond. (A) vol. 85, pp. 363-376, 1911.
12. Nikuradse, J.: Investigation of the velocity distribution in turbulent flows. Forsch. Arb. Ing. Wis. no. 281, Berlin, 1926.
13. Kármán, Th. v.: Mechanical similitude and turbulence. Nachr. Ges. Wiss. Göttingen. Math. Phys. Class, p. 58, 1930.
14. The author presented a brief account of these in Aachen at the Congress of aerodynamics and related subjects. J. Nikuradse: On turbulent water flow in straight pipes at very high Reynolds numbers. Lectures from the field of aerodynamics and related subjects, Aachen 1929, published by A. Gilles, L. Hopf, and Th. v. Kármán, Berlin 1930, p. 63. In the same volume on p. 69 there is a report by L. Schiller on experiments carried out in Leipzig simultaneously with ours, which will be referred to several times in the following.
15. The quick closing valve of 150 mm diameter, which otherwise is generally used for experiments with supersonic velocities, was designed by Prof. J. Ackeret.
16. Stanton, T. E.: see footnote 11.
17. Bazin, M.: New experiments on the distribution of velocity in pipes. Mémoires, etc.
18. Prandtl, L.: On friction resistance of flowing air. Ergebnisse der Aerodynamischen Versuchsanstalt, Göttingen, III, p. 1, 1927 Edition. -- V. Kármán, Th: Laminary and turbulent friction. Z. Angew Math. Mech., Vol. 1, p. 233, 1921.

19. Prandtl, L.: On friction resistance of flowing air. Ergebn. d. Aerodyn. Versuchsanstalt zu Göttingen III, p. 1, 1927 edition. On turbulent flow in pipes and along plates. Ergebn. d. Aerodyn. Versuchsanstalt, Göttingen IV, p. 18, 1932 edition.
20. The author discussed this relationship in the summer of 1929 at the Colloquium on applied mechanics in Gottingen.
21. Boussinesq, J.: Essay on the theory of flowing water. Memoirs presented to the members of the Science Institute of France, 1877.
22. Prandtl, L.: Report on investigations of developed turbulence. Report on recent turbulence research. Z. angew. Math. Mech.,Vol. 5; p. 136, 1925. (Berlin, VDI-Verlag, p. 1, 1926).
Tollmien, W.: Calculation of turbulent propagation processes. Z. angew. Math. Mech. Vol. 6, p. 468, 1926.
Prandtl, L.: Developed turbulence. Verh. d. 2. intern. Kongr. f. techn. Mech., Zurich 1927.
Nikuradse, J.: Investigations on flows of water in convergent and divergent channels. Forsch.-Arb. Ing.-Wes. Nr. 289, 1929.
Nikuradse, J.: Turbulent water flows in straight pipes at very high Reynolds numbers. Lectures on Aerodynamics and related subjects, Published by A. Gilles, L. Hopf and Th. v. Kármán, Aachen, p. 63, 1929.
Fritsch, W.: The effect of wall roughness on turbulent velocity distribution in troughs. Z. angew. Math. Mech., Vol. 8, p. 215, 1928.
Swain, L. M.: On the turbulent wake behind a body of revolution. Proc. Roy. Soc., Lond., Vol. 125, p. 647, 1929.
Betz, A.: Turbulent friction layers on curved walls. Lectures on Aerodynamics and related subjects, published by A. Gilles, L. Hopf and Th. v. Kármán, A chen, p. 10, 1929.
Nikuradse, J.: Law of resistance and velocity distribution of turbulent water flows in smooth and rough pipes. Verh. d. 3. intern. Kongr. f. techn. Mechanik. Stockholm, p. 239, 1930.
Schlichting, H.: On the flat lee problem. Göttingen thesis. Ing.-Arch., Vol. 1, p. 533, 1930.
23. Prandtl, L.: Turbulence and its origin. Tokyo lecture 1929. Rep. Aeron. Res. Inst., Tokyo, No. 65, 1930.
24. cf. footnote 13., p. 2
25. Betz, A.: The von Kármán hypothesis of similarity for turbulent processes in physical interpretation. Z. angew. Math. Mech., Vol. 11, p. 397, 1931.
26. This hypothesis was advanced by Prandtl in a survey lecture on hydrodynamics, Summer semester 1931.
27. Lees, Ch. H.: Proc. Roy. Soc., Lond. (A), Vol. 91, p. 46, 1915.
28. Schiller, L. and R. Hermann: Resistance of plates and pipes at high Reynolds numbers. Ing.-Arch. Vol. 1, No. 4, p. 392, 1930.
29. Schiller, L.: Pipe resistance at high Reynolds numbers. Lectures from the field of aerodynamics and related disciplines. ublished by A. Gilles, L. Hopf and Th. v. Kármán, Berlin, p. 78, Aachen, 1929.

## BIBLIOGRAPHY


1. Blasius, H.: The law of similarity in friction processes in fluids. Forsch.-Arb. Ing.-Wes., No 131, Berlin, 1913.
2. Saph, V. and E. H. Schoder: An experimental study of the resistance to the flow of water in pipes. Trans. Amer. Soc. civ. Engr. Vol. 51, Paper 944, 1903.
3. Nusselt, W.: Heat transfer in pipes. Forsch.-Arb. Ing.-Wes. No. 89, Berlin 1910.
4. Ombeck, H.: Pressure loss of flowing air in straight cylindrical pipes. Forsch.-Arb. Ing.-Wes. No. 158 and 159, Berlin 1914.
5. Stanton, T. E. and J. R. Pannell: Similarity of motion in relation to the surface Friction of Fluids. Proc. Roy. Soc., Lond. (A) Vol. 214, p. 199, 1914.
6. Lees, Ch. H.: On the flow of viscous Fluids through smooth circular pipes. Proc. Roy. Soc., Lond. (A), Vol. 91, p. 46, 1915.
7. Jakob, M. and S. Erk: The pressure drop in smooth pipes and the coefficient of flow of normal nozzles. Forsch.-Arb. Ing.-Wes. No. 267, Berlin, 1924.
8. Hermann, R.: Experimental investigation with reference to the law of resistance of circular pipe at high Reynolds numbers and long starting lengths. Leipziger Dissertation, Akadem. Verlagsges. m.b.H. Leipzig 1930.
9. Schiller, L.: Pipe resistance at high Reynolds numbers. Lectures on Aerodynamics and related subjects, published by A. Gilles, L. Hopf and Th. v. Kármán, Aachen 1929 (Berlin: J. Springer) p. 69, 1930.
10. Prandtl, L.: Comments on the above lecture by L. Schiller. Aachen 1929. Published by A. Gilles, L. Hopf and Th. v. Kármán (Berlin: J. Springer) p. 78, 1930.
11. Stanton, T. E.: The mechanical viscosity of fluids. Proc. Roy. Soc., Lond. (A), Vol. 85, p. 366, 1911.
12. Nikuradse, J.: Investigation with reference to the velocity distribution in turbulent flows. Forsch.-Arb. Ing.-Wes. No. 281, Berlin 1926.
13. von Kármán, T.: Mechanical similarity and turbulence. Gottinger Nachrichten. Math. Phys. Klasse p. 58, 1930.
14. Nikuradse, J.: Turbulent water flows in straight pipes at very high Reynolds numbers. Lectures on Aerodynamics and related subjects, published by A. Gilles, L. Hopf and Th. v. Kármán, Aachen 1929. (Berlin: J. Springer), p. 63, 1930.
15. Bazin, M.: New experiments on the distribution of velocities in pipes. Memoirs presented to the members of the Science Institute of France, Vol. 32, No. 6, 1902.
16. Prandtl, L.: Friction resistance of flowing air. Ergebnisse der Aerodynamics Versuchstalt zu Gottingen, Edition 3, p. 1, 1927.
17. Boussinesq, J.: Essay on the theory of flowing water. Memoirs presented to the members of the Science Institute of France, 1877.
18. Prandtl, L.: Turbulent flow in pipes and along plates. Ergebnisse der Aerodynamischen Versuchsanstalt zu Gottingen, 4th Edition, p. 18, 1932.
19. von Kármán, T.: Laminar and turbulent friction. Z. angew. Math. Mech., Vol. 1, p. 233, 1921.

20. Prandtl, L.: Report on research concerning developed turbulence. Z. angew. Math. Mech. Vol. 5, p. 136, 1925.
21. Prandtl, L.: Report on recent turbulence research. p. 1. (Berlin: VDI-Verlag 1926).
22. Tollmien, W.: Calculation of turbulent propagation processes. Z. angew. Math. Mech. Vol. 6, p. 468, 1926.
23. Prandtl, L.: Developed turbulence. Verh. d. 2. intern. Kongr. f. techn. Mech. Zürich, 1927.
24. Nikuradse, J.: Experiments concerning water flows in convergent and divergent channels. Forsch.-Arb. Ing.-Wes. No. 289, Berlin, 1929.
25. Fritsch, W.: The effect of wall roughness on turbulent velocity distribution in troughs. Z. angew. Math. Mech. Vol. 8, p. 21, 1928.
26. Swain, L. M.: On the turbulent wake behind a body of revolution. Proc. Soc. Roy., Lond., Vol. 125, p. 647, 1929.
27. Betz, A.: Turbulent friction layers at curved walls. Lectures from the field of aerodynamics and related subjects, published by A. Gilles, L. Hopf, and Th. v. Kármán, Aachen 1929 (Berlin: J. Springer, 1930), p. 10.
28. Nikuradse, J.: Law of resistance and velocity distribution of turbulent water flows in smooth and rough pipes. Verh. d. 3. intern. Kongr. f. techn. Mech. Stockholm, p. 239, 1930.
29. Schlichting, H.: On the flat lee problem. Göttinger Dissertation, Ing.-Arch. Vol. 1, p. 533, 1930.
30. Prandtl, L.: Turbulence and its origin. Tokyo lecture. Journal of the Aeronautical research Institute, Tokyo Imperial University No. 65, 1930.
31. Betz, A.: The von Kármán hypothesis of similarity for turbulent process in physical interpretation. Z. angew. Math. Mech., Vol. 11, p. 397, 1931.
32. Schiller, L. and R. Hermann: Resistance of plate and pipe at high Reynolds numbers. Ing.-Arch. Vol. 1, p. 392, 1930.

Translated for National Aeronautics and Space Administration by
INTERNATIONAL INFORMATION INCORPORATION.